IRN - CNRS
Hydrobio

“ This workshop aims to consolidate and strengthen collaborations through scientific exchange. It will provide a platform for academic researchers and industry experts in hydrodynamics and bioengineering to discuss recent trends.”

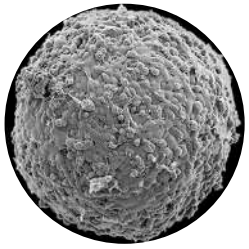
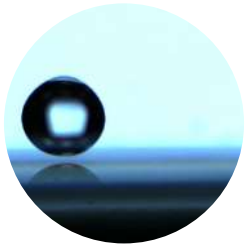
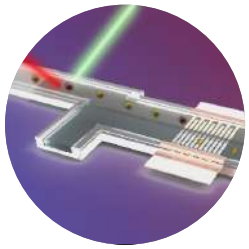


Sponsors

HOLMARC OPTO-MECHATRONICS LTD

AIP Publishing

Hydrodynamics at small scales

From Soft matter to bioengineering

October 25- 27, 2024

IRN - CNRS
Hydrobio

Table of Contents

Oral Presentations

Poster Presentations

A Bloody Tale

Saptarshi Basu
Department of Mechanical Engineering, Indian Institute of Science, Bengaluru, Karnataka, India

We study the mechanics of sessile blood drop evaporation using optical diagnostics, theoretical analysis, and micro/nano-characterization. The transient evaporation process has three major phases (A, B, and C) based on the evaporation rate. Phase A is the fastest, where edge evaporation dominates and forms a gelated three-phase contact line. Gelation results from sol-gel phase transition that occurs due to the accumulation of red blood cells, as they get transported due to outward capillary flow generated during drop evaporation. The intermediate phase B consists of a gelation front propagating radially inwards due to the combined effect of outward capillary flow and drop height reduction evaporating in pinned mode, forming a wet gel phase. We unearthed that the gelation of the entire droplet occurs in Phase B, and the gel formed contains trace amounts of water that are detectable in our experiments. Phase C is the final slowest stage of evaporation, where the wet gel transforms into a dry gel and leads to desiccation induced stress, forming diverse crack patterns in the dried blood drop precipitate. We observe radial and orthoradial cracks in the precipitate's thicker coronal region, mud-flat cracks in the drop center, and the outer contact line where thickness and curvature are relatively small. We also study the evaporation of bacteria-laden droplets to simulate bacterial infection in human blood and show that the drop evaporation rate and final dried residue pattern do not change appreciably within the parameter variation of the bacterial concentration typically found in bacterial infection of living organisms. However, at exceedingly high bacterial concentration we observe the cracks formed in the coronal region of the precipitate deviates from the typical radial cracks found in lower concentrations.

A novel particle-induced instability of a simple shear flow

Anu V. S. Nath*, Anubhab Roy* and M. Houssem Kasbaoui†

We investigate the instability of a dusty simple shear flow with non-uniformly distributed dust particles. While a simple shear flow is typically stable to infinitesimal perturbations, and a band of particles remains unaffected in the absence of any background flow, we demonstrate that their combination can lead to destabilisation through two-way interactions. This instability arises solely from the momentum feedback from the particle phase to the fluid phase, which significantly alters the dynamics of the system. By employing Eulerian-Lagrangian simulations, we illustrate the presence and characteristics of this instability, highlighting how particle-fluid interactions can drive new flow behaviours. Fig. shows the simulation results illustrating the evolution of vorticity perturbations in typical one-way and two-way interaction cases. The perturbations grow when the two-way interactions are activated, whereas they decay when only one-way interaction is considered.

A linear stability analysis using an Eulerian-Eulerian model further corroborates our simulation results, providing a comprehensive understanding of the underlying mechanisms. Our findings reveal that the instability is inviscid in origin, characterised by a critical wavelength below which it does not persist. This critical wavelength marks the threshold for the onset of instability, emphasising the importance of particle concentration and distribution in determining flow stability. Overall, this research provides new insights into the dynamics of particle-laden flows, underscoring the significant role of particle-fluid interactions in generating and sustaining flow instabilities. These insights have potential implications for a wide range of natural and industrial processes where a non-uniform particle distribution is affected by shearing from the background flow, such as sea-spray dynamics in the ocean-atmospheric boundary layer under shear turbulence and dust particles in a planetary accretion disk under Keplerian shear.

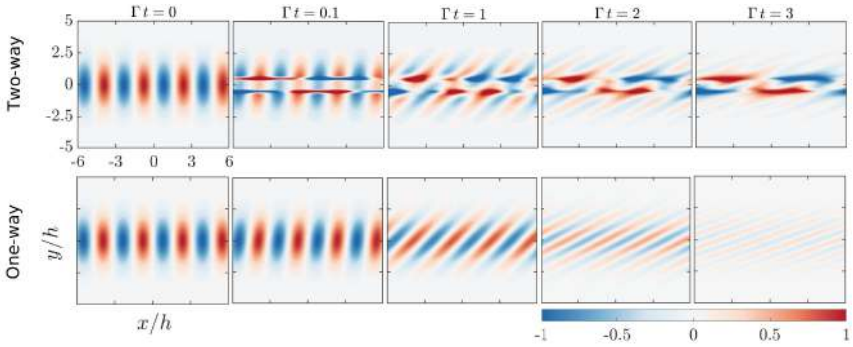

Figure 1: Time evolution of vorticity perturbations in one-way and two-way coupled Euler-Lagrange simulations.

*Dep. of Applied Mechanics and Biomedical Engineering, IIT Madras, Chennai 600036, India
†School for Engineering of Matter, Transport and Energy, Arizona State University, Tempe, AZ 85281, USA

A solution to the moving contact line problem using the Lightning Stokes solver

V.S.A. Sangadi [1] and Harish. N. Dixit[1,2]

[1]*Department of Mechanical & Aerospace Engineering, Indian Institute of Technology Hyderabad, India, ME20M22P100001@iith.ac.in*

[2] *Centre for Interdisciplinary Programs, Indian Institute of Technology Hyderabad, India, hdixit@mae.iith.ac.in*

I. ABSTRACT

When a fluid-fluid (or more commonly, a liquid-gas) interface comes in contact with a solid substrate, the three-phase line of intersection is referred to as the *contact line*. Understanding the flow field in the vicinity of a moving contact line can potentially lead to important insights into dynamic wetting transitions. Huh & Scriven[1] in their seminal paper, solve the biharmonic equation for flow in a wedge between a moving solid and a flat interface and show the presence of a logarithmic singularity at the contact line. Kirkinis & Davis[2] proposed a slip-based model at the vicinity of the contact line by solving for the biharmonic equation in stream function. For the same set of physical parameters, multiple solutions are found making it unsuitable to compare the results against experiments. To overcome this challenge, we employ a novel complex variable technique developed by Trefethen and co-workers[3] to solve the biharmonic equation. In this method, the streamfunction is described in terms of two unknown functions, also known as Goursat functions, as given below:

$$\psi(z\,,\bar{z}) = Im\{\bar{z}\,f(z) + g(z)\}$$

The unknown complex functions, f (z) and g(z), are approximated in terms of rational functions and polynomial functions. A linear least-square fitting of the boundary condition values on the assumed basis is done to get the coefficients for the arbitrary functions. The computed solution is then used to reconstruct the earlier derived physical quantities as a function of the independent variable, here z, which allows us to get a solution in the entire domain. The approach is extended to incorporate a curved interface with the gaseous phase fluid being passive i.e. it only exerts the surface tension force. This modified Lightning Stokes Solver (LSS) is used to model the moving contact line problem as shown in the figures below.

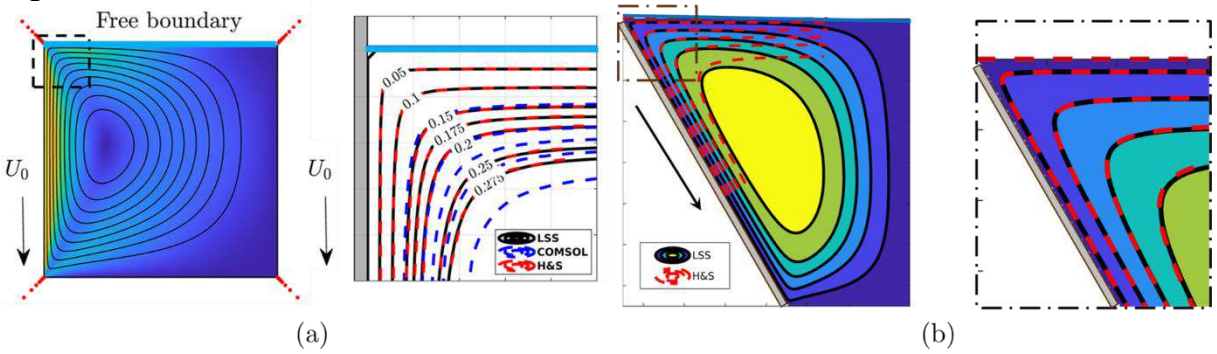

FIG. 1The figure (a) shows the results generated by LSS for the 90° contact line problem. The figure shows the direct comparison of the results with analytic study, namely Huh & Scriven[1][H&S] and with simulations done on COMSOL. Similarly, the figures (b) shows the same analysis for the case of 60° contact angle.

[1] Huh and Scriven, JCIS 35(1), 85-101, (1971).
[2] Kirkinis, E., and S. H. Davis. JFM 746 (2014): R3.
[3] Brubeck, P. D., & Trefethen, L. N. (2022).SIAM JSC, 44(3), A1205-A1226.

Acoustic field and particle transport in a viscoelastic fluid

T Sujith[1], Lokesh Malik[1] and Ashis Kumar Sen[1]

[1] *Department of Mechanical Engineering, IIT Madras, Chennai 600036, Tamil Nadu, India,*
sujitht996@gmail.com

Bio-fluids are crowded suspensions of cells and bio-particles and are extremely diverse in nature. These fluids, such as blood, saliva, sputum, and synovial fluid, exhibit viscoelastic properties due to the presence of various cells, structural proteins, and other macromolecules [1]. Among various microfluidic techniques, acoustofluidics has emerged as a promising method for manipulating cells and particles in these fluids for medical diagnostics [2]. Although earlier studies involve the use of complex bio-fluids, prevailing modeling techniques often oversimplify by presuming Newtonian characteristics, thereby disregarding their inherent viscoelastic properties. To address this gap, we conduct a comprehensive study by investigating the behavior of viscoelastic fluids and suspended particles under the influence of a standing bulk acoustic wave (S-BAW) in a micro-confinement using theory, simulations, and experiments. Our study examines the effect of viscoelastic parameters: μ^* (the ratio of viscosity of the viscoelastic fluid to the base Newtonian fluid) and De (= $\tau\omega$, the product of the fluid's relaxation time and the angular frequency of actuation) on the acoustic force parameters, which govern particle migration dynamics.

We classify ultrasound responses of fluids in micro-confinement into three categories: low, moderate, and high elasticity fluids, based on De. This classification reflects the transition from viscous to elastic behavior, where the fluid transits from an energy dissipation state (relaxation mode) to an energy storage state (frozen mode), as shown in Fig. 1. Our findings show that elastic effects accelerate particle migration due to the frozen mode, while viscous effects decelerate it due to the relaxation mode. Consequently, a viscoelastic fluid-filled micro-confinement functions as an energy dissipation device at low De and as an energy storage device at high De. Particle migration can be controlled by adjusting viscoelastic and acoustic parameters at a fixed power input. We validate our theoretical and numerical fndings with experimental data, which show very good agreement. Our study could find significance in understanding migration of cells and extracellular vesicles in bio-fluids.

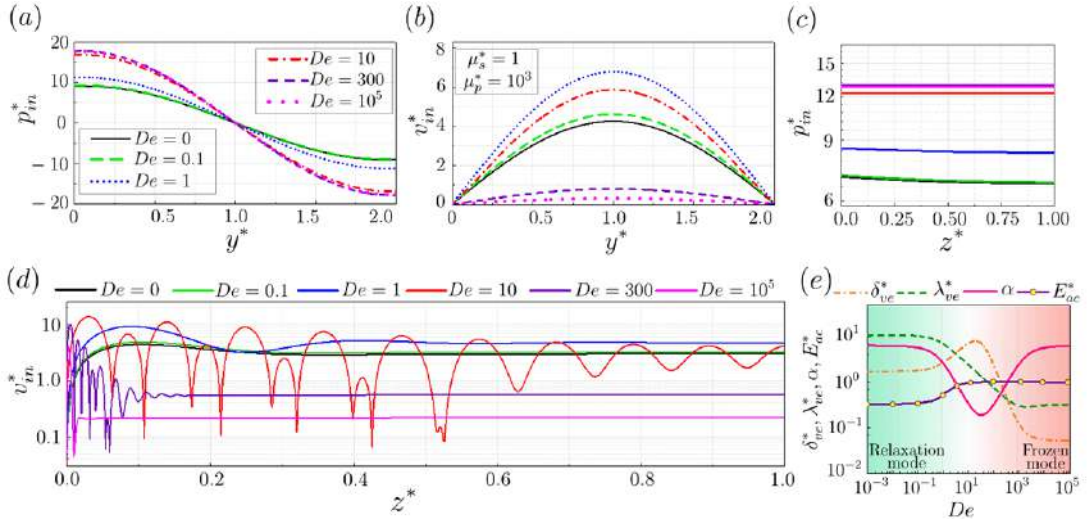

FIG. 1. Variation of incoming fields (p_{in}^* and v_{in}^*) in Newtonian ($De = 0$) and viscoelastic fluid ($De = 0.1, 1, 10, 300, 10^5$) at $\mu^* = 1001$, $\mu_s^* = 1$, $\mu_p^* = 1000$, (a) p_{in}^* along y^*,(b) v_{in}^* along y^*,(c) p_{in}^* along z^*, (d) v_{in}^* along z^*. Variation of (e) $\delta_{ve}^*(\delta_{ve}/a)$, $\lambda_{ve}^*(=\lambda_{ve}/a)$, α $(=\lambda_{ve}^*/\delta_{ve}^*)$, and $E_{ac}^*(=E_{ac}/E_{ac}^{bf})$with De.

[1] M Brust et al., *Rheology of Human Blood Plasma: Viscoelastic Versus Newtonian Behavior*, Phys. Rev. Lett. **110**, 078305 (2013).

[2] T. Laurell, F. Petersson and A. Nilsson, *Chip integrated strategies for acoustic separation and manipulation of cells and particles*, Chem. Soc. Rev. **36**, 492-506 (2007).

Acoustophoresis-assisted Fluid Jet Polishing

Anomitra Saha[1] and Abhijit Dhamanekar, Diwakar S. Venkatesan[2]

[1] *Engineering Mechanics Unit, JNCASR, 560064, Bengaluru, India,* anomitra.98@gmail.com
[2] *Engineering Mechanics Unit, JNCASR, 560064, Bengaluru, India,* diwakar@jncasr.ac.in

Fluid Jet Polishing (FJP) is a method of contouring and polishing a surface by aiming a jet of slurry from a nozzle and eroding the surface to create a desired shape. FJP finds its application in finishing micro-lens mold arrays, polishing microchannels, smoothing of micro-cusps, and generating functional surfaces. However, conventional FJP suffers from some drawbacks, such as a non-homogeneous erosion profile due to random particle impacts & formation of stagnation zone, unwanted erosion of the nozzle wall, and wastage of particles. Here, the acoustophoretic effect is being proposed as a possible means to overcome these drawbacks of conventional FJP.

Acoustophoresis is the process of manipulating the particles within a fluid stream by means of sound waves. The scattering of acoustic waves on the particles suspended in the liquid leads to momentum transfer from the sound field to particles giving rise to a 2nd order time-averaged acoustic radiation force, which results in particle migration. The main objective is to focus the impinging particles towards the center of the issuing nozzle to get a "U" shaped erosion profile as opposed to the "W" shaped profile.

The numerical analysis has been performed using ANSYS Fluent Software. The assumption of one-way coupling holds due to the small size & mass concentration of the abrasive particles. The fluid flow is solved using the Eulerian multi-phase approach, and the particle tracking is done using the Discrete Phase Model (DPM). The supplemental acoustic force is included via the User Defined Function (UDF) functionality.

The modeled geometry consists of two different nozzles with circular and square cross-sections respectively. In the case of circular nozzles, acoustic excitation results in precise and controllable annular erosions. Here, the particles are focused on concentric pressure nodes that do not occur at the axis of the impinging jet, making the inhomogeneity of the erosion process inevitable. On the other hand, composite one-dimensional acoustic excitations in square cross-sections enable the focusing of particles along the jet axis. This results in U-shaped erosion profiles for specific operating conditions.

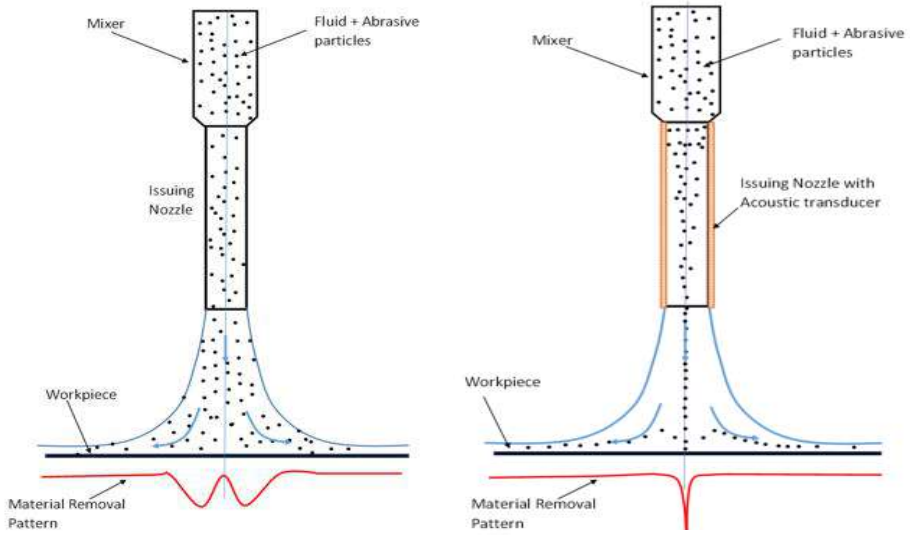

Fig.1. Left: Erosion profile without acoustic forcing; Right: Erosion profile with acoustic forcing

[1] A Mansouri, A combined CFD-experimental method for developing erosion equation for both gas-sand and liquid-sand flows, PhD Thesis, University of Tulsa

[2] M. Barmatz, P. Collas, Acoustic radiation potential on a sphere in plane, cylindrical and spherical standing wave fields, J. Acous. Soc. of America. 77, 928-945(1985)

Blood on Paper

Suman Chakraborty
Institute Chair Professor & Sir J. C. Bose national Fellow
Mechanical Engineering Department, Indian Institute of Technology Kharagpur
suman@mech.iitkgp.ac.in

Blood dynamics plays a crucial role in paper microfluidics, influencing the design, functionality, and accuracy of diagnostic devices. A thorough understanding of blood behaviour in these systems enables the development of more efficient, reliable, and innovative diagnostic tools. This talk explores three key aspects of blood flow on paper matrices: the impact of red blood cell (RBC) concentration on blood spreading on dry filter paper, blood flow dynamics on moist filter paper, and the selective aggregation-disaggregation of RBCs through the fibrous microporous pathways of the paper.

First, we present an unexpected observation where a finite volume of blood exhibits a universal time-dependent spreading on filter paper, largely independent of haematocrit levels (RBC volume fraction) within the healthy physiological range, though distinct from the spreading patterns of blood plasma and water. This is demonstrated through controlled wicking experiments on filter papers of varying grades. High-speed imaging and microscopy are used to track the spreading of human blood samples with haematocrit levels from 15% to 51%, as well as plasma. A semi-analytical theory is applied to explain the underlying physics, revealing the influence of cellular aggregates obstructing the randomly structured porous pathways and the hindered diffusion induced by networked plasma proteins.

Screening anaemic patients in resource-limited settings poses challenges, as gold-standard diagnostic technologies are impractical and alternative methods face issues like reduced accuracy, high costs, complexity, and reagent stability. To address these challenges, we introduce a smartphone-based sensor for rapid anaemia screening. This device analyses the patterns formed by blood spreading on a wet paper strip, where the blood displaces a more viscous fluid in the porous matrix, creating “finger-like” projections at the interface. Using smartphone-enabled image analysis, we correlate these patterns with RBC occupancy in the blood, enabling label-free screening and classification of blood samples for moderate to severe anaemia. The method shows a strong correlation ($R^2 = 0.975$) with gold-standard haematology reports, offering a cost-effective and reliable solution for resource-constrained environments.

Finally, we explore how reduced RBC deformability, often linked to impaired blood flow and oxygen delivery, can result in intriguing dynamics on a paper matrix. By integrating in vitro microfluidic techniques with mesoscopic simulations, we quantify the selective aggregation-disaggregation of RBCs as they move through randomly distributed fibrous microporous

pathways. Interestingly, contrary to expectations of phase separation at high RBC concentrations, our results reveal that RBCs can phase-separate even at low concentrations, driven by their aggregability and interactions within the tortuous microfluidic pathways. These findings provide crucial insights into blood flow dynamics in cellulose-based porous matrices, offering a decisive indicator of RBC deformability for diagnostic applications.

Brownian motion at interfaces

T. Salez
LOMA, CNRS & Univ. Bordeaux

Brownian motion near interfaces is a canonical situation, encountered from fundamental biophysics to nanoscale engineering. Using a combination of experimental, theoretical and numerical methods, we study the thermally-induced random tridimensional trajectories of individual microparticles, within salty aqueous solutions, in the vicinity of rigid walls, and in the presence of surface charges. We construct the time-dependent position and displacement probability density functions, and study the non-Gaussian character of the latter which is a direct signature of the hindered mobility near the wall. Furthermore, we implement a robust multifitting method, allowing for the thermal-noise-limited inference of diffusion coefficients spatially resolved at the nanoscale, equilibrium potentials, and forces at the femtonewton resolution. Finally, we discuss more complex situations, such as the ones involving soft boundaries, external flows or active microswimmers.

Collision rate of like-charged aerosol particles in a uniaxial compressional flow

Srikumar Warrier*, Pijush Patra† and Anubhab Roy*

Collision of aerosol particles can lead to the formation of larger droplets which precipitate out of the cloud. Cloud droplets acquire electric charge by diffusion of ions, convection charging, and inductive charging. Unlike the accepted wisdom of an always repulsive interaction of same-signed point charges, the scenario for finite-sized particles is remarkably different. Like-charged finite-sized particles attract each other at close separation, while the interaction is repulsive at large distances. These effects play an important role in the collision process and thus influence the droplet size distribution in the cloud.

We present the trajectory analysis and calculate the collision rates of like-charged unequal dielectric spheres in a uniaxial compressional background flow. Non-continuum lubrication interactions are incorporated in the limit of vanishing separation gap, resulting in particle-particle contact in finite time. We calculate the collision rate and study the modifications of pair trajectories for a range of size ratios, charge ratios, Knudsen number and as a function of the strength of the electrostatic force relative to the flow. As the size ratio increases, the efficiency increases for small charge ratios. The collision efficiencies are higher for small-size ratios and decrease as the size ratio increases. For small charge ratios, the collision efficiency is greater for large size ratios, irrespective of the strength of the electrostatic force to the flow strength. However, as the charge ratio increases, the collision rates decrease for larger ratios beyond a certain strength of the electrostatic force relative to the flow. For a charge and size ratio combination for which the near field electrostatics is attractive, the radial component of the relative velocity is negative and thus results in colliding trajectories. We quantify this using a non-dimensional parameter, N_e, that quantifies the relative strength of electrostatic force to flow strength. Above a critical value of N_e, no collisions are possible due to an outward radial component of the relative velocity at some region in the domain. For repulsive near-field electrostatics, collision is still possible below a critical value when the incoming uniaxial compressional flow is strong enough to overcome the near-field repulsive electrostatic force.

*Dept. of Applied Mechanics and Biomedical Engineering, Indian Institute of Technology, Madras, Chennai 600036.

†Nordita, KTH Royal Institute of Technology and Stockholm University, Stockholm 10691, Sweden.

Consistent wetting boundary condition and solid surface projection-based capillary force calculation scheme for diffuse interface framework

Malyadeep Bhattacharya[1], Snigdhadyut Dash[2] and Amol Subhedar[1]

[1] *Department of Chemical Engineering, Indian Institute of Technology Bombay, Mumbai, Maharashtra 400076, India,* amol.subhedar@iitb.ac.in

[2] *Department of Chemical Engineering, Indian Institute of Technology Delhi, Delhi 110016, India*

The numerical analysis of suspensions in multiphase flow presents several challenges, particularly regarding the application of capillary forces on solid bodies and the implementation of wetting boundary conditions in diffuse interface models. In these models, fluid-fluid interfaces are treated as diffuse, while solid-fluid interfaces are considered sharp. To address these issues, we introduce two key advancements: (i) a novel wetting boundary condition and (ii) a new capillary force computation scheme. Our wetting boundary condition utilizes phase-field theory to define phase-field values at ghost nodes within the solid phase. Unlike current methods [1], our approach avoids the need for special handling of neutral wetting conditions and eliminates complex interpolation requirements. In the second part, our capillary force computation scheme is designed to be independent of delta distribution choices, reduces discrete errors, and is effective for both curved boundaries and scenarios where capillary forces do not cancel out due to symmetry. Numerical tests conducted with the lattice Boltzmann method demonstrate that both our wetting boundary condition and capillary force scheme significantly outperform existing methods in terms of accuracy [2,3].

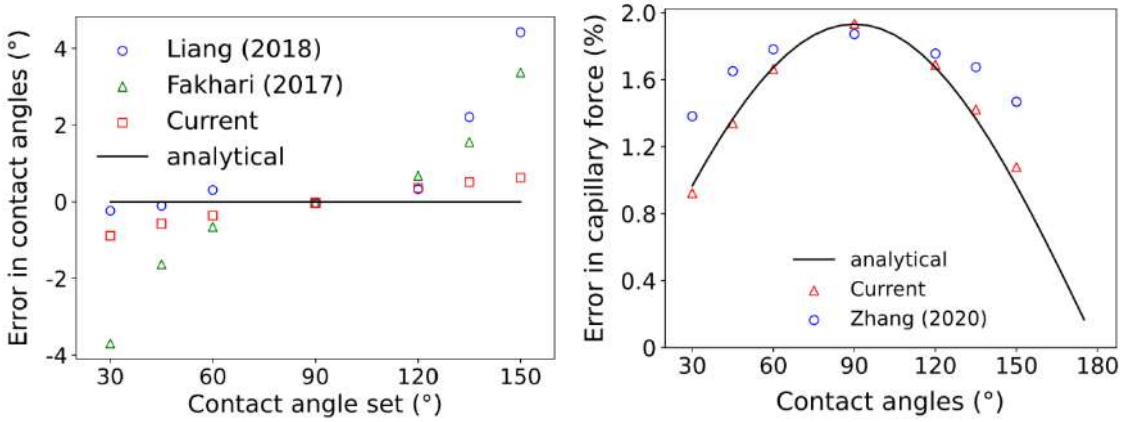

(a) (b)

FIG. 1. (a) Error in contact angles from the simulations for various set contact angles for a drop resting on a flat plate. (b) Error in capillary forces for various contact angles for a drop resting on an inclined plate. Notice how the proposed methods produce the least amount of errors for both cases.

[1] A. Fakhari and D. Bolster, Diffuse interface modeling of three-phase contact line dynamics on curved boundaries: A lattice Boltzmann model for large density and viscosity ratios, J. Comput. Phys. **334**, 620 (2017)

[2] K. W. Connington, T. Lee and J. F. Morris, Interaction of fluid interfaces with immersed solid particles using the lattice Boltzmann method for liquid–gas–particle systems, J. Comput. Phys. **283**, 453 (2015)

[3] X. Zhang, H. Liu and J. Zhang, A new capillary force model implemented in lattice Boltzmann method for gas–liquid–solid three-phase flows, Phys. Fluids **32**, 10 (2020)

Abstract: Indo French Workshop, IIT Madras

Uddipta Ghosh
Mechanical Engineering, IIT Gandhinagar

Title of the presentation: Coupled interfacial and bulk surfactant transport govern the movement of drops.

Surfactant-like impurities are omnipresent in multiphase emulsions, either naturally or introduced artificially for stability. They are known to have significant impact on the motion of small droplets by altering their interfacial properties through generation of Marangoni stresses or imparting viscosity to the droplet interface. Sometimes these surfactants are soluble in the bulk and undergo adsorption–desorption onto the interface which modifies their surface concentration and hence their overall influence on droplet motion. Yet, the impact of transport of surfactants on droplet dynamics, especially that of the interactions between the transport in the bulk and the interface, remain poorly explored till now. As such, we address a few canonical scenarios in this talk, where the impact of the aforementioned interactions on the drop's motion and trajectory is probed.

We shall start with the simplest problem where the settling of a single drop in an otherwise stationary unbounded medium is considered. Here, we analyse how the nature of the surfactant may influence a drop's settling velocity. To this end, the surface active agents are assumed to be bulk-insoluble and non-ideal, while the interface itself is assumed to have its own rheology, described by the Boussinesq-Scriven model. The diffusive fluxes of the surfactants are expressed in a thermodynamically consistent manner as proportional to the chemical potential gradient, which results in concentration dependent diffusivity. We subsequently derive semi-analytical solutions for approximately spherical drops without any other restrictions on the transport processes. Our results reveal that stresses originating from interfacial rheology tend to decrease the settling velocity and at the same time make the surfactant concentration uniform across the surface. Remarkably, this settling velocity is revealed to be independent of the choice of the free-energy isotherms and the extent of packing of the surfactants, when a variable diffusivity is correctly accounted for.

The next step is to consider the impact of the bulk solubility of the surfactants along with the presence of a bounding surface. Usually the surfactants are soluble in the bulk and undergo adsorption–desorption onto the interface which modifies their surface concentration and hence their overall influence on droplet motion. Yet, the impact of the bulk solubility and transport of surfactants on droplet dynamics, especially in the presence of bounding walls, remains poorly understood. As such, we construct a semi-analytical framework for arbitrary values of 'bulk interaction parameter', which dictates the strength of adsorption–desorption kinetics compared with bulk diffusion. Our results indicate that while mass exchange between the bulk and the interface can remobilize the drop, a finite bulk diffusion rate restricts this process and therefore slows down the drop. This also results in bulk concentration depletion near the south pole and accumulation near the north pole, the extent of which becomes strongly asymmetric with an enhanced intensity of depletion, as the drop approaches the wall. Presence of the wall and bulk solubility are found to aid each other towards remobilizing the drop by aptly modifying the interfacial concentration.

The above studies only consider surfactant solutions with relatively low bulk concentrations, whereas in many scenarios of practical interest, high concentration levels, even above the critical micelle concentration (CMC) levels are maintained. We address such a scenario in the last part, where the impact of the interactions between bulk and interfacial transport of surfactants on the cross-stream migration of a passive drop suspended in a Poiseuille flow

is investigated, with the bulk concentration being larger than the CMC. This results in an intriguing dynamical coupling between the transport and formation of micelles and the free surfactant molecules and their interfacial adsorption-desorption processes. It is found that bulk soluble surfactants actually slow down the migration of a drop as compared to bulk insoluble ones, the extent of which strongly depend on the times scales of bulk and interfacial diffusion as well as the times scales of adsorption-desorption processes. However, the increasing the bulk concentration beyond CMC may significantly alter coupling between the interfacial and bulk transport, leading to changes in the migration patterns, which we aim to explore in this final piece.

Critical Fluid Shear for Sperm Rheotaxis

Pulak Roy[1] and Ashis Kumar Sen[2]

[1] *Department of Mechanical Engineering, IIT Madras, Chennai, India,* me22d040@smail.iitm.ac.in
[2] *Department of Mechanical Engineering, IIT Madras, Chennai, India,* ashis@iitm.ac.in

Sperm rheotaxis is a fundamental biophysical process that plays a crucial role in guiding sperm cells towards the oocyte (egg cell) during fertilization. It is characterized by the ability of sperm cells to orient their heads against the direction of fluid flow and swim upstream, a mechanism that is essential for successful navigation through the female reproductive tract (FRT). In recent years, the study of sperm hydrodynamics has attracted significant attention from researchers seeking to understand the biophysical principles governing fertilization, for addressing concerns such as declining fertility rates. During fertilization, sperm cells must traverse considerable distances, often thousands of times their own body length, within the complex and dynamic environment of the FRT to reach the fertilization site [1]. This journey is facilitated by a variety of navigational mechanisms, including chemotaxis (the ability to move toward higher concentrations of specific chemical signals) and thermotaxis (the ability to move toward regions with higher temperatures). However, recent studies have demonstrated that rheotaxis, the ability to swim against fluid flow, plays a dominant role in guiding sperm cells over much of their journey within the reproductive tract, thereby attracting more research into the underlying mechanisms of rheotaxis and how it affects sperm motility and fertilization. The biophysical mechanism of sperm rheotaxis involves a complex interplay between the sperm cell's flagellar motion and the external hydrodynamic forces exerted by the surrounding fluid. Sperm cells can sense the direction of fluid flow and align themselves so that they swim upstream, counteracting the drag forces imposed by the flow. This upstream swimming is facilitated by the helical beating of the sperm's flagellum, which generates forward propulsion. However, the ability of sperm cells to maintain upstream movement is highly dependent on the flow rate of the surrounding fluid. At low to moderate flow rates, sperm cells exhibit positive rheotaxis, successfully orienting themselves against the flow and swimming upstream. Conversely, at sufficiently high flow rates, the drag forces become too high for the sperm to overcome, and they are passively swept downstream [2]. One key focus of research in sperm rheotaxis is identifying the operational flow regimes in which sperm cells can effectively swim upstream. This is particularly relevant for understanding the conditions under which sperm cells exhibit progressive motility i.e., sustained, directional movement that is critical for successful fertilization. Additionally, understanding the hydrodynamic constraints on sperm motility has important implications for in vitro fertilization techniques, as it can help optimize the fluid environments in which sperm cells are cultured and assessed for their motility.

In this study, we investigated the rheotactic behavior of bovine sperm cells under varying flow rate conditions, ranging from low to high flow rates. At low flow rates, sperm cells exhibited clear positive rheotaxis, swimming upstream against the flow. As the flow rate increased to moderate levels, sperm cells began to encounter greater resistance from the fluid, and their ability to swim upstream was diminished. At this stage, it is observed that sperm cells find it difficult to maintain their upstream orientation and are reoriented in the downstream direction due to the increased fluid drag forces acting on their heads. This loss of upstream orientation likely occurs because the forces on the sperm’s head and tail become unbalanced at higher flow rates, making it difficult for the sperm to control its upstream direction. At even higher flow rates, the drag forces became overwhelming, and sperm cells were unable to resist the fluid flow. As a result, they were passively carried downstream, unable to swim against the fluid current. These findings highlight the existence of a critical flow rate threshold beyond which sperm cells lose their ability to exhibit positive rheotaxis. This threshold is an important parameter for understanding the limits of sperm motility in both natural and artificial reproductive environments.

[1] S. S. Suarez and A. A. Pacey, Sperm transport in the female reproductive tract, Hum. Reprod. Update. **12**, 23 – 37 (2006).
[2] M. Zaferani, G. D. Palermo, A. Abbaspourrad, Strictures of a microchannel impose fierce competition to select for highly motile sperm, Sci. Adv. **5**, (2019).

Curvature, Flow, and Miniaturization: A Nematic Droplet's Journey on Water

Vinod Vanarse[1], Siddharth Thakur[1], and Dipankar Bandyopadhyay[1,2,3]

[1] *Department of Chemical Engineering, Indian Institute of Technology, Guwahati 781039, Assam, India,* vanarse@iitg.ac.in

[2] *Centre for Nanotechnology, Indian Institute of Technology, Guwahati 781039, Assam, India,* dipban@iitg.ac.in

[2] *Jyoti and Bhupat Mehta School of Health Science and Technology, Indian Institute of Technology, Guwahati 781039, Assam, India,*

Abstract

Self-organized contact line instabilities (CLI) in macroscopic liquid crystal (LC) droplets provide a novel route to generate a vast array of miniaturized LC droplets. For instance, when a larger volatile solvent droplet (e.g., hexane) is introduced near a smaller LC droplet resting on a soft, slippery non-solvent surface (e.g., water) as shown in FIG. 1, a unique twin vortex locomotion emerges within the droplets. This process is driven by the rapid counter-diffusion of hexane and LC, forming vortices and initiating CLI at the three-phase contact line (TPCL) of the LC droplet. Initially, the positive pressure gradient ($P_{\mathrm{L,5CB}} > P_{\mathrm{L,Hex}}$) drives the LC droplet toward hexane. However, as hexane evaporates and shrinks, the flow reverses due to the shifting pressure gradient ($P_{\mathrm{L,5CB}} < P_{\mathrm{L,Hex}}$). Hexane diffusion into the LC droplet triggers periodic oscillatory expansion and retraction at the TPCL, forming finger-like structures, which break into smaller LC droplets via Rayleigh-Plateau instability (RPI). The observed deviation in the satellite droplet spacing — $\lambda/R_{\mathrm{5CB}} \sim 3.15\sqrt{2}\pi$ compared to the theoretical value ($\sim 2\sqrt{2}\pi$) indicates that LC elasticity stabilizes these fingers. Control experiments reveal the significant roles of capillary, drag, solutal Marangoni, and osmotic forces in LC locomotion. Dimensional analysis reveals that finger spacing, ejected droplet diameter, and droplet spacing scale with the original LC droplet volume as $F_S \sim V_{\mathrm{5CB}}^{0.17}$, $S_{d,\mathrm{5CB}} \sim V_{\mathrm{5CB}}^{0.36}$, and $\lambda/R_{\mathrm{5CB}} \sim V_{\mathrm{5CB}}^{-0.5}$, with dependency on Reynolds and Strouhal numbers as $F_S \sim Re^4 St^{1.03}$ and $S_{d,\mathrm{5CB}} \sim Re^{2.26} St^{0.32}$.

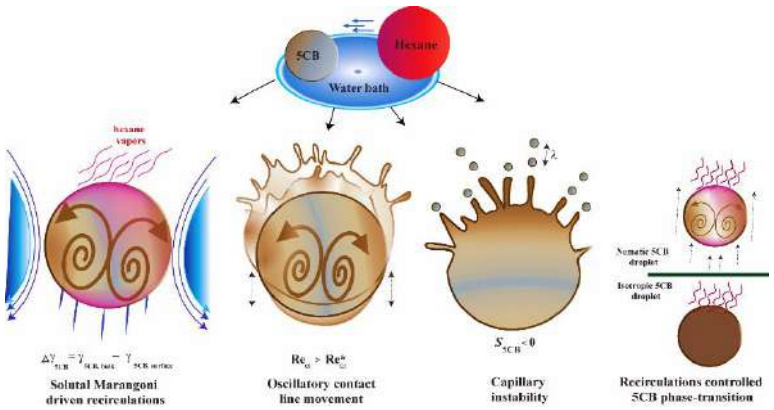

FIG. 1. Locomotion and morphological evolution of 5CB droplet on a water bath in the presence of hexane droplet.

Drop impact on a Superhydrophobic spot surrounded by superhydrophilic region

Aayanshu Kumar[1] and Ashis Kumar Sen[2]

[1] *Department of Mechanical Engg.,IIT Madras , Chennai* me23d009@smail.iitm.ac.in
[2] *Department of Mechanical Engg., IIT Madras, Chennai* ashis@smail.iitm.ac.in

I. Abstract

Droplet impact is a physical phenomenon that is visible in our everyday life be it the fall of raindrops on the ground, inkjet printing, or spray cooling. Droplet solid-surface interaction has been a topic of great interest in science and technology such as medicine, aerospace, and energy.

The dynamics of a liquid drop impacting a solid surface consists of initial spreading followed by recoiling. A water drop impacting a hydrophobic surface shows vigorous oscillation however the same drop spreads into a thin lens-like shape with almost no oscillations. During drop impact, the liquid spreads initially both on a hydrophobic surface as well as a hydrophilic surface until its Kinetic energy is converted into surface energy and Viscous dissipation. During the initial spreading of the liquid drop air is trapped inside the drop as the lubrication pressure inside the thin layer of air deforms the bottom surface of the drop into a dimple shape. Recently solid surfaces with wettability gradients have gained significant attention for droplet-based cell culture, cell encapsulation, anti-fogging, and water harvesting. Recently Satpathy[1] et al. studied the drop impact on a Superhydrophilic (SHL) spot surrounded by a Superhydrophobic(SHB) region. They identified 3 different regimes: no-splitting, jetting, and splashing for different Weber No., spot size, and drop sizes.

In this work, we show a convenient way to fabricate a Superhydrophobic (SHB) spot surrounded by a Superhydrophilic (SHL) region and its behavior during drop impact. We identify 3 different regimes namely Complete rebound of drop, migration of drop to SHL region, and complete spreading of water drop. We observe a complete rebound of drop at lower Weber No. , with the increase in Weber no. same drop migrates completely towards the super hydrophilic region, as Weber no. further increases drop completely spreads on the surface.

Figure 1

Complete rebound of drop

Figure 2

Migration to SHL side

Figure 3

Complete spreading

II. REFERENCES

[1] Niladri Shekhar Satpathy, Lokesh Malik, Alwar Samy Ramaswamy Ashis Kumar Sen* *Drop Impact on a superhydrophilic Spot Surrounded by a Superhydrophobic Surface,* Langmuir (2021*)*

Droplet behavior on superheated substrates – splashing to trampolining

Pranjal Agrawal[a], Susmita Dash[b]

[a]Interdisciplinary Center for Energy Research, Indian Institute of Science, Bangalore

[b]Department of Mechanical Engineering, Indian Institute of Science, Bangalore

Abstract

Two-phase interaction of droplets on heated substrates is ubiquitous and has applications in power plants, industrial cooling, and particle drying. At temperatures significantly higher than the saturation temperature of the liquid, the vigorous nucleate boiling is replaced by a rather quiescent film boiling in which the liquid contact with the solid is eliminated due to the formation of an intervening vapor layer over which the droplet levitates. This Leidenfrost (LF) phenomena, while detrimental to cooling, is useful in applications such as formation of supra-particles in pharmaceuticals and food processing industries and is marked by enhanced droplet mobility. Here, we report on the spontaneous bouncing, trampolining, and hovering behavior of an unconstrained LF water droplet. We observe that a droplet exhibits intermittent increase in bouncing height at specific radii and subsequent reduction in the height of bounce leading to a quiescent LF state. We propose that the trampolining behavior of the droplet at specific radii is triggered by harmonic excitation of the liquid-vapor interface. This mechanism of resonance-driven trampolining of LF droplets is applicable for different liquids irrespective of the initial volume and substrate temperatures, thus indicating a universality of the behavior. We also discuss the impact dynamics of droplets in different boiling regimes on heated substrates. We correlate the contact time and wetted area fraction during droplet impact on the heated substrate to the boiling regime and associated acoustic signal generated.

Droplet Impact on Curved Surface with relevance to eye drop administration on the human eye

Sruthi Kumar[1] and Kiran Raj. M[2]

[1] *Department of Applied Mechanics and Biomedical Engineering, Indian Institute of Technology, Madras, Tamil Nadu- 630006, India*
am23d312@smail.iitm.ac.in

[2] *Department of Applied Mechanics and Biomedical Engineering, Indian Institute of Technology, Madras, Tamil Nadu- 630006, India*
kiran@iitm.ac.in

Dry eye disease (DED) is characterized by symptoms such as photophobia, irritation, burning, ocular discomfort and disturbances. It occurs when there is an imbalance in the tear film, which leads to excessive tear evaporation or insufficient tear production. This imbalance can damage the epithelial cells of the eye and cause further tear film instability and inflammation. We aim to analyse the droplet impact on contact lenses by measuring the contact angle and spreading parameters, in order to understand the impact of eye drop administration on the human eye. We considered the critical fluid parameters such as the shear-thinning and temperature-dependent variations in the viscosity of various ocular lubricants currently available in the Indian market. We are also looking into the effects of the dimensions and design of the dropper tip and bottle and their effects on droplet size.

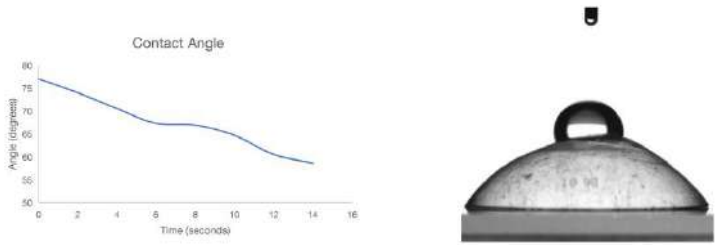

FIG. 1. Left: Change in contact angle of Genteal eye drops droplet on the lens over time; Right: Contact angle measurements of occular liquid on contact lens.

REFERENCES

[1] Alexandre Xavier et al., “Microbial Cross-contamination in Multidose Eyedrops: The Impact of Instillation Angle and Bottle Geometry.” Transl Vis Sci Technol. 2020 Jun; 9(7): 7.

C. Sykes et al., “Droplet splashing on curved substrates”. Journal of Colloid and Interface Science. 2022 Jun; 615:227-235.

Luc Van et al., “Determinants of eye drop size”. Survey of Optamology 2004 49:2 197-213.

Droplet Impact on Paper Cantilever

Aneesh V[1], Athira K P [2]and Kiran Raj M[1]

[1] *Dept. Applied mechanics and Biomedical Engineering IIT Madras Chennai, India*
[2] *School of Physics, Indian Institute of Science Education and Research, Thiruvananthapuram, Kerala, 695551, India*

Droplet impact dynamics on flexible surfaces play a pivotal role in technical applications. When a raindrop lands on the wings of a micro aerial vehicle or flying bug or a surface that harvests energy from raindrops, the droplet's wetting behaviour is quite significant [1]. It depends on many factors like surface morphology, interfacial tension, and the dynamics involved in the droplet impact [2]. To mimic such surfaces, a high-quality bond paper is taken as substrate in this experiment which is flexible, porous, and hydrophilic. It offers distinct characteristics on the droplet that influence droplet impact dynamics. The paper is fixed to a table at one end and used as a cantilever with fixed length and width. A high-speed imaging technique was utilized to capture impact from different heights (Figure 1(a)).

During the impact, the droplet undergoes deformation, imbibition, wicking, oscillation, and subsequent damped vibration due to the elasticity of the cantilever [3]. Droplet size, impact velocity, and wetting properties govern these responses. Here, we mainly look into the variation of the deflection and slope of the cantilever during the impact and divulge the limit of rigidity of the cantilever during impact as a result of the variation in the Weber number of the droplet. As the Weber number increases (We=185 to 383), the inertial forces dominate over surface tension forces, the cantilever deflected to the maximum and moves to its initial position similar to a rigid cantilever impact (Figure 1 (b)). However, at lower Weber numbers (We=185 to 85) the deflection and slope increases initially with time, but it become constant after a certain time, which is a consequence of the droplet adhering on the surface of the substrate. The pinning nature of the droplet is due to the hydrophilicity and the combined dynamics of the droplet and cantilever as well.

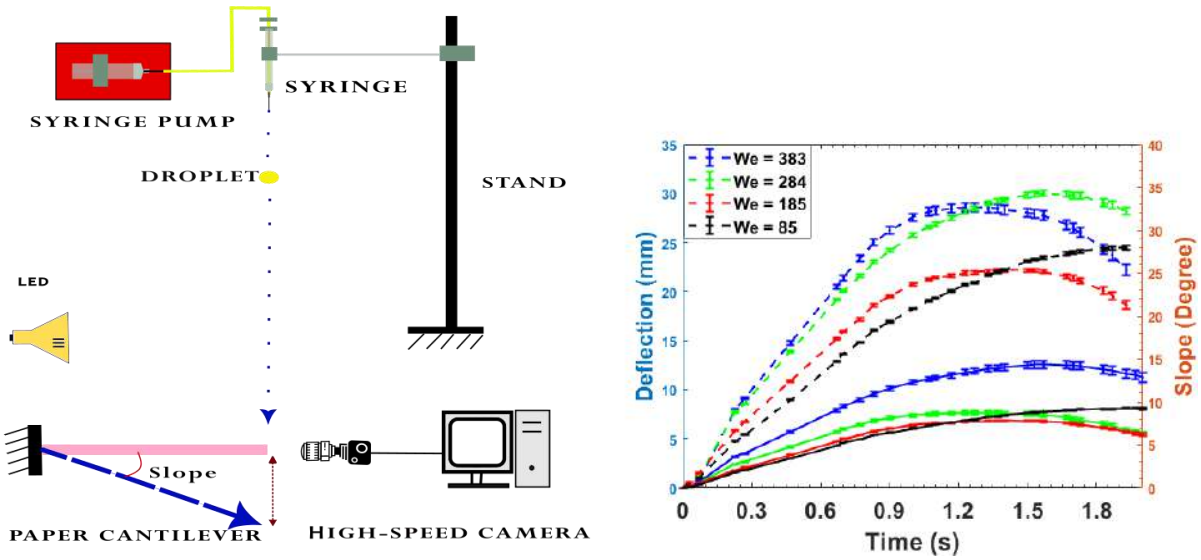

FIG. 1. (a) Schematic of the experiment set-up (b) Variation of the deflection of the cantilever with time for different Weber numbers.

[1] Fan, Yaxun, and Yilin Wang. "Deposition and spread of aqueous pesticide droplets on hydrophobic/superhydrophobic surfaces by fast aggregation of surfactants." Langmuir 39, no. 16 (2023): 5631-5640.

[2] Pepper, Rachel E., Laurent Courbin, and Howard A. Stone. "Splashing on elastic membranes: The importance of early-time dynamics." Physics of Fluids 20, no. 8 (2008).

[3] Law, Kock-Yee, Hong Zhao, Kock-Yee Law, and Hong Zhao. "Wetting on flat and smooth surfaces." Surface Wetting: Characterization, Contact Angle, and Fundamentals (2016): 35-54.

Dust in the wind

Anubhab Roy[1]

[1] *Department of Applied Mechanics and Biomedical Engineering, Indian Institute of Technology Madras, Chennai 600036, India.* anubhab@iitm.ac.in

Particles suspended in a flow can modify the stability characteristics and thus influence the transition from a laminar to a turbulent state. In dilute flows of inertial particles, the feedback force from the particles to the fluid induces an array of complex flow dynamics otherwise absent in particle-free cases. In this work, we investigate the role of the feedback force in two canonical problems in vortical flows - the stability of an isolated vortex and the merger of co-rotating vortices. In the first study, the two-way coupled Eulerian-Lagrangian simulations of a heavy core vortex laden with inertial particles reveal a remarkable disintegration of the vortex monopole. To probe further, we conduct a linear stability analysis of the continuum system, modelled using a two-fluid model. The small inertia approximation of the two-fluid model reveals that the first corrections of particle inertia manifest as variable density effects. Comparison with Eulerian-Lagrangian simulations shows that growth rates computed from simulations match well the theoretical predictions from linear stability analysis. Past the linear stage, we observe the emergence of high-wavenumber modes that turn into spiralling arms of concentrated particles emanating out of the core while regions of particle-free flow are sucked inward. In the second study, we investigate the effect of particle inertia on the merger of co-rotating dusty vortex pairs at semi-dilute concentrations. In single-phase flow, the merger is triggered once the ratio of vortex core size to vortex separation reaches a critical value. In dusty flows, we observe a substantial departure from the vortex dynamics previously established in particle-free flows. Most strikingly, dispersed particles with moderate inertia cause the vortex pair to push apart to a separation nearly twice as large as the initial separation. We identify that the antisymmetric vorticity generated by particles flung out of the rotational cores is responsible for the vortex pair repulsion.

Dynamics and rupture of liquid plugs in capillaries: cascades, memory effects and anti-Bretherton droplet formation

Michael Baudoin[1], C. Baroud[2], A. Duchesne[1], J.C. Magniez[1], P. Manneville[1], P. Favreau[1], S. Signe Mamba[1], Y. Song[2], F. Zoueshtiagh[1]

[1] *Univ. Lille, CNRS, Centrale Lille, Univ. Polytechnique Hauts-de-France, UMR 8520 - IEMN - Institut d'Électronique de Microélectronique et de Nanotechnologie, Lille F-59000, France,*
michael.baudoin@univ-lille.fr

[2] *Laboratoire d'Hydrodynamique (LadHyX) and Department of Mechanics, École Polytechnique, Centre National de la Recherche Scientifique*

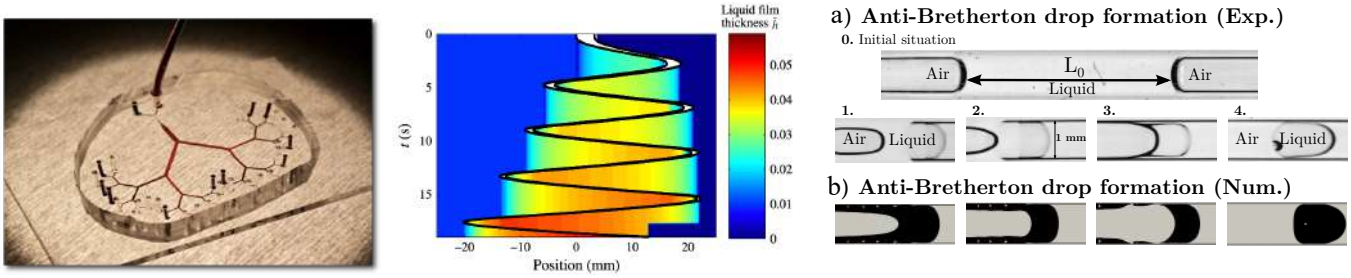

FIG. 1: Left: PDMS network used to study the dynamics of liquid plugs in complex networks [1]. Center: Graph illustrating memory effects induced by liquid film deposition during liquid plug cycles [2]. Right: Anti-Bretherton drop formation [3].

Liquid plugs play a pivotal role in diverse fields, ranging from chemical engineering processes to medicine, where they can form naturally in the lungs due to the instability of the mucus lining in patients suffering from pulmonary obstructive diseases. In this presentation we will delve into three distinct facets of liquid plug dynamics. First, we will explore the collective dynamics of a train of liquid plugs within both simple linings and complex microfluidic structures [1]. Our investigation reveals that a trains of liquid plugs, driven by a pressure delta, undergo an accelerating dynamic, culminating in a cascade of plug ruptures. This acceleration is intricately influenced by local interactions between plugs through the wetting films and global interactions involving the total resistance to the flow of the entire plug train. Second, we will present some findings on the response of a single plug subjected to a cyclic forcing [2]. Our experimental and theoretical study demonstrates that these cyclic dynamics exhibit memory effects stored in the length of the plug and the thickness of the trailing film. Last, we will describe how the rupture of an extended liquid plug in a channel can give rise to the formation of a lengthy levitating droplet, isolated from the tube by a thin air film—a negative configuration compared to Bretherton's long bubbles [3]. Our analysis indicates that the shape of the droplet and the lubricating air film can be recovered from an adapted Bretherton's analytical theory.

[1] M. Baudoin, Y. Song, P. Manneville, C.N. Baroud, Airways reopening through catastrophic events in a hierarchical network, **Proc. Nat. Ac. Sci.,** 110: 859-864 (2013)

[2] S. Signé Mamba, J.C. Magniez, F. Zoueshtiagh, M. Baudoin, Dynamics of a liquid plug in a capillary tube under cyclic forcing: memory effects and airway reopening, **J. Fluid. Mech.:** 838: 165-191 (2018)

[3] P. Favreau, A. Duchesne, F. Zoueshtiagh, M. Baudoin, The motion of long levitating drops in tubes in an anti-Bretherton configuration, **Phys. Rev. Lett**., 125: 194501 (2020)

Dynamics of mucus films in ciliated lung airways

Swarnaditya Hazra[1] and Jason R. Picardo[1]

[1]*Chemical Engineering Dept., IIT Bombay, Mumbai, 400076, India*

The healthy functioning of mucus-bearing airways (inset of Fig. 1a) is potentially compromised by the capillary-driven Rayleigh-Plateau instability that prevents the annular mucus film from staying uniform and instead causes it to form bulging lobes. If the lobes grow too large, then they can form a liquid bridge that blocks the flow of air. Several studies have analysed airway blockage [1] and shown how liquid-bridge formation is affected by airflow [2], viscoelasticity and surfactants [3]. Here we investigate how blockage is altered by the presence of cilia. In particular, we consider a finite airway (as opposed to an infinite periodic domain) with a constant input of mucus and an outlet boundary condition that allows cilia to evacuate the mucus. Can a dynamically-stable film be maintained? And if so, how is this stability affected by the cilia beat-rate, the mucus volume fraction, and other system properties?

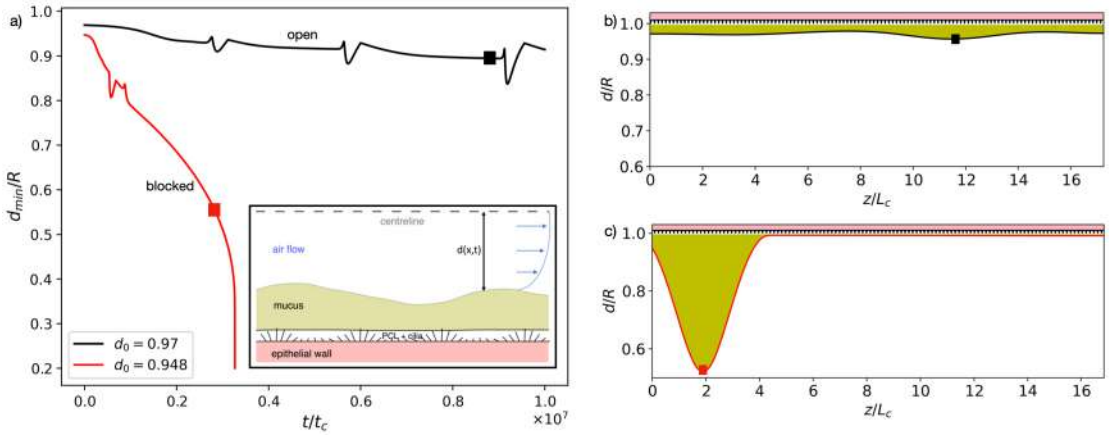

FIG. 1: (a) The inset shows a schematic of the ciliated airway with its mucus film, and the main panel traces the evolution of the minimum distance of the mucus from the centreline, $d_{\min}$, which approaches zero in a blockage scenario. Here, the mucus input rates is set so as to produce a base state with a uniform $d = d_0$. The red line corresponds to a slightly larger flow rate than the black line; snapshots of the respective interface profiles are shown in panels (b) and (c).

To answer these questions, we use the second-order WRIBL (Weighted-Residual Integral Boundary Layer) thin-film model for the coupled flow of mucus and air [2] and incorporate the effect of cilia via a coarse-grained boundary condition [4, 5] at the bottom of the mucus layer. This open-domain system admits a steady flat-film base state in which the constant input of mucus is balanced by cilia-induced transport and evacuation. Infinitesimal perturbations destabilize this state, however, and produce growing and translating lobes. Our results show that if the input (or secretion) rate of mucus is low, then the cilia is able to evacuate the lobes and keep the airway open (see Fig. 1a, black line). There is a critical input rate, however, beyond which this is no longer possible—strong capillary forces cause all incoming mucus to stay trapped in an ever growing lobe, near the inlet, that ultimately blocks the airway (see Fig. 1a, red line). Importantly, the critical volume fraction for blockage is less than that predicted by equilibrium calculations for a closed domain without cilia [6]; we calculate this critical volume and examine its dependence on the properties of the cilia and mucus.

---

[1] Levy R., Hill D.B., Forest M.G., Grotberg J.B., *Integr. Comp. Biol.* **54**:985–1000, 2014.

[2] Dietze G.F., Quil C.R., *J. Fluid Mech*, **762**:68–109, 2015.
[3] Halpern D., Hideki F., Grotberg J.B., *Phys. Fluids*, **22.1** :011901, 2010.
[4] Vasquez P. A., Jin Y., Palmer E., Hill D., Forest M.G., *PLoS Comput. Bio*, **12.8**:e1004872, 2016.
[5] Choudhury A., Filoche M., Ribe N.M., Grenier N., Dietze G. F. *J. Fluid Mech.*, **971**:A33, 2023.
[6] Everett D.H., Haynes J.M., *J. Colloid Interface Sci.* **38.1**:125–137, 1972.

Dynamics of self-propelling swimmers in complex micro-confinements

Smita S. Sontakke[1], Subhasish Guchhait[1], Aneesha Kajampady[1], and Ranabir Dey[1]

[1] *Department of Mechanical and Aerospace Engineering, Indian Institute of Technology Hyderabad, Kandi, Sangareddy, Telengana- 502285, India,* ranabir@mae.iith.ac.in

Biological microswimmers have developed various locomotion strategies to adapt to different changes in their micro-environment. For example, bacteria like *E. coli* and *Vibrio alginolyticus* exhibit run-and-tumble[1] and switch-and-flick[2] motility in response to the changing physico-chemical cues from their immediate surrounding; bacteria and sperm cells also exhibit unique swimming trajectories ranging from linear and helical to oscillatory to adapt to external flows in confinements[3,4]; and euglena swims through increasingly tighter confinements by deforming its cell shape[5]. Here, we investigate how self-propelling artificial microswimmers adapt their swimming dynamics in complex micro-confinements, by considering active droplets as a model system. These active droplets are oil droplets that are slowly dissolving in supramicellar aqueous solutions of ionic surfactants. The droplets spontaneously develop self-sustaining gradients in interfacial surfactant coverage, resulting in Marangoni stresses which lead to self-propulsion[6,7].

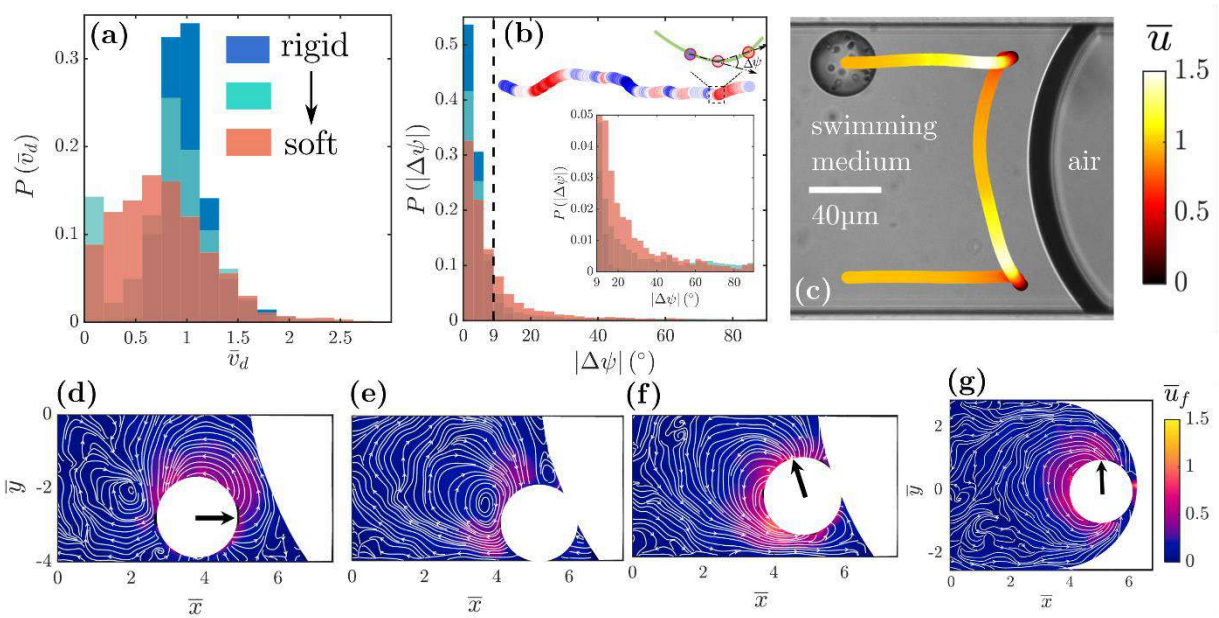

FIG. 1. Probability distributions for **(a)** instantaneous swimming velocity magnitude and **(b)** local reorientation in the swimming direction for active droplets swimming in microchannels of increasing softness. **(c)** Trajectory of an active droplet, colour-coded with the instantaneous swimming speed, as it swims along a convex liquid-air meniscus in a microchannel. **(d)-(f)** Alterations in the hydrodynamic signature of the active droplet as it reaches and swims out of the corner created where the liquid-air meniscus meets the microchannel wall. **(g)** Hydrodynamic signature of the active droplet as it swims along a concave liquid-air meniscus.

[1] H. C. Berg and D. A. Brown, Chemotaxis in Escherichia coli analysed by three-dimensional tracking, Nature **239**, 500 (1972).

[2] L. Xie, T. Altindal, S. Chattopadhyay and X-L Wu, Bacterial flagellum as a propeller and as a rudder for efficient chemotaxis, PNAS **108,** 2246 (2011).

[3] V. Kantsler, J. Dunkel, M. Blayney and R. E. Goldstein, Rheotaxis facilitates upstream navigation of mammalian sperm cells, eLife **3**, e02403 (2014).

[4] A. J. Mathijssen, N. Figueroa-Morales, G. Junot, E. Clément, A. Lindner and A. Zöttl, Oscillatory surface rheotaxis of swimming E. coli bacteria, Nature Communications **10(1)**, (2019).

[5] G. Noselli, A. Beran, M. Arroyo and A. DeSimone, Swimming Euglena respond to confinement with a behavioural change enabling effective crawling, Nature Physics **15**, 496 (2019).

[6] K. Pedireddy, P. Kumar, S. Thutupalli, S. Herminghaus and C. Bahr, Solubilization of thermotropic liquid crystal compounds in aqueous surfactant solutions, Langmuir **28,** 12426 (2012).

[7] S. Michelin, Self-propulsion of chemically active droplets, Ann. Rev. Fluid Mech. **55**, 77 (2023).

First, we experimentally investigate the effects of reducing stiffness (increasing softness) of the walls of a micro-confinement on the swimming dynamics of self-propelled artificial microswimmers, considering active droplets in microchannels of varying softness. We use a combination of double-channel fluorescence microscopy and micro-PIV analyses to reveal and characterize the alterations in microswimmer dynamics in the soft microchannels. In a microchannel with stiff walls, active droplets exhibit approximately unidirectional swimming along a wall with a steady velocity. However, in a soft microchannel of identical geometry, the droplet microswimmers exhibit unsteady swimming velocity with intermittent deceleration, stopping, and subsequent acceleration (Fig. 1a). These intermittent stopping events are followed by sharp reorientation in the subsequent swimming direction (Fig. 1b). Interestingly, the microswimmer exhibits autonomous changes in its hydrodynamic signature over such stopping events in the soft microchannel. Second, we experimentally investigate the dynamics of these self-propelled active droplets near confined liquid-air and liquid-liquid menisci in microchannels. We highlight the alterations in the swimming velocity (Fig. 1c), orientation, and hydrodynamic signature (Figs. 1d-g) as the microswimmer traverses the curved, confined meniscus. Specifically, we delineate the effects of the corners in the immediate vicinity of the three-phase contact lines, formed where the meniscus meets the microchannel walls, on the microswimmer dynamics.

Understanding these alterations in swimming dynamics for artificial microswimmers (model systems) in complex micro-environment serves two main purposes- one, it provides better insight into the underlying adaptation mechanisms which to a certain extent are applicable even for biological microswimmers (specifically, pusher-types); two, it helps in devising accurate methodologies for possible use of active droplets as state-of-the-art autonomous microrobots in many biotechnology/biomedical applications.

Effect of particles on Rayleigh-Benard convection

Thota Srinivas and Gaurav Tomar
Department of Mechanical Engineering, Indian Institute of Science Bangalore

We investigate the settling of small and heavy particles suspended in a Rayleigh-Benard convection in a 2D shallow cavity at a Rayleigh number Ra = 10^5 and Prandtl number Pr = 0.701 using Eulerian-Lagrangian simulations. We consider momentum coupling between the particles and the underlying flow, while thermal energy coupling is neglected. In this momentum two-way coupling formulation, the particle volume fraction is varied systematically and studied for its effect on the settling dynamics of the particles by keeping the particle Stokes number (St_p = 10^{-3}) and particle-to-fluid density ratio (ρ_p/ρ_f = 1000) constant. It is observed that the rate and the fraction of particles settled are higher when the initial particle volume fraction is of the order of $\varphi^*_v = (\rho_f/\rho_p)F r^2$ (ρ_f and ρ_p are densities of fluid and particle, respectively, and Fr is the Froude number) due to a strong coupling between the particles and flow at this concentration. We study the time history of fraction of particle ($\Delta N_p/N_p$) for various initial particle concentrations. By the time $t/\tau_r \sim 1$ (t is time and τ_r is residence time of the particle) almost all particles are settled down when the initial particle concentration $\varphi_v \in (0.8\varphi^*_v, \varphi^*_v)$ and around 85% of particles settle when $\varphi_v \in (0.3\varphi^*_v, 0.4\varphi^*_v)$. Finally, only around 35% of particles settle when the particle concentration is small $\varphi_v \in (0.1\varphi^*_v, 0.05\varphi^*_v)$ due to weak coupling between the two phases. At this small volume fractions particles effect on the flow is negligible and behaves like one-way coupled and most of the particles trapped inside the closed streamlines and very few particles starts leaking and leads to a small positive slope the curves corresponding to $0.05\varphi^*_v$ and $0.1\varphi^*_v$ for concentrations.

Electrohydrodynamic stability of a two-layer Poiseuille flow in the presence of interfacial surfactant: an asymptotic analysis

Sarita Yadav and Geetanjali Chattopadhyay
Department of Mathematics, Malaviya National Institute of Technology Jaipur, 302017, Rajasthan, India

The electrohydrodynamic stability of a two-layer Poiseuille flow has been considered under the influence of an electric field acting normally to the interface of the two viscous immiscible fluids. The two fluids considered here for the asymptotic stability analysis are leaky dielectrics. The study on the influence of a monolayer of insoluble surfactant at the fluid-fluid interface reveals that the interfacial surfactant further enhances or suppresses the electric field-induced instability. The long-wave linear stability analysis is carried out in the framework of Orr-Sommerfeld analysis for leaky dielectrics. In the context of long-wave linear stability study, the phase speed is expressed as a function of the ratio of viscosities (m), layer thicknesses (d), densities (r), permittivities (ε) and conductivities (l) of the two fluids. The electric field is observed to have either a destabilizing or a stabilizing effect, primarily non-monotonic, depending upon the ratios of permittivities and conductivities of the two fluids. It is found that when $m > d^2$, the region of instability in the ε − l plane increases with increasing Marangoni number (Ma); however, when $m < d^2$, the scenario reverses. The electrohydrodynamic interface instability among two viscous fluids with varying electrical properties in plane Poiseuille flow has applications in microfluidic devices for mixing and droplet formation. Therefore, the present study aims to propose a control mechanism for the instability occurring at the interface through the modified interface tension.

Eukaryotic chemotaxis in the travelling wave of chemoattractant

Richa Karmakar[1], Alex Groisman[2], Wouter-Jan Rappel[2]
[1]*Department of Biotechnology, Indian Institute of Technology Madras, India*
[2]*Department of Physics, University of California, San Diego, USA*

Eukaryotic chemotaxis plays a significant role in many biological processes like tumour dissemination, immune system, wound healing and many more. Cells respond in natural chemical gradients by temporal sensing or spatial sensing. The rate-limiting step of the process governs the maximum speed of cell migration. While individual steps in chemotaxis have been studied, few investigations have explored the overall limits of chemotaxis as a complete process. Using microfluidic devices to generate chemoattractant waves with precisely controlled size and speed, we measured the migration speeds of *Dictyostelium* cells in response to these conditions. In this talk, we will focus on the collective migration of *Dictyostelium discoideum*, a social amoeba that aggregates into large clusters as a survival strategy during starvation. This process requires precise coordination of signalling and movement. We will highlight two examples where experiments and modelling provide insights into this coordination. First, we will demonstrate that small *Dictyostelium* aggregates can exhibit dispersal behaviour, where cells move away from the cluster instead of toward it. Through experiments and modelling, we show that this dispersal arises from the interaction between the diffusible chemoattractant and the enzyme responsible for its degradation.

(1)

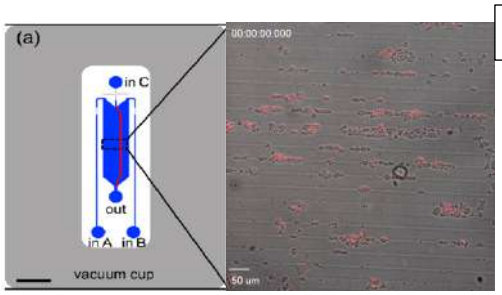

2

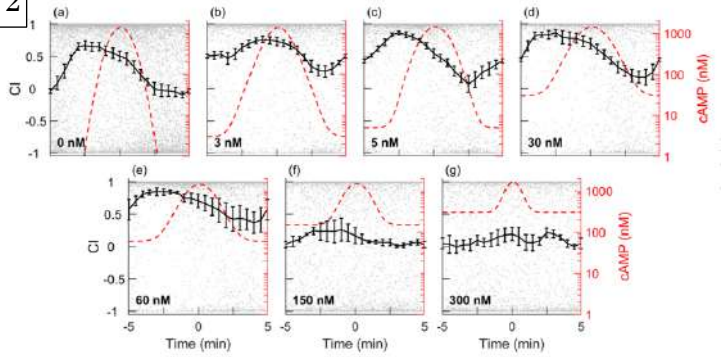

Fig1: (a) The microfluidic setup and (b) cells on the substrate and the travelling wave generated in the chip. Fig2: the chemotactic index of the cell over the travelling wave of chemoattractant (cAMP) with the background concentration of cAMP.

---

1. Karmakar R, Karanam A, Tang M, Rappel W J. (2024) *Eukaryotic chemotaxis under periodic stimulation shows temporal gradient dependence.* Physical Review Letter. 133: 068401.
2. Karmakar R, Tyree T, Gomer R H, Rappel W J. (2021). *Cell dispersal by localized degradation of a chemoattractant.* Proceedings of the National Academy of Sciences of the United States of America. 118(6): e2008126118.
3. Karmakar R, Tang M, Yue H, Lombardo D, Karanam A, Camley B A, Groisman A, Rappel W J. (2021) *Cellular memory in eukaryotic chemotaxis depends on the background chemoattractant concentration.* Physical Review E. 103, 012402.

Evidence of an inertialess Kapitza instability due to viscosity stratification

Shravya Gundavarapu[1], Darish Jeswin Dhas[2] and Anubhab Roy[1]

[1] *Department of Applied Mechanics and Biomedical Engineering, Indian Institute of Technology, Madras, Chennai, India, 600036.*

[2] *Department of Engineering and Architecture, University of Udine, Italy, 33100.*

We investigate the linear stability of a flow down an inclined plane in the inertialess limit, focusing on exploring different models of viscosity-particle concentration relationships. Here, we use a long-wave asymptotic analysis and a Chebyshev collocation based spectral method to investigate the stability of the film under various scenarios. By considering different models of viscosity-particle concentrations, we gain critical insights into how variations in these relations impact the stability of the film. Our findings indicate that viscosity stratification, occurring due to shear-induced migration in dense suspensions, can lead to instability in the Stokesian regime[1], which otherwise is impossible in the particle-free scenario[23]

1. Dhas, D. J., & Roy, A, et al. Journal of Fluid Mechanics, 938, A29, 2022.

2. Yih, C. S. Physics of Fluids, 6(3), 321-334, 1963

3. Benjamin Journal of Fluid Mechanics, 2(6), 554-573 1957.

Evolution of interfacial instability due to bulk acoustic wave in a microchannel

Debasish Ghosh[1], Sazid Z Hoque[1], Niladri Sekhar Satpathi[1], Lokesh Malik[1] and Ashis Kumar Sen[1]

[1] *Micro Nano Bio –Fluidics Group, Department of Mechanical Engineering, Indian Institute of Technology Madras, Chennai-600036, India*

The manipulation of micro-objects using ultrasonic waves in microfluidics has recently garnered significant attention for its diverse applications. Research has extensively explored the dynamics of inhomogeneous miscible liquids and their manipulation through bulk acoustic waves (BAW), focusing on the acoustic force density arising from differences in density and sound speed at interfaces [1]. However, the interaction of sound waves with coflowing immiscible liquids in microchannels remains less studied. When acoustic waves interact with a fluid-fluid interface, the discontinuity in fluid properties—such as density and sound speed—causes scattering that generates time-averaged, second-order acoustic radiation forces. These forces can deform the interface between the fluids. Our group has previously shown that a higher impedance fluid (HIF) moves to the center of the microchannel under the influence of BAW. This phenomenon is explained by the acoustocapillary number (Ca_{ac}), which represents the ratio of acoustic radiation force to interfacial tension force [2]. While it is established that HIF relocation to the channel center occurs when $Ca_{ac} \geq 1$, the effects of parallel-flowing streams and droplet generation in this context have not been thoroughly investigated. In this study, we address this gap by exploring different intermediate regimes by varying flow rates and acoustic power.

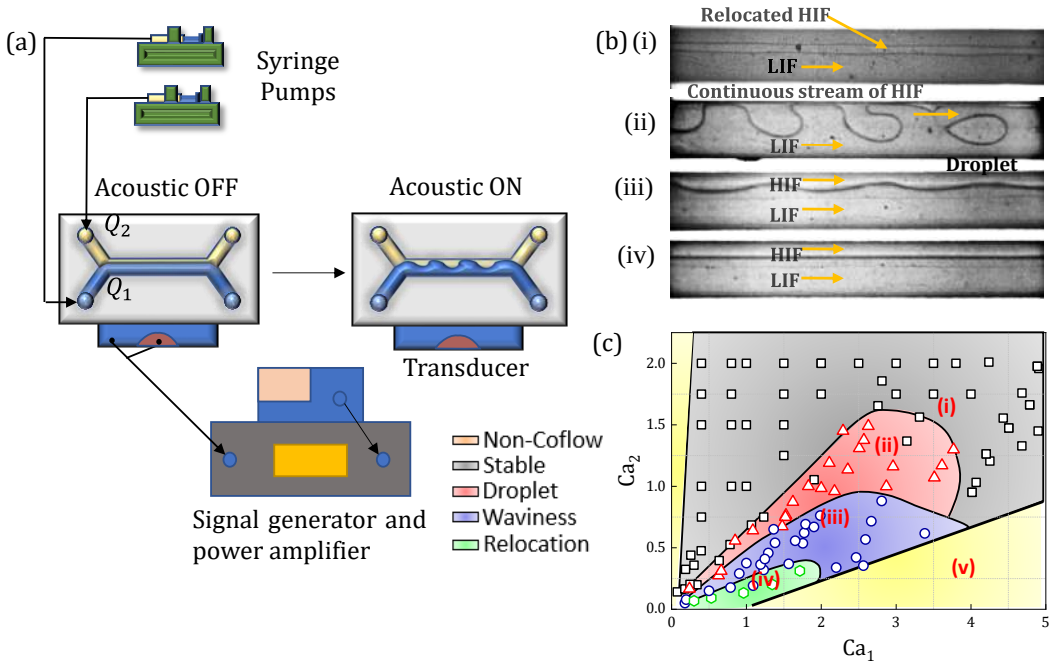

FIG. 1. (a) Shows the schematic of the experimental set-up. (b) The snapshots of experimental results of different regimes, where (b)-(i) $Q_{LIF} = 15\ \mu L/m$, $Q_{HIF} = 1\ \mu L/m$ (Relocation configuration), (b)-(ii) $Q_{LIF} = 15\ \mu L/m$, $Q_{HIF} = 7\ \mu L/m$ (Droplet configuration),(b)-(iii)$Q_{LIF} = 15\ \mu L/m$, $Q_{HIF} = 12\ \mu L/m$ (Waviness configuration) and (b)-(iv) $Q_{LIF} = 15\ \mu L/m$, $Q_{HIF} = 15\ \mu L/m$ (Stable configuration), (c) The different regimes obtained by varying the capillary number at constant power.

[1] J. T. Karlsen, P. Augustsson, and H. Bruus, *Acoustic Force Density Acting on Inhomogeneous Fluids in Acoustic Fields*, Phys. Rev. Lett. **117**, 1 (2016)..

[2] S. Hawking, *A brief history of time: from Big Bang to black holes*, Transworld Publishers, London (2011).

Extremely high clustering among droplets in turbulence at the dissipative scales

K. Shri Vignesh[1], Ambedkar Sanket[1], K. N. Arya[1] and R. I. Sujith[1*]

[1] *Department of Aerospace Engineering, Indian Institute of Technology Madras, Chennai - 600 036, India,*
**sujith@iitm.ac.in*

Due to their inertia, droplets tend to form clusters in turbulent flow [1]. This phenomenon can enhance the collision rate among droplets and is believed to play a crucial role during the onset of rain in warm clouds [2]. In this context, the inertia of the droplets is characterized using the Stokes number (*St*), defined as the ratio between the time taken by the droplet to respond to changes in flow and the characteristic time scale experienced by the droplet.

In this study, we experimentally create cloud-like conditions in a laboratory setting and investigate droplet clustering when interacting with homogeneous isotropic turbulence. We obtain the spatial distribution of droplets from high-speed planar Mie-scattering images and characterize clustering using the radial distribution function (*g(r)*). When droplets are randomly distributed throughout space, *g(r)* equals 1; conversely, when droplets exhibit clustering, *g(r)* exceeds 1. Figure 1 shows the *g(r)* variation at different scales normalized with Kolmogorov's scale for droplets with differing Stokes numbers. It is evident that the clustering strongly depends upon the St. Intriguingly, for $St \sim O(1)$, we observe two distinct regimes of clustering, a distinctly very high clustering in the dissipative scales ($r/\eta \sim 1$) and a weak clustering in inertial scales ($r/\eta \sim 10$). This extremely high clustering at the dissipative scales could be a consequence of hydrodynamic interactions between droplets.

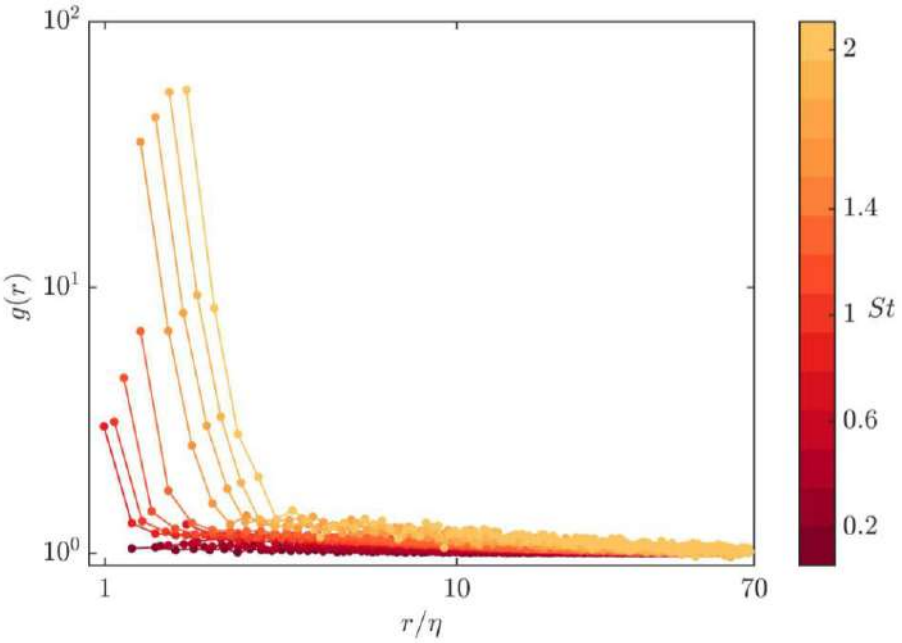

FIG. 1. Variation of Radial Distribution Function (*g(r)*) with r/η for droplets with different Stokes numbers (*St*). The hue of the color marks the variation in St. For $St \sim O(1)$, we observe extremely high clustering at the dissipative scales

REFERENCES

[1] Saw, E.W., Shaw, R.A., Ayyalasomayajula, S., Chuang, P.Y. and Gylfason, A., 2008. *Inertial clustering of particles in high-Reynolds-number turbulence*. Physical review letters, 100(21), p.214501.

[2] Devenish, B.J., Bartello, P., Brenguier, J.L., Collins, L.R., Grabowski, W.W., IJzermans, R.H.A., Malinowski, S.P., Reeks, M.W., Vassilicos, J.C., Wang, L.P. and Warhaft, Z., 2012. *Droplet growth in warm turbulent clouds.* Quarterly Journal of the Royal Meteorological Society, 138(667), pp.1401-1429.

Falling films on a slippery wall

Christian Ruyer-Quil[1] and Khawla Msheik[1]

[1] *Université Savoie Mont-Blanc, LOCIE UMR CNRS 5271, 73000, Chambéry, France* christian.ruyer-quil@univ-smb.fr

[2] *Université Savoie Mont-Blanc, LOCIE UMR CNRS 5271, 73000, Chambéry, France* khawlamk3@gmail.com

Natural and engineered surfaces are never smooth, but irregular at different scales. They generally are porous or superhydrophobic. For all these cases, the momentum transfer at these surfaces can be modeled by a Navier slip boundary condition with a slip length whose magnitude is of the order of the surface roughness or large [1]. In this paper, we propose to revisit the problem of a falling liquid film over a slippery surface.

Modeling attempts on this problem either assume a small slip length l with respect to the film thickness or lack mathematical structure as the model coefficients are functions of the local ratio of the slip length to film height l/h which is a function of time and space[2]. As a consequence, the inclusion of inertia is limited to first-order consistency with respect to the film parameter $\varepsilon=hN/\lambda$, where hN and λ refer to the Nusselt film thickness and typical wavelength respectively. We will present a novel formulation which overcomes those difficulties. Our model is second-order accurate and present a clearer mathematical structure. In particular, coefficients are independent on l/h and the classical Saint-Venant averaged momentum balance is included in the model. This guarantees that the inviscid classical shallow-water equations are recovered in the limit $l \gg 1$. Besides, surface tension terms appear only in the averaged momentum equation, which enables to propose an augmented formulation of our model and therefore to account for complete surface tension forces, i.e. without the linear approximation of the curvature that is generally employed in thin-film studies [3]. The second-order four-equation model proposed by Ruyer-Quil and Manneville[4] is recovered in the appropriate limit. In particular, our new formulation being much simpler, is easily implemented numerically.

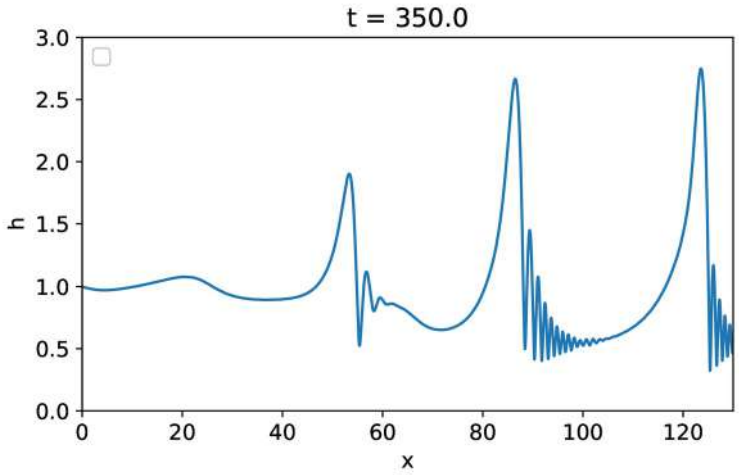

FIG. 1. Simulation of a water film on a vertical wall (Re = 69, Ka=3650, l/hN =0.01)

[1] A. Bottaro, Flow over natural or engineered surfaces: an adjoint homogenization perspective, J. Fluid Mech. (2019), **877**, P1

[2] A. Samanta, C. Ruyer-Quil and B. Goyeau, A falling film down a slippery plane, J. Fluid Mech. (2019), **684**, 353-383

[3] D. Bresch, N. Cellier, F. Couderc, M. Gisclon, P. Noble, G.-L. Richard, C. Ruyer-Quil, J.-P. Vila, Augmented skew-symmetric system for shallow-water system with surface tension allowing large gradient of density, J. Comp. Phys. **419** (2020) 109670

[4] C. Ruyer-Quil and P. Manneville, Improved modeling of flows down inclined planes, Eur. Phys. J. B **15**, 357–369 (2000)

Finite amplitude standing water-waves.

Nikhil Yewale[1] and Ratul Dasgupta[1]
[1] *Department of Chemical Engineering, IIT Bombay, Powai, Mumbai 400 076 (Maharashtra)*
dasgupta.ratul@iitb.ac.in

I. INTRODUCTION

The physics of standing water waves is a fundamental problem in hydrodynamics for more than two centuries. The mathematical description of nonlinear finite-amplitude standing waves have a presence of the time-dependent terms that cannot be omitted by any suitable frame of reference unlike progressive waves. The first such calculation of standing waves in deep water limit was carried out up-to third order accuracy by *Lord Rayleigh*[1]. *Penney and Price*[2] further improved the perturbative solution up-to fifth-order using successive expansion method. For standing waves in uniform finite-depth, *Tadjbakhsh and Keller*[3] estimated a third order approximation.
We present mathematical description of *Tsai and Jeng*[4] for plane standing waves of finite-amplitude and finite-depth up-to arbitrary order of accuracy.

II. BRIEF METHODOLOGY

By assuming appropriate scales as mentioned in section 2 of *Tsai and Jeng*[4] ,the dimensionless potential flow equations governing water-waves (of amplitude *H* , in a rectangular vessel of depth *d)* with the relevant boundary conditions are mentioned below:

$$\nabla^2\phi = 0 \tag{1}$$

Along with, (2a) Kinematic boundary condition and (2b)stress-free surface boundary condition at the free surface, (3) bottom and wall boundary conditions, and (4) mass conservation.

$$\omega\eta_t + \phi_x\eta_x = \phi_z, \text{at} \quad z = \eta \tag{2a}$$

$$\eta + \omega\phi_t + \frac{1}{2}(\phi_x^2 + \phi_z^2) = Q, \text{at} \quad z = \eta \tag{2b}$$

$$\phi_z = 0 \quad \text{at} \quad z = -d \qquad \phi_x = 0 \quad \text{at} \quad x = 0 \tag{3}$$

$$\int_0^{\pi}\int_0^{\pi} \eta(x,t)dxdt = 0 \tag{4}$$

One may eliminate η by combining equations (2a) and (2b) to derive a modified dynamic boundary condition at the free surface $z = \eta$.
Now, by assuming the form of velocity potential for any general depth *d*

$$\phi = \sum_{n=1}^{\infty}\sum_{n=0}^{\infty} B_{mn}\frac{\cosh m(z+d)}{\cosh md}\cos mx \sin nt \tag{5}$$

One may now setup a numerical method as described in section (3) *Tsai and Jeng*[4] to find velocity potential ϕ and free surface η.

We summarize some preliminary results for a standing wave of fixed depth(*d/L*) with increasing wave-

amplitude(H/L) as given below.(L is the wavelength of standing waves). These are time-periodic solutions to the equations (1-4).

III RESULTS

Fig. 1 shows free-surface profile at various wave-amplitudes at $t=0$, when the velocity potential $\phi = 0$.

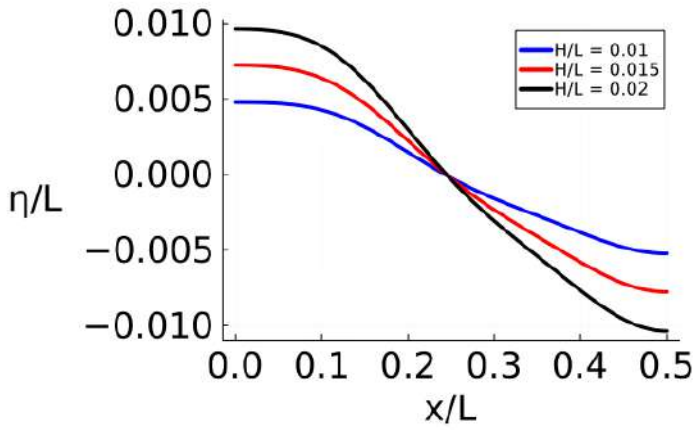

Figure 1 : Free surface profile at various wave-amplitudes H/L for $d/L = 0.5$.

IV PLANNED STUDIES FOR THE PRESENTATION

We plan to show the accurate calculation of time-periodic standing wave solutions at various wave amplitudes and depth of the container. Benchmarking numerical solution with CFD solver that proves the time-periodic behaviour of waves shall prove the accuracy of the numerical implementation. Also its comparison with existing solutions [2,3] will shed more light on the free-surface profiles as well as the higher-order dispersion relation.

V REFERENCES

[1] L. Rayleigh . *Deep water waves, progressive or stationary, to the third order of approximation*. Proceedinggs of Royal Society A, Mathematical , Physical and Engineering Sciences(1915)

[2] W.G.Penney and A.T.Price, *Finite periodic stationary gravity waves in a perfect liquid*, Proceedinggs of Royal Society A, Mathematical , Physical and Engineering Sciences:244- 254-284(1952)

[3] Tadjbakhsh I, Keller JB. Standing surface waves of finite amplitude. *Journal of Fluid Mechanics*. 1960;8(3):442-451

[4] Ching-Piao Tsai and Dong-Sheng Jeng, Numerical Fourier solutions of standing waves in finite water depth, *Applied Ocean Research* 16 (1994) 185-193

Fluttering without wind: Stokesian quasiperiodic settling

Harshit Joshi[1] and Rama Govindarajan[2]

[1] *International Centre for Theoretical Sciences, Bengaluru* harshit.joshi@icts.res.in
[2] *International Centre for Theoretical Sciences, Bengaluru* rama@icts.res.in

Fluid inertia imparts rich dynamics to leaves falling from trees. We show that bodies with two planes of symmetry can display a range of behaviors even without inertia. Any such body supports a conserved quantity in its dynamics, and is either a settler, a drifter or a flutterer, depending only on its shape. At large time, settlers and drifters respectively fall vertically and obliquely, while flutterers rotate forever while executing intricate patterns. These three types of behaviors are shown in figure 1. The dynamics of flutterers decouples into a periodic and a Floquet part with different time scales, giving periodicity or quasi-periodicity. We design a set of bodies and use the boundary integral method to show that settlers, drifters and flutterers, all lie in this set. This work is currently under review [1].

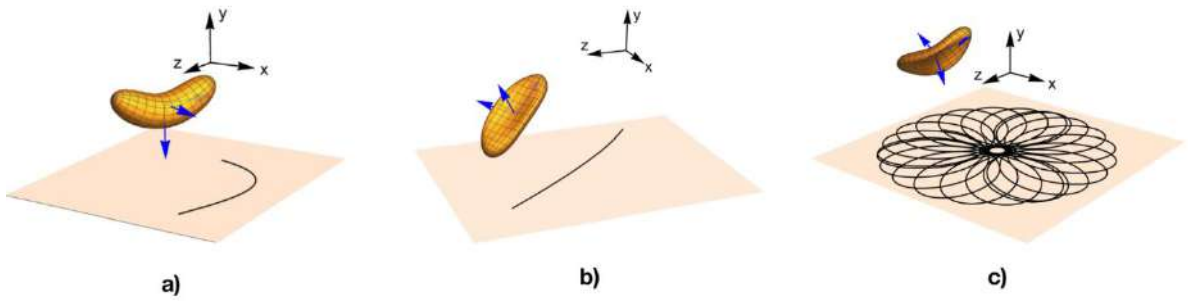

FIG. 1. Gravity is along negative 'y'. a) Settlers and b) Drifters eventually fall along their stable orientations. The black lines in the horizontal planes show their translational trajectories. This black line extends till infinity for drifters. c) Flutterers can display quasi-periodic motion and form intricate patterns in the horizontal plane.

[1] Harshit Joshi and Rama Govindarajan, Fluttering without wind: Stokesian quasiperiodic settling, arXiv:2403.10643 (2024).

Focusing of concentric free-surface waves

Lohit Kayal[1], Vatsal Sanjay[2], Nikhil Yewale[1], Anil Kumar[1] and Ratul Dasgupta[1]

[1] *Department of Chemical Engineering, IIT Bombay, Mumbai, India* kayal.lohit@gmail.com

[2] *2Physics of Fluids Group, Max Planck Center for Complex Fluid Dynamics, Department of Science and Technology, and J. M. Burgers Centre for Fluid Dynamics, University of Twente, Enschede, The Netherlands*
vatsalsanjay@gmail.com

Gravito-capillary waves at free-surfaces are common in several natural and industrial processes involving quiescent liquid pools [1[1], 2[2]]. These waves generate from the relaxation of initial interface perturbation, which often take the form of a cavity (depression). For a bounded domain, these surface waves reflect from the container walls, leading to a radially inward propagating wave-train converging onto the symmetry. Under the inviscid approximation and for sufficiently shallow cavities, the relaxation is well-described by the linearised potential-flow equations. Naturally, adding viscosity to such a system introduces viscous dissipation that enervates energy and dampens the oscillations at the symmetry axis.

However, for viscous liquids and deeper cavities, these equations are qualitatively inaccurate. In this work, we show a modal approach to observe the initial-value problem for concentric gravito-capillary waves. For a sufficiently deep cavity, the inward focusing of waves results in large interfacial oscillations at the symmetry, necessitating a quadratic order nonlinear theory. We demonstrate that this theory effectively captures the interfacial behaviour and highlights the crucial role of nonlinearity at $r=0$. Similar to the observations in bubble bursting [3[3]], the addition of slight viscosity further intensifies the oscillations at the symmetry axis. This finding underscores the limitations of the potential flow model and suggests avenues for more accurate modelling of such complex free-surface flows.

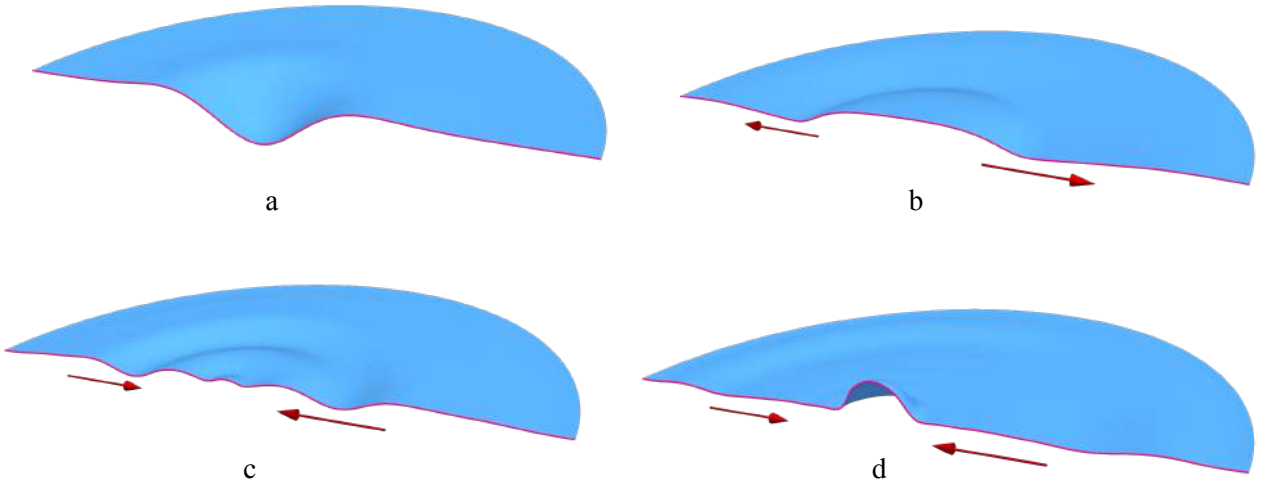

Fig 1. Relaxation of an initial cavity (panel a), and its inward and outward propagation (panels b, c, d)

[1] 1. Liquid jet eruption from hollow relaxation." *Journal of fluid mechanics* 761 (2014): 206-219.

[2] 2. "Singularity dynamics in curvature collapse and jet eruption on a fluid surface." *Nature* 403.6768 (2000): 401-404.

[3] 3. "Capillary waves control the ejection of bubble bursting jets." *Journal of Fluid Mechanics* 867 (2019): 556-571.

Forces acting on a small spherical droplet and Mass transfer

Eric Climent[1], D. Legendre[1], P. Shi[1], H. Godé[1-2], F. Lamadie[2], S. Charton[2].

[1] *Institut de Mécanique des Fluides de Toulouse (IMFT), Université de Toulouse, CNRS, Toulouse, France.*
[2] *CEA, DES, ISEC, DMRC, Univ. Montpellier, Marcoule, France, France*

I. CONTEXT AND OBJECTIVES

The dispersion of droplets or the separation of a dispersed phase from a fluid stream are encountered in many industrial, biological and environmental processes. The improvement and optimization of those processes, such as in liquid-liquid extraction columns, micro-fluidic high throughput devices are based most importantly on a thorough understanding and precise modeling of the hydrodynamic coupling between the two phases. Very often the model to predict the motion of small objects such as spherical droplets is based on a force balance which includes the major contributions of the fluid flow (drag, history, added-mas and lift forces) and gravity. Although the knowledge on the formulation for these forces have been significantly advanced for the two extreme cases of solid particles and bubbles, the specific case of fluid spheres (viscosity ratio $\mu^* \sim 0.1$ - 10) needs to be carefully addressed due to the coupling of internal flow circulation and the carrying fluid flow.

We are going to elaborate on droplet dynamics when the viscosity and density ratios between the internal and external fluids are of order one. Finally, I will comment on mass transfer across the interface and possibly the effect of a chemical reaction. This is of particularly high importance for chemistry and biotech industries. Chemical reaction in the extracting solvent is often used to enhance interfacial mass transfer. Given the complexity of an accurate description of the different coupling phenomena, the investigation of mass transfer at the microscale around a single droplet is still an open question.

A wide numerical investigation has been carried out using Direct Numerical Simulations to investigate the coupling between the internal and the external flows and their respective effects on the forces acting on the droplet and mass transfer coefficient. The CFD code developed at IMFT was adapted and used to this aim. We consider that the droplet has a constant spherical shape. Appropriate boundary conditions for the hydrodynamics have been implemented as well as a specific jump condition in order to accurately represent the convection/diffusion and mass transfer coupling at the interface between the droplet and the surrounding liquid. The finite volume code JADIM, together with the use of an orthogonal curvilinear refined mesh close to the interface permit accurate simulations of flow dynamics and interfacial phenomena over a large range of fluid flow regimes and conjugate mass transfer.

II. RESULTS

1 - History force

The effect of the history force is often neglected, due to numerical difficulties for its time integration, but also because no analytic expression is available in the time domain for droplets. The contribution of the history force acting on a spherical droplet in an oscillatory flow is determined using direct numerical simulation. Variation of the viscosity ratio makes the analysis relevant to bubbles, droplets, and solid particles. By changing the flow oscillation frequency, we can determine the range of physical parameters for which the contribution of the history force is significant [1].
We demonstrate that a kernel based on an analogy with a partially slipping sphere can be used to model history effects for droplets, especially when the contribution of the history force to the total force is important. The proposed history force expression provides a significant improvement for droplet trajectory prediction in unsteady flows when the history force contribution cannot be neglected.

2 - Path instabilities

Path instabilities of rising objects are known to be the result of coupling the particle dynamics with wake flow bifurcations. We investigate the specific case of viscous droplets rising under gravity in a quiescent

[1] The Basset-Boussinesq history force acting on a drop in an oscillatory flow. H. Godé, D. Legendre, S. Charton and E. Climent (2023) Phys. Rev. Fluids. 8, 073605.
[2] Lift force on a spherical droplet in a viscous linear shear flow. P. Shi, E. Climent and D. Legendre (2024), under revision for publication in J. Fluid Mech.

fluid. We consider only the case of spherical droplets and we aim at investigating trajectory oscillations with respect to internal or external flow instabilities which may depend on the Reynolds number and the viscosity ratio μ^*. By means of experiments and numerical simulations, we identify the range of physical properties yielding flow instability (inside the droplet and in the wake), as well as their consequences on the drop unsteady dynamics. The numerical study is based on direct numerical simulations: the Navier-Stokes equations are solved in both phases (i.e. inside and outside the droplet). Two types of bifurcation are evidenced depending on the viscosity ratio and Reynolds number. In agreement with existing literature on 3D flows around a solid sphere, we observe an increase of the drag and the appearance of a lift force (possibly unsteady) when the bifurcation occurs. A full map of bifurcations is proposed together with the identification of the origin of the droplet path instability. These numerical evidences are successfully compared to experiments.

3 - Lift force

Determining the lift (transverse) force on particles, bubbles, and drops in non-uniform flows is a longstanding problem in fluid dynamics. In this work [2], we examine a spherical droplet subjected to a linear shear flow, the most common situation in which a lift force on a sphere is known to exist.

Figure 1(a) displays the results for the lift coefficient, C_L, as a function of μ^* at Re = 200. As expected, C_L approaches that of a clean bubble [3] in the limit $\mu^* \to 0$ and that of a rigid sphere [4] as $\mu^* \to \infty$. However, the variation between these two limits is not monotonic, with C_L reaching a local maximum at $\mu^* \approx 0.5$.

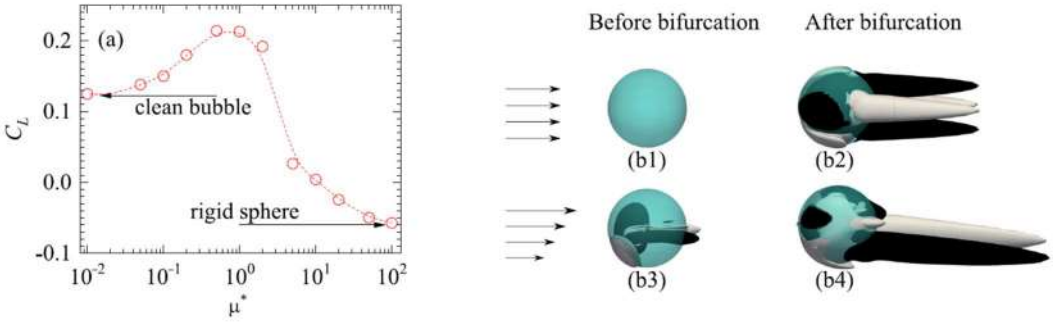

FIG. 1. (a) Lift coefficient as a function of μ^* at Re = 200; (b) Structure of the streamwise vorticity at $\mu^* = 0.5$.

This behavior is related to the same internal flow bifurcation also occurring under uniform-flow conditions, causing the flow to evolve from axi-symmetry to biplanar symmetry. In the presence of shear, this bifurcation enhances the streamwise vortices generated in the wake of the droplet. Consequently, under certain conditions, the lift force may exceed that in the inviscid limit.

4 - Mass transfer and chemical reaction

Dedicated simulations have been carried out to investigate the effect of the internal and external flows on mass transfer across the interface of a single droplet, and the evolution of the Sherwood number [5]. The results revealed very good agreement with available experimental and numerical data for validation on external and internal mass transfer coefficients varying the dimensionless numbers that control the physical and chemical system (Reynolds, Schmidt and Hatta numbers). Moreover, the respective effect of internal flow circulation and external convection was evidenced. Drastic changes of the internal and external resistances to mass transfer with increasing values of the Péclet number were predicted. Under specific flow conditions, 3D instabilities of internal and external fluid circulations were observed leading to drastic modifications of mass transfer. The effect of an external chemical reaction [6] has been correlated to the classic Hatta number with very good collapse of all the data on a scaling law.

[3] Legendre, D. and Magnaudet, J., The lift force on a spherical bubble in a viscous linear shear flow, J. Fluid Mech., 368, pp. 81-126, 1998.
[4] Kurose, R. and Komori, S. Drag and lift forces on a rotating sphere in a linear shear flow, J. Fluid Mech., 384, pp. 183-206, 1999.
[5] Towards more predictive correlations for conjugated mass transfer across a droplet interface. H. Godé, E. Climent, D. Legendre, S. Charton. (2023) Chem. Eng. J. – 478 (2023) 147110.
[6] Conjugate mass transfer from a spherical moving droplet: Direct numerical simulations of enhancement by a chemical reaction. H. Godé, E. Climent, D. Legendre, S. Charton. (2024) Chem. Eng. J. – 489, 151073.

Generation of waves on a free surface by quadratic shear currents

Harishankar Muppirala[1], Ramana Patibandla[1] and Anubhab Roy[1]

[1] *Department of Applied Mechanics, IIT Madras, Chennai, India* anubhab@iitm.ac.in

Surface waves are ubiquitous in nature. They range from large amplitude waves on the ocean, small-scale ripples in a pond, to thin films flowing down an incline in engineering applications. In an oceanic context, they grow by extracting energy from the shear flow, subsequently breaking due to various nonlinear processes, thereby generating sea spray and communicating between the ocean and the atmosphere, dictating the mass, momentum and energy exchanges.

In this study, we look at the growth of waves in a shear flow bounded between a rigid wall and a free surface, using linear stability analysis and characterizing the instabilities in the system. The base state shear flow in water is chosen to be a single-parameter family of quadratic velocity profiles, allowing us to access various kinds of flows ranging from a forward bulging to a backward bulging profile along with intermediate monotonic profiles, which can be concave or convex. We perform both viscous and inviscid calculations for this family of shear flows, using exact analytical, asymptotic and numerical methods.

Homeostatic ordering of cells in tissues

Shuvrangsu Das[1], Patrick McGarry[2] and Vikram Deshpande[1]
[1] Department of Engineering, University of Cambridge, Cambridge, UK
[2] Biomedical Engineering, College of Engineering and Informatics, National University of Ireland, Galway, Ireland

Artificial tissues are created by growing cells on scaffolds that mimic the shape and function of in-vivo tissues. Cells organize themselves in response to confinements provided by scaffolds, which in turn dictate mechanical functions of the tissues. In this work, we demonstrate that cells sense the confinement geometry while stochastically changing cell positions and morphologies driven by subcellular biochemical reactions. We show that cells align along the long axis of a rectangular tissue but randomly oriented in a square tissue, without any appreciable collagen fiber alignment. More importantly, cell statistics are relatively uniform, within experimental error, across the tissue width. This motivated us to consider tissues with identical aspect ratio but different areas, and we find that cell statistics demonstrate weak dependence on tissue areas. The experimental results suggest that classical theory of nematic ordering would be inadequate to explain the observations and it is necessary to develop a new statistical ensemble for cells in tissues. In this work, we propose the homeostatic ensemble for cells where cellular ordering emerges as cells fluctuate in tissue to maximize the total morphological and positional entropy of the system consisting of cell and collagen while each cell individually maintains homeostasis. We show that the homeostatic ordering can explain the long-range ordering of cells observed in the experiments.

Impact of soft-gel coated wall on evolution of Faraday waves

G. Balram[1], R. Kumar[1] and B. Dinesh[1]

[1] *Department of Chemical Engineering and Technology, Indian Institute of Technology-BHU, Varanasi, UP 221005, India dinesh.che@iitbhu.ac.in*

I. Abstract

This work studies the behavior of Faraday waves [1] on the surface of a fluid overlying a soft-gel layer. The fluid is treated as Newtonian, and the soft-gel is modeled as a linear viscoelastic material [2]. First, we use a heuristic model to analyze the natural frequency of the soft-gel layer alone. Our results show that the elastic properties of the soft-gel have a stabilizing effect on the natural frequency at its free surface. Next, we perform numerical calculations of the natural frequency of a fluid layer over the soft-gel layer. These results show that the presence of the soft-gel layer can either increase or decrease the fluid's natural frequency. The increase is due to the added inertia from the soft-gel layer, while the decrease is caused by the elastic stresses in the gel, which absorb stresses from the fluid. As a result of this increment and decrement in the natural frequency, the thresholds for the onset of Faraday instability at the free surface of the fluid are also affected. This leads to either a reduction or increase in the threshold, depending on whether the soft-gel layer has a stabilizing or destabilizing effect.

[1] Dinesh, B., Livesay, J., Ignatius, I. B. & Narayanan, R. 2023 Pattern formation in Faraday instability—experimental validation of theoretical models. Philosophical Transactions of the Royal Society A 381 (2245), 20220081.

[2] Dinesh, B & Narayanan, R 2021 Branching behaviour of the Rayleigh–Taylor instability in linear viscoelastic fluids. Journal of Fluid Mechanics 915, A63.

Influence of Joule Heating on Capacitance Dynamics in Supercapacitors

Kiran Prakash[1] and Sarith P Sathian[1]
[1]*Department of Applied Mechanics and Biomedical Engineering, IIT-Madras, India, kiran.prakash1987@gmail.com*

Introduction

One of the critical factors affecting the performance of supercapacitors is thermal management. The design of supercapacitors that operates across a broad temperature range and at high charge/discharge rates necessitates understanding the correlation of molecular characteristics of the device (such as interfacial structure and inter-ionic and ion-electrode interactions) with its macroscopic properties. The temperature dependence of electrical double layer (EDL) in room-temperature ionic liquids (RTILs) has been studied in various experimental and computational studies[1,2]. Most previous molecular simulations have focussed on studying temperature-dependent EDL capacitance using a rigid-wall approach to model the electrodes. However, the interfacial EDL is sensitive to the electrode's internal dynamics (wall-wall interactions) at the ionic liquid (IL)-electrode interface during the working of the supercapacitors. In the present study, we investigate joule heating in a supercapacitor by applying a temperature gradient along the electrode using molecular dynamics (MD) simulations. We examine the temperature-dependent behaviour of the electrical double layer (EDL) and differential capacitance-potential (C_D - V) curves for two different IL-graphene pairs under various thermal gradients in the range 1.83 K nm^{-1} to 9.01 K nm^{-1}.

Methodology

We performed non-equilibrium molecular dynamics simulations on two different IL-graphene systems. The imidazolium-based cation,1-butyl-3-methylimidazolium $[Bmim]^+$, is paired with tetrafluoroborate $[BF_4]^-$ and hexafluorophosphate $[PF_6]^-$ anion to form two different ILs pairs [Bmim][BF_4] and [Bmim][PF_6] shown in Fig.1(a). For each ILs-graphene supercapacitor system, 600 ion pairs are assembled between the graphene electrodes shown in Fig.1(b). The ILs are modelled using the nonpolarizable OPLS-AA (Optimized Potential for Liquid Simulations/All Atom)based all-atom force field without scaling the charges. The dimensions of the sheets are l_x x l_y = 4 nm x 12 nm.

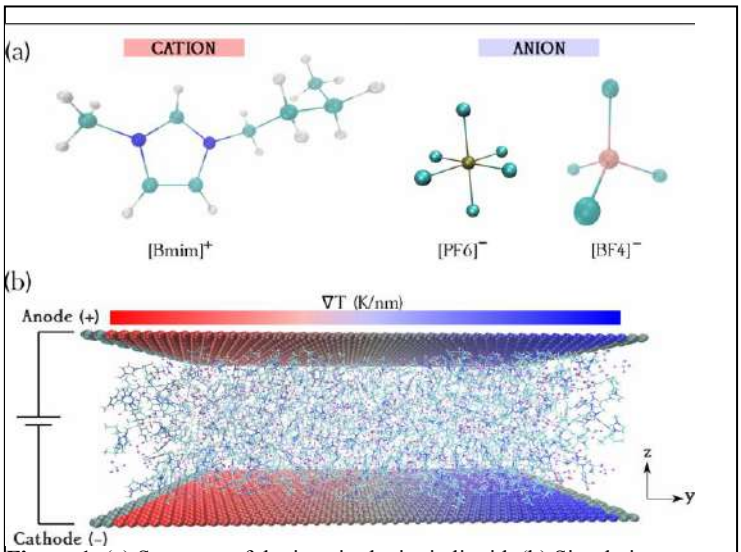

Figure 1: (a) Structure of the ions in the ionic liquid. (b) Simulation setup: Ionic liquid confined between two graphene sheets that act as electrodes. A thermal gradient is applied along the length (y-direction) of the graphene electrodes**.**

1 M. Drüschler, N. Borisenko, J. Wallauer, C. Winter, B. Huber, F. Endres, B. Roling. *New insights into the interface between a single-crystalline metal electrode and an extremely pure ionic liquid: slow interfacial processes and the influence of temperature on interfacial dynamics,* Physical Chemistry Chemical Physics. **14**, 5090-5099 (2012).

2 X. Liu, Y. Han, T. Yan. *Temperature Effects on the Capacitance of an Imidazolium-based Ionic Liquid on a Graphite Electrode: A Molecular Dynamics Simulation,* ChemPhysChem. **15**, 2503-2509 (2014).

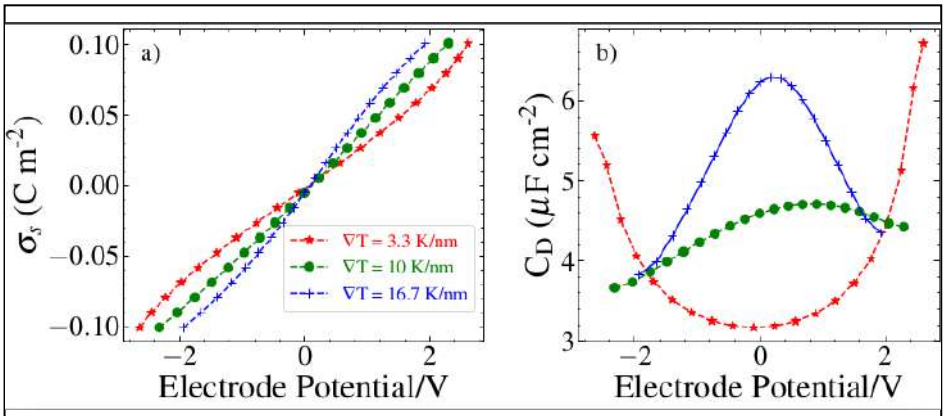

Figure 2: (a) Surface charge density(σ_s) as a function of electrode potential and (b) Differential Capacitance(C_D) as a function of electrode potential, for [Bmim-BF_4] system.

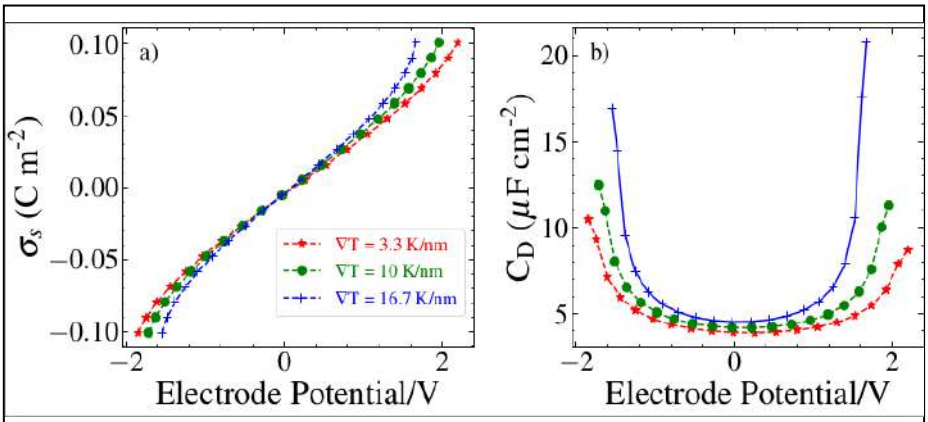

Figure 3: (a) Surface charge density (σ_s) as a function of electrode potential and (b) Differential Capacitance(C_D) as a function of electrode potential, for [Bmim-PF_6] system.

Results and Discussion

Figure 2(b) and 3(b) presents the differential capacitance, C_D as a function of electrode potential for [Bmim][BF_4] and [Bmim][PF_6] for different temperature gradients. As the temperature gradient increases, for the [Bmim][BF_4] system, the C_D - V curve transitions from 'U' to the bell shape. In contrast, for [Bmim][PF_6] system, we find a positive dependence of capacitance with temperature. The distinct variation in C_D - V with ∇T for [Bmim][BF_4] and [Bmim][PF_6] systems is attributed to the existence of high steric hindrance to the movement of charges at the interface [3] and high binding energy of adsorption for [Bmim][PF_6] with graphene [4]. This results in $[Bmim]^+$ cations forming a more stable interfacial layer with co-absorbed $[PF_6]^-$ anions compared to the [Bmim][BF_4]. The [Bmim][BF_4] makes distinctively higher anodic capacitance for different ∇T, whereas cathodic capacitance was higher for [Bmim][PF_6] due to differences in anionic characteristics in the IL.

Conclusion

The capacitive performance of [Bmim][BF_4] and [Bmim][PF_6] under different heating conditions are compared. The C_D - V curves for [Bmim][BF_4] transition from 'U' to the bell shape with the increase in thermal gradients. For the [Bmim][PF_6], we find a positive dependence of the capacitance with ∇T. The higher steric hindrance for $[PF_6]^-$ compared to $[BF_4]^-$ restricts the movement of charges at the interface, as well as the high adsorption energy of [Bmim][PF_6] with graphene, results in $[Bmim]^+$ cations forming a more stable interfacial layer with co-adsorbed $[PF_6]^-$ anions.

3 M. Shakourian-Fard, Z. Jamshidi, A. Bayat, and G. Kamath. *Meta-hybrid density functional theory study of adsorption of imidazolium-and ammonium-based ionic liquids on graphene sheet, The Journal of Physical Chemistry C.* **119**, 7095-7108 (2015).

4 C. Wei, K. Jiang, T. Fang, X. Liu. *Insight into the adsorption of Imidazolium-based ionic liquids on graphene by first principles simulation,* Journal of Molecular Liquids. **338**, 116641-116650 (2021).

Instability of a dusty vortex

Shraddha Mandloi[1], Darish Jeswin Dhas S[1], M. Houssem Kasbaoui[2] and Anubhab Roy[1]

[1] *Department of Applied Mechanics, Indian Institute of Technology Madras, Chennai, 600036, India.*
[2] *School for Engineering of Matter, Transport and Energy, Arizona State University, Tempe, AZ 85281, USA.*

In this work, we study the three-dimensional stability of a particle-laden vortex - an isolated columnar vortex with non-uniformly distributed inertial particles. We perform a temporal linear stability analysis by considering an Eulerian-Eulerian framework of a two-fluid model for the particle and fluid phases, further reduced to a single-fluid model for weakly inertial particles. We obtain a 'particle modified Rayleigh criterion', identifying the possibility of an axisymmetric instability of a monotonically decaying vorticity profile due to particle feedback force. For the specific scenario of a vortex column, our calculations reveal that the axisymmetric perturbations render the system unstable for non-zero mass loading, even in the limit of vanishing particle inertia. With increasing particle inertia, the growth rates of the unstable modes are reduced; however, for large wavenumbers, the stationary unstable modes morph into a pair of oscillatory unstable modes with an increase in particle inertia. Thus, a novel axisymmetric instability is observed in a columnar vortex due to the presence of inertial particles.

Interaction of two charged spherical soft-particles with uncharged polymer coating

Anirban Chatterjee[1] and Ameeya Kumar Nayak[2]

[1] *Department of Mathematics, IIT Roorkee, India, chatterjeeanirban001@gmail.com*

[2] *Department of Mathematics, IIT Roorkee, India, ameeyakumar@gmail.com*

ABSTRACT

Micro-bio molecules that exist everywhere in nature are usually modeled as having a rigid inner core along with a thin polymer coating over it. These bio particles are usually defined as a softparticle. The polymeric nature of the interface separating the inner core of the bio molecules from the suspending fluid pose great challenges in deciphering their interaction mechanism. Usually, the bio molecules are inherently charged and being suspended in fluid medium develop a Debye layer, which shields the effects of the surface charges from the bulk fluid medium. The interaction of such soft-particles leads to a multifold coupling of the electrokinetic, hydrodynamic, polymeric repulsion and short ranged Van der Waals attraction. In the current study we have attempted to study the interaction dynamics of soft-particles under simplifying assumptions of weak charge limit, moderate Debye layer thickness and the simplified de Gennes scaling law [1] for deformable polymer brushes. The electroviscous effect arising due to the coupling of the electrokinetic and the hydrodynamics has been handled in a self-consistent manner by following the works of Zhao et al [2]. As the two soft-particles approach each other, the squeeze flow results in the development of a streaming current, which couples with the flow hydrodynamics to give rise to the electroviscous effect. Furthermore, we take into account the DLVO interaction and the steric repulsion effect due to the compression of the polymer layers. The complex interaction gives rise to a variety of attractive and repulsive forces that decides upon the fate of the two interacting soft-particles, finally yielding a critical compression length of the polymer chains where the attractive force overpowers the repulsive forces and finally, we obtain instantaneous velocity of the approaching particle.

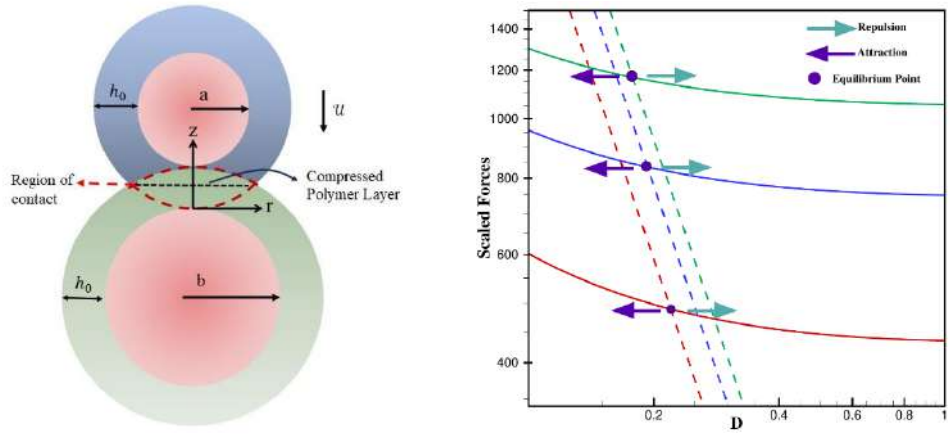

FIG. 1. Left: The motion of a soft-particle towards a stationary soft particle, Right: The lengths at which Net Force balance occurs.

[1] de Gennes and Pierre Gilles. Polymers at an interface; a simplified view, *Advances in colloid and interface science* 27.3-4, 189-209 (1987).

[2] C. Zhao, W. Zhang, D. van den Ende and F. Mugele, Electroviscous effects on the squeezing flow of thin electrolyte solution films. *Journal of fluid mechanics* 888, A29 (2020).

Levy walks and superdiffusion

Mahesh Panchagnula[1] and Satish Akella[2]
[1]*Department of Applied Mechanics, Indian Institute of Technology Madras, Chennai, 600036 - India*
[2]*Department of Physics, Indian Institute of Technology Jammu, Jagti Campus, 181221 - India*

Levy walks are a class of non-Gaussian random walks which occur in many different physical phenomena from animal foraging to the motion of light in amorphous media. In this talk, we will present experimental evidence of the occurrence of Levy walks in fluid mechanical systems involving activity. We introduce an experimental system using an octanoic acid (OA) drop placed on aqueous solutions containing unsaturated OA to investigate Lévy walks in a controlled setting. The motion of the drop is driven by unbalanced Marangoni forces, leading to spontaneous movement similar to the propulsion mechanisms observed in biological systems. This movement is identified as a Lévy walk, exhibiting characteristics of superdiffusive transport, with the step lengths following a Lévy-stable distribution and the velocity autocorrelation function decaying according to a power law. The exponents of this behaviour align with theoretical predictions, confirming the Lévy walk nature of the drop's motion. This setup provides a simplified and controlled way to explore complex transport phenomena observed in natural systems like foraging. Finally, we will discuss the broader implications of the work to show that where ‘activity’ or ‘propulsion’ aids diffusion, one could expect Levy walks.

Light Scattering in Droplets within Optofluidic Devices: A Ray Optics Simulation Analysis

Kanimozhi Kumaresan[1,2], Ashis Kumar Sen[2] and Anil Prabhakar[1]
[1] *Department of Electrical Engineering, Indian Institute of Technology Madras, Chennai, India.*
[2] *Department of Mechanical Engineering, Indian Institute of Technology Madras, Chennai, India.*

I. INTRODUCTION

Droplet microfluidics has gained considerable attention due to its ability to facilitate high-throughput analysis of single cells and other biological entities. Optofluidic devices, which integrate optical and microfluidic systems, have emerged as powerful tools for non-invasive analysis, offering precise control over droplet behavior and enabling real-time monitoring of cellular interactions. Understanding the optical properties of droplets, particularly how light interacts with them, is crucial for optimizing these devices for applications in healthcare, biotechnology, and bioanalysis. One key observation in optofluidic systems is the side scattered (SSC) signal generated when light interacts with droplets. Historically, SSC signals were attributed to various optical phenomena, but recent investigations suggest that light refraction within droplets plays a central role. This study focuses on using Ray Optics simulations to explore how droplet size influences SSC signals, aiming to improve our understanding of the underlying physics and enhance the design of optofluidic systems for more effective single-cell and particle analysis.

II. NUMERICAL SIMULATIONS RESULTS

A comprehensive 3D numerical model was developed using the Ray Optics module in COMSOL Multiphysics 5.6 to simulate light interaction with droplets in an optofluidic device. The simulation was based on Hamiltonian optics principles, where the propagation of light rays is described by Hamilton's equations. Snell's Law was applied at interfaces to account for refraction and reflection as light rays passed through droplets of varying sizes. The geometry modeled a standard polydimethylsiloxane (PDMS)-based optofluidic device, with fluid channels and multimode fibers (MMF) positioned at specific angles to a single-mode excitation fiber (SMF). Spherical water droplets were introduced into the fluidic channel, simulating their movement through the optical interrogation region. The refractive indices of the materials PDMS, water, and oil were set according to their respective optical properties to replicate realistic interactions.

Conical rays, emitted from the SMF, were directed toward the droplets, where they were refracted or reflected depending on the interface. The refracted light reaching the MMF, which was positioned at varying angles, was analyzed for energy flux to determine the intensity of light scattering. The simulation performed a parametric sweep over different droplet positions and sizes, ranging from 50 µm to 125 µm in diameter, to evaluate the effect of droplet size on SSC signal intensity.

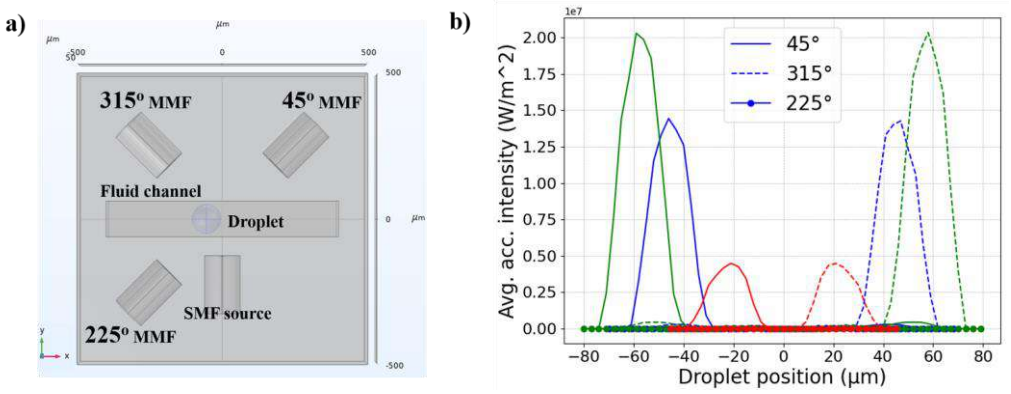

FIG. 1. Optofluidic device (a)3D optofluidic device model. (b) Average accumulated intensity decreases with a decrease in droplet diameter, and the distance between the leading and lagging peaks decreases. g-125 µm, b-100 µm, r-50 µm.

Conical rays guided through the SMF interacted with the droplets, resulting in refraction and reflection. The interacted rays reaching the MMF positioned at various angles were analyzed for total incident energy flux. A parametric sweep study of droplet position across the optical interrogation region evaluated the refracted light. The study performed for different droplet sizes, ranging from 50 μm to 125 μm.

III. SIMULATIONS RESULTS

The Ray Optics simulations revealed a strong correlation between droplet size and the intensity of SSC signals. As the droplets moved through the interrogation region, the curved surface of the droplet refracted the incoming light, directing it towards the collection fibers. The simulations demonstrated that larger droplets resulted in increased accumulated intensity, while the distance between the leading and lagging peaks of the SSC signal was directly related to the droplet diameter.

IV. DISCUSSION AND CONCLUSION

.

The Ray Optics simulations conducted in this study confirmed that side scattered (SSC) signals in optofluidic devices originate from light refraction within droplets. This refraction is influenced by droplet size, with larger droplets refracting more light and producing higher SSC signal intensities. These findings highlight the critical role of droplet size in shaping SSC signals, which is essential for improving the performance of optofluidic systems in applications such as single-cell analysis. The Ray Optics simulation confirms that SSC signals arise from refracted light, using the Ray Optics module to validate this hypothesis. Although earlier studies have linked SSC signals to refraction, this work is the first to use ray optics simulations for concrete evidence[1].

Furthermore, these findings align with recent advancements in light-scattering-based droplet screening (LSDS) technologies, which offer high-throughput, label-free analysis of single cells[2]. By integrating these insights into device design, researchers can enhance the sensitivity and accuracy of optofluidic systems, making them more effective for bioanalytical tasks.

In future work, simulations will be expanded to investigate the interaction of light with beads encapsulated within droplets. This focus will aim to enhance the fluorescence intensity from the beads, which could further improve the detection capabilities of optofluidic devices. These advancements are expected to pave the way for more precise and efficient optofluidic platforms, facilitating high-throughput, label-free analysis in biomedical and biotechnological applications.

[1] J. N. Schianti, I. Y. Abe, M. I. Alayo, and D. O. Carvalho, Real time water-in-oil emulsion size measurement in optofluidic channels, Sens. **22**, 4999 (2022).

[2] L. Liang, M. Liang, Z. Zuo, and Y. Ai, Label-free single-cell analysis in microdroplets using a lightscattering-based optofluidic chip, Biosens. Bioelectron. **253**, 116148 (2024).

Marangoni wakes in a viscous fluid

Thomas Bickel[1] and François Detcheverry[2]

[1] *LOMA, University of Bordeaux, F-33400 Talence, France,* thomas.bickel@u-bordeaux.fr
[2] *ILM, University of Lyon, F-69622 Villeurbanne, France,* francois.detcheverry@univ-lyon1.fr

Marangoni surfers are active particles having the ability to self-propel along the liquid-air interface. Their actuation mechanism relies on the asymmetric release of surface-active agents by the particle. Indeed, variations of surface tension along the contact line lead to a net force that pulls the particle toward the region of higher surface tension. The motion of a Marangoni surfer is also accompanied by a flow in the liquid subphase.

Despite general agreement on the actuation mechanism, a definite quantitative description is still lacking. This is especially true for symmetric particles, such as circular disks loaded with camphor, that exhibit rapid translational or rotational motion when placed at the air-water interface [1]. In this case, the initial axial symmetry is broken by a convective instability, which results in directed motion. Yet, little is known regarding the onset of the instability. In particular, the existence of a critical Péclet number as well as the effect of fluid inertia are questions that remain largely unexplored.

To address these issues, we focus on the Stokes flow due to a point source of surfactants at the interface of an unbounded, viscous liquid at low Reynolds number ($\mathrm{Re} \ll 1$). Although the advection-diffusion equation for surfactant spreading is both nonlinear and nonlocal [2], we manage to derive analytical results in the limit of large Péclet number ($\mathrm{Pe} \gg 1$). For a steady source, the interfacial velocity is shown to decay as $r^{-\alpha}$, where r is the radial distance to the source. The power-law exponent is equal to $\alpha = 1/2$ for insoluble surfactants, and $\alpha = 1$ for perfectly soluble surfactants. For a source that is moving at constant speed, we characterize the 3D wake of the Marangoni flow both in the vicinity and far away from the source. As shown in Fig. 1, the flow field separates into two distinct regions that eventually meet at a stagnation point in front of the surfactant source. Our findings, that are expected to shed new light on the actuation mechanism of Marangoni surfers, are finally discussed in relation to experiments.

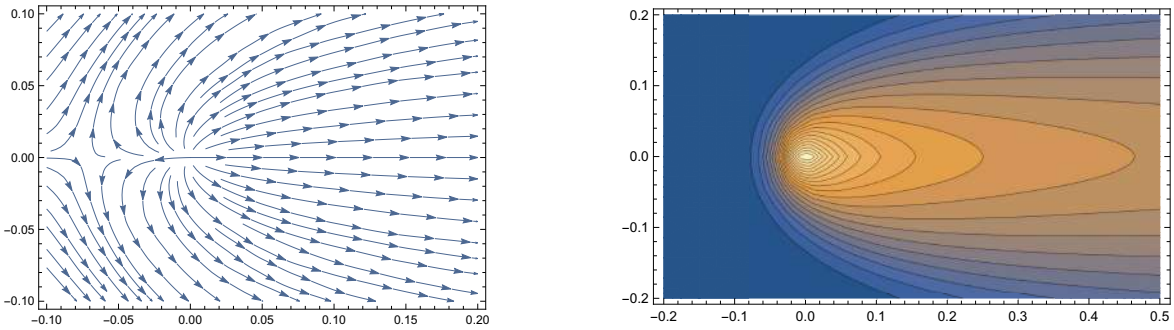

FIG. 1. Interfacial flow streamlines (left) and concentration field (right) for a moving source of insoluble surfactants, in the reference frame of the source (x and y in arbitrary units).

[1] D. Boniface, C. Cottin-Bizonne, F. Detcheverry and C. Ybert, Role of Marangoni forces in the velocity of symmetric interfacial swimmers, Phys. Rev. Fluids **6**, 104006 (2021).

[2] T. Bickel and F. Detcheverry, Exact solutions for viscous Marangoni spreading, Phys. Rev. E **106**, 045107 (2022).

Modelling liquid plugs in the pulmonary airways

Georg F. Dietze[1]

[1]*Université Paris-Saclay, CNRS, FAST, 91405 Orsay, France, georg.dietze@cnrs.fr*

Abstract

We validate a long-wave model based on the weighted residual integral boundary layer (WRIBL) approach of Ruyer-Quil and Manneville (Eur. Phys. J. B, vol. 15, 2000, pp. 357–369) in terms of representing liquid plugs in a narrow vertical cylindrical tube lined by a liquid film in contact with a core gas flow and subject to gravity. We apply this model to predict airway occlusion and epithelial cell damage in the human tracheobronchial tree.

Keywords: *Liquid plugs, airway occlusion, integral boundary layer models*

Introduction

We study the flow of a liquid film lining the inner surface of a narrow cylindrical tube in contact with a core laminar gas flow and subject to gravity (figure 1), focusing on parameters representative of mucus films in the pulmonary airways. We aim to predict the formation and properties of liquid plugs and the wall stresses they generate, in the context of airway occlusion. It is known that the threshold for liquid plug formation is given by a limit point (w.r.t. the liquid volume, V_1) on the solution branch of nonlinear travelling-wave solutions (TWS), which can be predicted by numerical continuation, using low-dimensional models based on the long-wave approximation [1,3]. Here, we apply the augmented Weighted Residual Integral Boundary Layer (WRIBL) model of [3] to go beyond this limit point and to predict travelling-plug solutions (TPS).

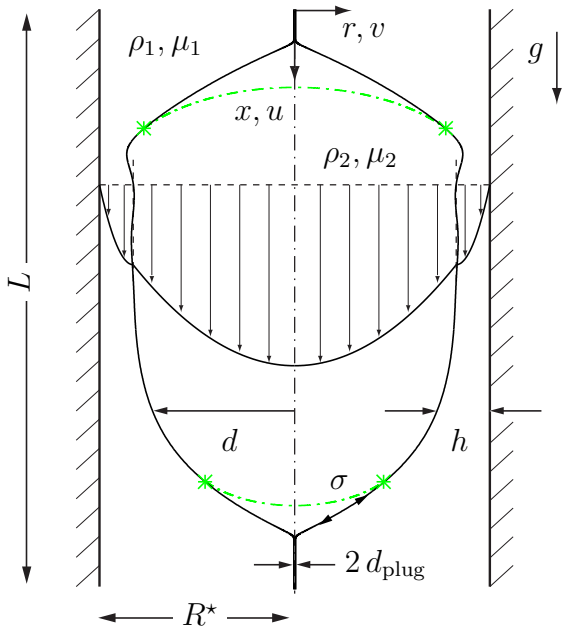

Figure 1: Liquid plugs (subscript 1) enclosing a gas bubble (subscript 2) formed by the occlusion of a narrow cylindrical tube by a liquid film lining its inner surface.

Mathematical formulation

The augmented WRIBL model, which accounts for the full coupling between the liquid (i,j=1) and gas (i,j=2), consists of three equations written here in non-dimensional form, assuming Einstein summation, i.e. the momentum equation:

$$S_i\partial_t q_i + F_{ij}q_i\partial_x q_j + G_{ij}q_iq_j\partial_x d = \frac{\mathrm{We}}{2\pi}\partial_x\kappa + \Pi_\varphi + \frac{1}{2\pi}\mathrm{Fr}^{-2}\left(1-\Pi_\rho\right) + \frac{1}{2\pi}C_iq_i + J_iq_i\partial_x d^2 + K_i\partial_x q_i\partial_x d + L_iq_i\partial_{xx}d + M_i\partial_{xx}q_i, \tag{1a}$$

and the phase-specific continuity equations (dimensional tube radius, $R^\star$, used as length scale throughout):

$$\partial_t d - \frac{1}{2\pi d}\partial_x q_1 = 0, \quad \partial_t d + \frac{\Pi_u}{2\pi d}\partial_x q_2 = 0, \tag{1b}$$

where d, q_1, and q_2 denote the core radius and the phase-specific cross-sectional flow rates, and We and κ=κ_x+κ_φ denote the Weber number and the film surface curvature. The source term, Π_φ, is designed to cancel the azimuthal curvature contribution, κ_φ, in (1a) in the limit d=$d_{\rm plug}$$\ll$1:

$$\Pi_\varphi = -\frac{\mathrm{We}}{2\pi}\Pi_{\rm CRL}\exp\left[\lambda\left(1-\frac{d(x,t)}{d_{\rm plug}}\right)\right]\partial_x\kappa_\varphi. \tag{1c}$$

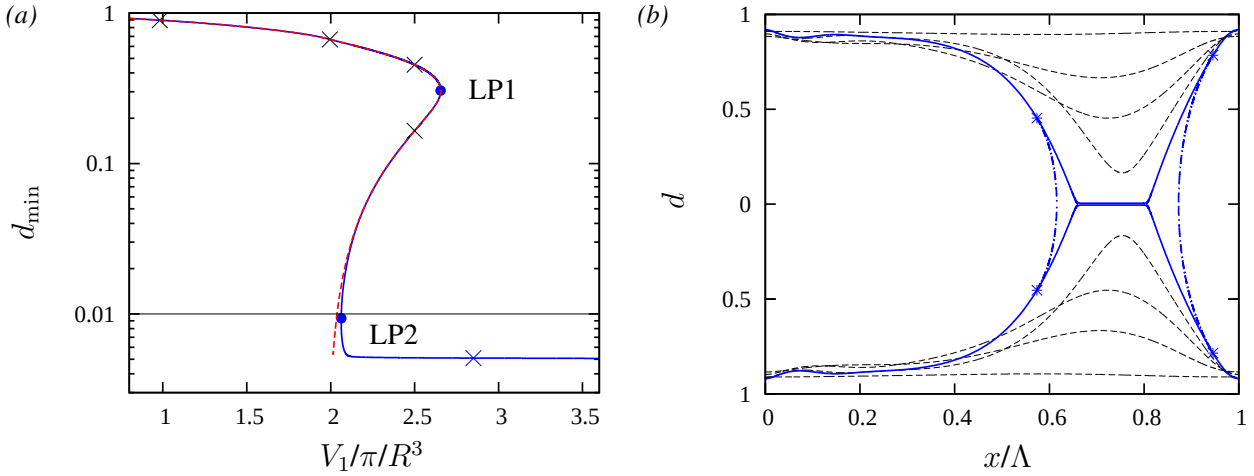

Figure 2: Transition from TWS to TPS: silicone oil film (Ka=121.4) in contact with air under an aerostatic pressure gradient, $R^\star$=1.5 mm, L=Λ=5.4. *(a)* Minimal core radius, $d_{\min}$, in terms of normalized liquid volume. Solid blue: Π_{CRL}=λ=1, d_{plug}=0.01; dashed red: Π_{CRL}=0; *(b)* profiles corresponding to crosses in panel *a*. Toward tube axis: $V_1/\pi/R^3$=1, 2, 2.5, 2.5, 2.85. Dot-dashed blue lines correspond to spherical-cap reconstruction.

Thus, the Plateau-Rayleigh instability mechanism is deactivated when the liquid-gas interface comes close to the tube axis. This allows to obtain pseudo-plugs, which consist of a liquid annulus filling almost the entire tube cross section except for a thin gas filament in the core (panel 2b). In the current work [2], we show that the augmented WRIBL model (1) accurately predicts the plug speed, the associated wall stresses, and the flow field within the liquid and gas, in good agreement with direct numerical simulations (DNS) and experiments.

Results and discussion

The augmented WRIBL model allows to predict the transition from TWS to TPS, as shown in figure 2. We apply it to predict airway occlusion within the conducting zone of the tracheobronchial tree [2], based on the Weibel lung architecture model. We find that plug formation can be avoided in all airway generations by increasing the tracheal gas flow rate, but at the expense of maintaining high levels of the axial wall stress derivatives. The derivatives of both the tangential wall shear stress and the wall pressure are found to attain levels that are sufficient to cause epithelial cell damage. By contrast, reducing the liquid surface tension, allows to avoid airway occlusion while significantly reducing wall stress levels. Also, we observe a significant effect of gravity on the nature of travelling-state solutions. For the counter-current configuration, where the gas flows opposite to gravity, breathing is significantly hindered even in the absence of liquid plugs.

Conclusion

We have validated the augmented WRIBL model of [3] in terms of predicting liquid plugs forming in a narrow cylindrical tube under the effects of a core gas flow and gravity. We have applied this model to predict airway occlusion and epithelial cell damage throughout the tracheobronchial tree, identifying the parameter range for avoiding plug formation via assisted ventilation or surfactant treatment.

Acknowledgments: The author gratefully acknowledges funding provided by “CNRS Ingénierie” via équipe-project MUCUS.

References

[1] Camassa, R., Ogrosky, H. R. & Olander, J. 2014 Viscous film-flow coating the interior of a vertical tube. part 1. gravity-driven flow. *J. Fluid Mech.* **745**, 682–715.

[2] Dietze, G. F. - Liquid plugs in narrow tubes: application to airway occlusion. *J. Fluid Mech.* **in print**.

[3] Dietze, G. F., Lavalle, G. & Ruyer-Quil, C. 2020 Falling liquid films in narrow tubes: occlusion scenarios. *J. Fluid Mech.* **894**, A17.

New insights into flow near a moving contact line: resolution of the singularity and role of hysteresis

Charul Gupta[1], Tejasvi Hegde[2], Rishabh Sharma[3], V. S. Anvesh Sangadi[4], Anjishnu Choudhury[5], Lakshmana Dora Chandrala[6], Harish N Dixit[7]

[1] *Dept. of Mechanical & Aerospace Engg., IIT Hyderabad, India,* ME18RESCH11001@iith.ac.in

[2] *Dept. of Mechanical & Aerospace Engg., IIT Hyderabad, India,* me22mtech12006@iith.ac.in

[3] *Dept. of Mechanical & Aerospace Engg., IIT Hyderabad, India,* me22mtech12009@iith.ac.in

[4] *Dept. of Mechanical & Aerospace Engg., IIT Hyderabad, India,* me20m22p100001@iith.ac.in

[5] *PMMH, CNRS, ESPCI Paris, Sorbonne Université, France,* anjishnu.choudhury@espci.psl.eu

[6] *Dept. of Mechanical & Aerospace Engg., IIT Hyderabad, India,* lchandrala@mae.iith.ac.in

[7] *Dept. of Mechanical & Aerospace Engg. & Centre for Interdisciplinary Programs, IIT Hyderabad, India,* hdixit@mae.iith.ac.in

ABSTRACT

A moving contact line is a region where the interface between two immiscible fluids intersects a moving solid surface. The theoretical study by Huh & Scriven [1] reported a stress singularity near a moving contact line. The stress singularity is primarily caused by the application of the no-slip boundary condition on the moving plate, which is directly in conflict with a moving contact line. Several models have been proposed to resolve this singularity. A popular choice is to relax the no-slip condition and allow a finite amount of slip in the vicinity of the moving contact line [2,3]. The current study provides evidence for slip flow near a moving contact line using high-resolution PIV experiments. The experiments reveal the presence of variable slip in the vicinity of the moving contact line and no slip further away, thus offering a direct pathway for the resolution of the moving contact line paradox. Furthermore, often the contact angle does not assume a constant value, but exbibits hysteresis. Experimentally, this value is difficult to detect dynamically. We show that hysteresis can have a dramatic effect on the flow field. Hysteresis induces a high-frequency fluctuation at the contact line due to the localised 'stick-slip' motion. The effect of this fluctuation is investigated in the present study using experiments and numerical simulations.

I. INTRODUCTION

Moving contact lines, between two immiscible liquids A and B shown schematically in figure 1(a), can be observed in several applications, such as ink-jet printing, coating, secondary oil recovery, etc. Huh & Scriven [1] studied the flow field near a moving contact line assuming the interface to be flat and the no-slip condition was employed on the moving solid. This leads to the formation of a stress singularity, sometimes referred to as the Huh & Scriven paradox. Several models [2, 3] have subsequently been developed to resolve the moving contact line singularity. A common theme in all these models is the incorporation of additional physics at the moving contact line such as intermolecular forces, phase-field models or slip near the contact line. It is well known that introducing slip near the moving contact line resolves the stress singularity and is one of the most popular choices for modelers. In a recent model, Kirkinis & Davis [3] introduced a variable slip model where a region of finite but variable slip occurs near the contact line and no-slip condition is enforced away from the contact line as shown in figure 1(b). This model shows that the fluid slips along the plate near the moving contact line and the slip velocity eventually disappears when the standard no-slip condition is enforced. But the model lacks information on the exact length scale over which the slip velocity persists.

In a recent discovery [4,5], it was shown that slip flow indeed occurs in the vicinity of the moving

[1] Huh, C. & Scriven, L. E., Hydrodynamic model of steady movement of a solid/liquid/fluid contact line. J. Coll. Int. Sci., **35(1)**, 85-101 (1971)

[2] Cox RG., The dynamics of the spreading of liquids on a solid surface. Part 1. Viscous flow, J. Fluid Mech., 168, 169-194, (1986)

[3] Kirkinis E, Davis SH, Moffatt vortices induced by the motion of a contact line. J. Fluid Mech.,746:R3 (2014)

[4] Gupta, C., Chandrala, L.D. and Dixit, H.N., An experimental investigation of flow fields near a liquid–liquid moving contact line. The Euro. Phys. Journal Special Topics, pp.1-11. (2024)

[5] Gupta, C., Choudhury, A., Chandrala, L.D. and Dixit, H.N., An experimental study of flow near an advancing contact line: a rigorous test of theoretical models. arXiv:2311.09560 (2023)

contact line. Further, systematic deviations of interface velocity were also observed from the theoretical predictions of Huh & Scriven's theory. The current study systematically investigates the slip flow near the moving contact line and its relation to various operating parameters such as Reynolds and capillary number.

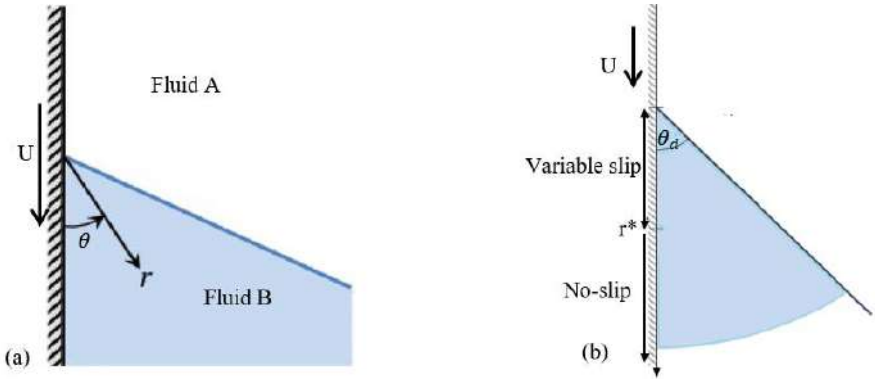

Fig. 1: (a) Flow configuration and geometry showing plate immersion resulting in an advancing contact line, and (b) the variable slip model of Kirkinis & Davis [3]

Figure 2(a) shows a typical flow field in the liquid showing 'rolling motion' of the flow field. We then extract the velocity field along the moving plate and define a non-dimensional slip parameter, defined as

$$v_s = 1 - \frac{v(r)}{U},$$

where U is the speed of the plate, $v(r)$ is the fluid velocity along the moving plate with $r = 0$ indicating the contact line. Perfect slip is indicated by $v_s = 1$ whereas no-slip is indicated by $v_s = 0$. As is clearly evident, slip velocity Figure 2(b) shows the non-dimensional slip velocity measured along the moving plate. To the best of our knowledge, this is the first experimental evidence of slip in moving contact lines, and this provides direct evidence of how the singularity is being resolved.

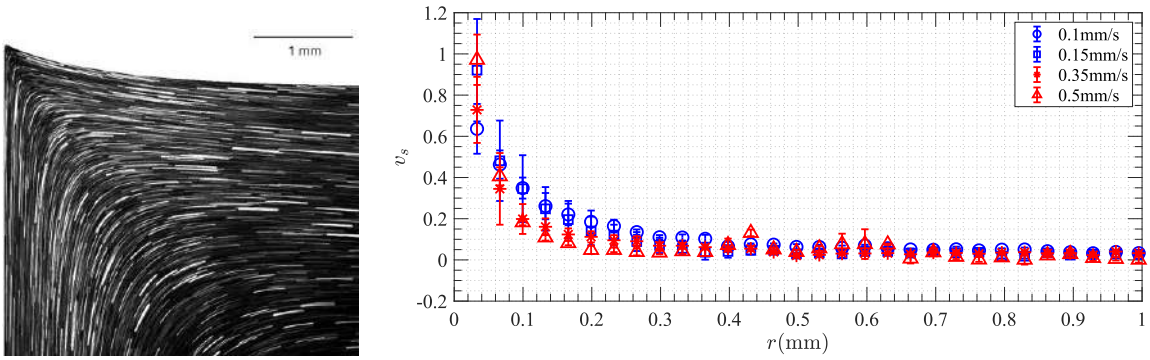

Fig. 2: (a) Streakline image of flow feild in air-silicone oil system, (b) non-dimensional slip velocity along the plate in air-silicone oil system at various plate speeds

The slip observed near the contact line was also found to have an effect on the interface velocity. Gupta et al. [4,5] showed that material points along the interface slow down as they approached the contact line. Thus, a consolidated view of the flow near the contact line emerges by combining the motion of fluid along the interface and along the moving plate. While the flow field in figure 2(a) is shown to be of rolling-type, other types of motion such as the split-streamline motion can also occur. This flow field involves a streamline from the bulk splitting the flow into two distinct parts. Preliminary experimental evidence, with support from numerical simulations, suggests that hysteresis has the potential to alter the flow from rolling to a split-streamline motion.

ACKNOWLEDGEMENTS

HND gratefully acknowledges funding from the Science & Engineering Research Board, Department of Science and Technology for financial support through grant CRG/2021/007096.

Non-Newtonian drop impact dynamics on superhydrophobic surfaces

K. Kamaluddin[♠], G.C. Pal[♠], P. Dhar[♣], C.S. Sharma[♠] and Devranjan Samanta[♥]

Non-Newtonian droplets were known to inhibit rebound suppression on hydrophobic surfaces[1]. Various factors such as extensional viscosity, normal stress, molecular level adsorption of polymer molecules at the substrate are shown to be responsible factors for slowing down the retraction dynamics and subsequently reduce the kinetic energy enough to suppress the drop rebound. We have experimentally studied the non-Newtonian drop impact dynamics on superhydrophobic (SH) substrates[2]. We showed that polymer concentrations and impact velocities have certain threshold values to trigger the non-Newtonian dynamics responsible for rebound suppression. Eventually, we showed that the rebound suppression mechanism is effective only if the Weissenberg number (*Wi*) based on the shear rate during the onset of retraction exceeds one. Subsequently we tried to test this hypothesis on four different types of SH surface and test the universality of the hypothesis of *Wi*>1 for onset of rebound suppression [3]. Contrary to our expectations, we didn't observe the rebound suppression on all the surfaces. The surfaces where rebound suppression was observed were termed as 'Type-I' surface whereas the other surfaces were categorized as ''Type-II' surfaces. The role of Cassie-Wenzel transformation (CWT) or impalement was further examined for the surfaces. For the occurrence of CWT, the dynamic pressure (P_D) has to exceed the minimum capillary pressure (P_c). The capillary pressure is inversely proportional to the characteristic spacing of the finer structures of the SH surfaces. For the 'Type-I' surface, the characteristic spacing was or micron order whereas the characteristic spacing for the 'Type-II' surfaces were of nanometres order i.e. at least three order of magnitudes less. Naturally, it was far more probable for the 'Type-I' surface to exhibit rebound suppression where the criterion of $P_D/P_C > 1$ can be achieved. It is worth mentioning that even at $P_D/P_C > 1$, water droplets would imply fragment and rebound off the surfaces. The slowing down of retraction dynamics due to polymer dynamics is also essential for the drop to stay intact and prevent rebound off the SH surface. The role of extensional viscosity was also highlighted. Overall, the dual role of fluid elasticity (*Wi>1*) and CWT ($P_D/P_C > 1$) has been highlighted as the two mechanisms which have to simultaneously act for causing the non-Newtonian drop rebound on SH surfaces.

♠ IIT Ropar

♣ IIT Kharagpur

[1] Bergeron et al, Nature 2000

[2] P. Dhar et al, Phys. Rev. Fluids 4, 103303 Published 22 October 2019

[3] K Kamaluddin et al., Colloids and Surfaces **A**, 2024

Numerical simulation of clustering of nano particles in aqueous medium

Bahni Ray[1] and Gaurav Nath[2]

[1]*Department of Mechanical Engineering, IIT ,110016, Delhi,India, gulam95070@gmail.com*
[2]*Department of Mechanical Engineering, IIT,110016, Delhi, India, bray@mech.iitd.ac.in*

Clustering of particles has found to play an important role in food and pharmaceutical processing, colloidal suspensions, mineral extraction and waste water treatment. The wet granulates can form if the particles are suspended over an underlying fluid at the liquid-air interface. Capillary bridges are formed due to the presence of a secondary “sticky" liquid, which can lead to clustering. Clustering of particles in wet granulates can have a significant role in altering the rheological and physical characteristics of materials In this work simulation of various conditions of shear on a single wet aggregate of spherical and non-spherical particles in a couette cell via Lattice Boltzmann method is done and their behavior is studied. Single relaxation time *Bhatnagar-Gross-Krook* lattice Boltzmann model has been used for the continuous phase. *Ladd's (1994)* particle model has been used for the dispersed phase. Two particles, wetted by a second liquid, tend to cluster. In the simulations, instead of introducing another fluid, the particles are considered to be attracted by a constant force *(Sarkar and Dubey, 2016)*.

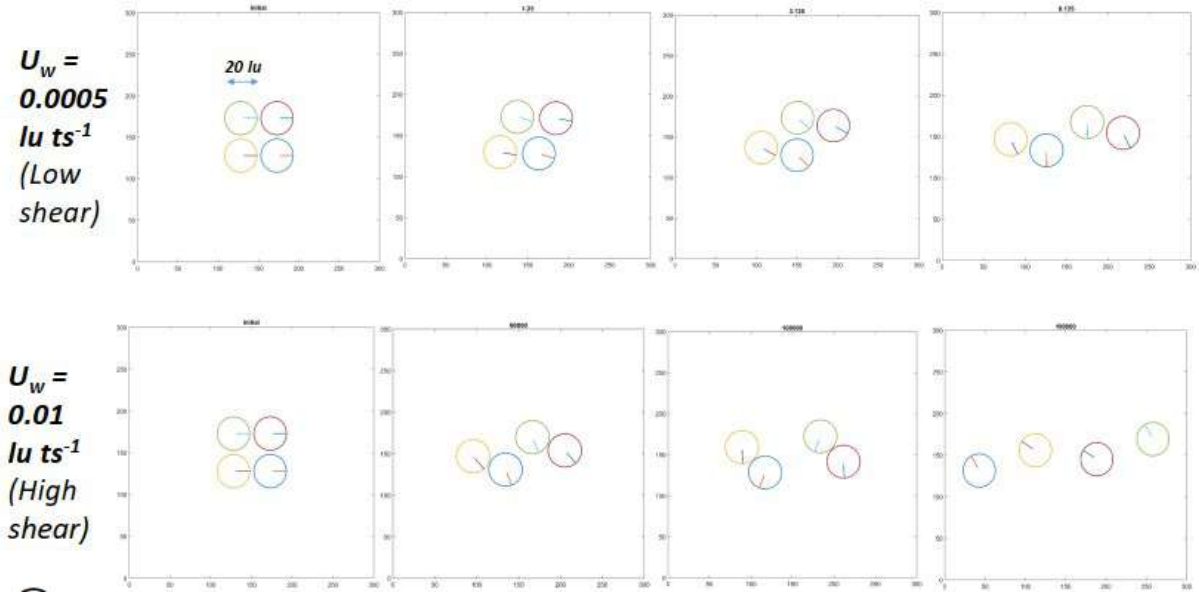

FIG.1 **Above**: For **low shear** the cluster deforms gradually, and eventually breaks with the top and bottom pair remaining after breakup, **Below:** For **high shear** the cluster breaks abruptly in half followed by separation of all particles.

REFERENCES

[1] Ladd, A.J., 1994. Numerical simulations of particulate suspensions via a discretized Boltzmann equation. Part 1. Theoretical foundation. Journal of fluid mechanics, 271, pp.285-309

[2] Sarkar, J. and Dubey, D., 2016. Failure regimes of single wet granular aggregate under shear. Journal of Non Newtonian Fluid Mechanics, 234, pp.236-248

On dynamics of inflating a soap bubble

Saini Jatin Rao, Siddhant Jain and Saptarshi Basu*

Department of Mechanical Engineering, Indian Institute of Science, Bengaluru, Karnataka, India

*sbasu@iisc.ac.in

Despite their widespread occurrence, bubbles demonstrate complex behaviour that is not only visually captivating but also evokes scientific inquiry. This study examines the dynamics of soap bubble inflation by methodically regulating airflow through a nozzle, focusing on the motion of the soap film and the characteristics of the internal airflow. The source pressure was varied to examine its effect on the bubble growth rate, and the unexplored internal airflow was visualized [1], unlike earlier studies [2,3]. Observations indicated that air is introduced into the bubble as a jet, which subsequently generates a toroidal vortex upon impingement with the expanding concave internal surface of the bubble. Scaling laws governing the characteristics of this vortex and the associated flow dynamics within the bubble have been established. The interaction between the incoming jet and the vortex induces flow instabilities at remarkably low Reynolds number ($\mathrm{Re_{jet}} \sim 250$).

These findings present new insights into the physics of bubbles and establish a foundational basis for confined, continuously or intermittently fed small-scale vortex rings. This can be extended to other systems involving interface, membrane or flexible cavity such as droplet microfluidics, vesicle formation, balloons in soft robotics, medical devices, heart chambers, artificial organs and bio-propulsion such as jellyfish locomotion. A comprehensive understanding of internal flow dynamics may prove imperative for the effective design and control of these processes.

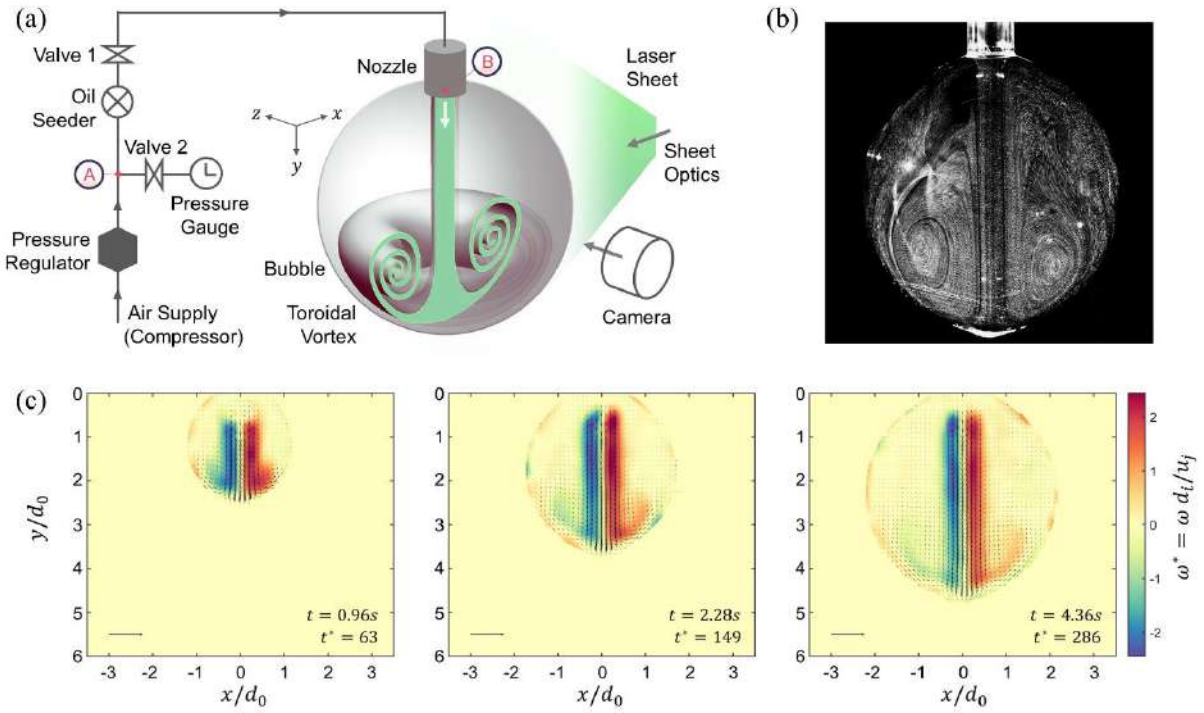

FIG. 1. (a) Schematic of the experimental setup (b) Long exposure mie-scattering images illustrating toroidal vortex motion of the seeded internal airflow within soap bubble (c) Vorticity field obtained using particle image velocimetry (PIV)

[1] S.J. Rao, S. Jain and S. Basu, Dynamics of soap bubble inflation, Phys. Rev. Fluids 9, L051602 (2024).

[2] L. Salkin, A. Schmit, P. Panizza, and L. Courbin, Generating Soap Bubbles by Blowing on Soap Films, Phys. Rev. Lett. 116, 077801 (2016).

[3] M. Grosjean and E. Lorenceau, Unstable growth of bubbles from a constriction, Phys. Rev. Fluids 8, 053602 (2023).

On the fluid dynamics of electrospinning: A novel method to generate stable cone-jet simulations in truncated domain

Ghanashyam K C[1]*, Swasthika Arunachalam[2], Satyavrata Samavedi[3], Harish N Dixit[1].
[1] *Department of Mechanical and Aerospace Engineering, IIT Hyderabad, Hyderabad, India,* me21resch11001@iith.ac.in
[2]*Department of Chemical Engineering, IIT Hyderabad, Hyderabad, India,* ch21resch11007@iith.ac.in
[3]*Department of Chemical Engineering, IIT Hyderabad, Hyderabad, India ,* samavedi@che.iith.ac.in
[1]*Department of Mechanical and Aerospace Engineering, IIT Hyderabad, Hyderabad, India,* hdixit@mae.iith.ac.in

ABSTRACT

Electrospinning is a technique that creates polymeric non-woven meshes by applying high voltage to a viscoelastic polymer solution from a metal needle at a fixed flow rate. Numerous prior efforts have aimed to simulate stable cone-jet formation in electrospinning and study the underlying physics. Herrada et al. [1] utilised a truncated domain method, only focusing on the stable cone-jet regime while avoiding the formation of instabilities. Their approach was based on the analytical expression of Gañán-Calvo et al. [2] for voltage distribution across the domain. Their method utilizes the far-field electrostatic field around a semi-infinite cylinder and applies it as the boundary condition on a truncated numerical domain. Since the extent of the cone-jet region is much smaller than the typical tip-to-collector distance in experiments, the truncation method proposed by Herrada et al. is computationally attractive. In this study, we show that the analytical expression used in the literature for the electrostatic field underpredicts the strength of the field. As a result, a reduced electrostatic force near the needle tip leads to a mismatch between experiments and simulations. We further propose a robust alternative for truncated domain electrohydrodynamic simulations that accurately predicts the electric field distributions in the vicinity of the needle. Through a careful choice of appropriate domain sizes that exactly match the experimental domain size, we set up a simulation protocol resulting in different modes, including the stable cone-jet mode. We will present a detailed study of these modes, as well as direct comparisons of mode maps against experimentally generated data using PEG-200. We shall also present interface comparisons for the stable cone-jet mode against experimental shapes obtained with PEG-200.

Keywords: Electrohydrodynamics, Electrospinning, Taylor cone, Instability, Leaky dielectric model.

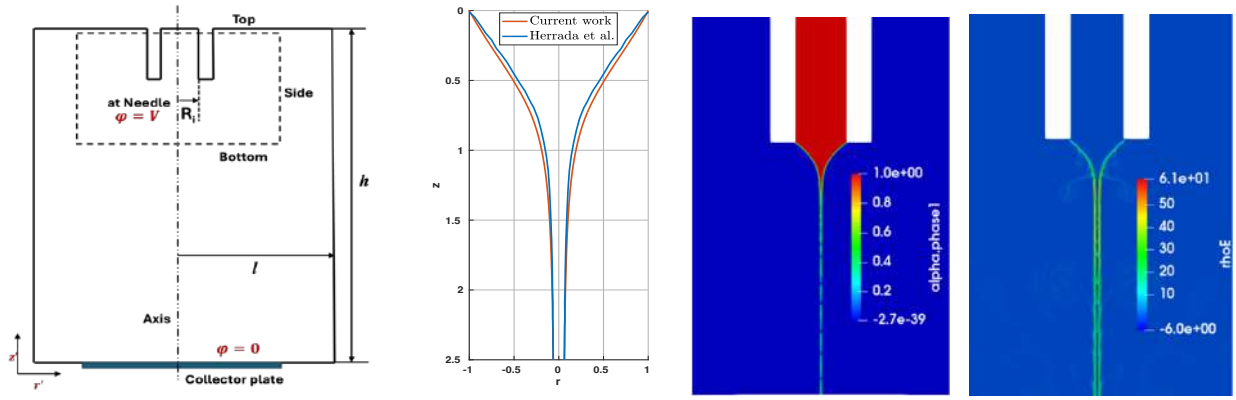

(a) **(b)** **(c)** **(d)**

Figure 1: (a) Overall domain with dotted lines indicating truncation lines for the stable cone-jet and boundary conditions in red, where ϕ represents voltage. (b) Validation with Herrada et al.'s [1] experimental results using 1-octanol, comparing interfaces. (c) Volume fraction distribution. (d) Charge density (C/m^3) distribution

REFERENCES

[1] M.A. Herrada, J.M. López-Herrera, Alfonso M Gañán-Calvo, E.J. Vega, J.M. Montanero, S. Popinet, *Numerical simulation of electrospray in the cone-jet mode*, Physical Review E **86**(2), 026305 (2012).

[2] A.M. Gañán-Calvo, J.C. Lasheras, J. Dávila, A. Barrero, *The electrostatic spray emitted from an electrified conical meniscus*, Journal of Aerosol Science **25**(6), 1121–1142 (1994)

Onset of Chaotic mixing in asynchronous time-periodic Stokes flows

Prabhash Kumar Prahallada Jutur, Anubhab Roy and Mahesh Panchagnula

Department of Applied Mechanics and Biomedical Engineering, Indian Institute of Technology Madras

We experimentally and numerically investigate the influence of asynchronous time oscillation on particle trajectories in time-periodic Stokes flows. Using a T-section model equipped with stepping motors and piston assemblies, we introduce pulsation dynamics that generate oscillating Stokes flow characteristics. Our findings demonstrate that geometric asymmetry, quantified by the parameter ϕ in time-periodic flow at vanishing Reynolds number, is crucial for initiating convective mixing. This mixing transitions to chaos under specific combinations of ϕ and the non-dimensional oscillation frequency *Sr*. We explain how the stretch-and-fold mechanisms at finite asymmetry drive convective mixing across different ϕ and *Sr* values through detailed experimental and numerical analyses. We construct a regime map in the generalized ϕ-*Sr* parameter space, identifying a chaotic mixing region and marking the boundary of this zone. Our findings highlight the critical role of geometric asymmetry in wall-bounded, time-periodic Stokes flows, with significant implications for particle transport in various physical, biological, and industrial systems.

Orientation dynamics of an anisotropic particle in homogeneous isotropic turbulence and in the presence of an external electric field

Himanshu Mishra*, Pijush Patra†, and Anubhab Roy*

We investigate the orientation dynamics of a spheroid in homogeneous isotropic turbulence and in the presence of an external electric field. At the scale of the spheroid, we assume that viscous effects dominate the flow, and thus, the dynamics can be studied in the Stokesian regime. Further, when the size of the spheroid is smaller than the Kolmogorov scale, the flow field around the particle can be modeled locally as a stochastic linear flow. This approximation becomes particularly useful when studying the orientation dynamics of spheroids in homogeneous isotropic turbulence and when the orientation dynamics of the spheroid is governed by the Jeffery equation[1], which involves the local fluctuating velocity gradient. The turbulent velocity gradient is obtained from the stochastic model given by Girimaji and Pope[2]. The model uses the log-normal distribution of the pseudo-dissipation rate. In the presence of an external electric field, the spheroid aligns in the direction of the electric field. We study the competition due to the torque induced by the turbulent velocity gradient and the electric field. The orientation dynamics is analyzed by varying a non-dimensional parameter Σ, which is defined as a ratio of the Kolmogorov time scale and the electric relaxation time scale. For lower values of Σ, we show that the spheroid exhibits an isotropic orientational distribution, whereas it fluctuates along the direction of the electric field at higher values of Σ. We calculate moments of the orientation distribution at large electric field limits using asymptotic methods and compare them with numerical calculations. A second-order moment in the orientation, which quantifies the fluctuations in the orientation, depends on Σ and the shape of a spheroid. The fourth-order moment of the orientation, a measure of the non-Gaussian statistics of the orientation distribution, increases from its Gaussian value with the increase in Taylor-scale Reynolds number.

*Dept. of Applied Mechanics and Biomedical Engineering, Indian Institute of Technology Madras, Chennai, India, 600036

†Nordita, KTH Royal Institute of Technology and Stockholm University, Hannes Alvéns väg 12, 23, SE-106 91 Stockholm, Sweden

[1]Jeffery, *Proc. R. Soc. London, A.* **102**, 161-179 (1922).

[2]Girimaji and Pope, *Phys. Fluids* **2**, 242-256 (1990).

Oscillating ultrasonic contrast agents near a deformable wall

Shambhu Anil*, Pushpavanam S†

Indian Institute of Technology, Madras, Chennai – 600036, Tamil Nadu, India

Ultrasound contrast agents are microbubbles encapsulated with a biocompatible shell that can oscillate radially in the presence of ultrasound with minimal interface deformation. UCAs are injected directly into an area of interest in the human body and used for ultrasonic vascular imaging, drug delivery and tumour detection. However, issues like allergic reactions and premature collapse of the encapsulated bubble renders UCAs as the lesser used imaging tool. Previous studies [1, 2, 3] consider potential flow around the bubble and focus on radial flow dynamics of the bubble using method of images. This results in generation of an undesirable slip at the walls.

In this study, we consider two cases (i) a UCA near a wall in 3D spherical coordinates and solve for the fluid flow around the bubble using Navier Stokes and Continuity equation. We perturb the system using the inverse of Strouhal number as the smallness parameter and use stream function formulation and matched asymptotic expansions near the wall to rectify the non – zero wall slip problem faced when using method of images. The shear stress at the wall is calculated from the non – oscillatory second order flow field. (ii) a UCA trapped equidistantly between two rigid walls. Method of images fails to deliver in this case because of infinite reflections leading to divergent Bjerknes force. Instead, we take the one wall problem and use method of reflections to satisfy no slip and no penetration in the other wall. Also, the effect of various parameters like radius of the bubble (R_0) and distance from the wall (L) on resonance frequency and shear stress at the walls is also studied to determine stability and biological feasibility of the UCA.

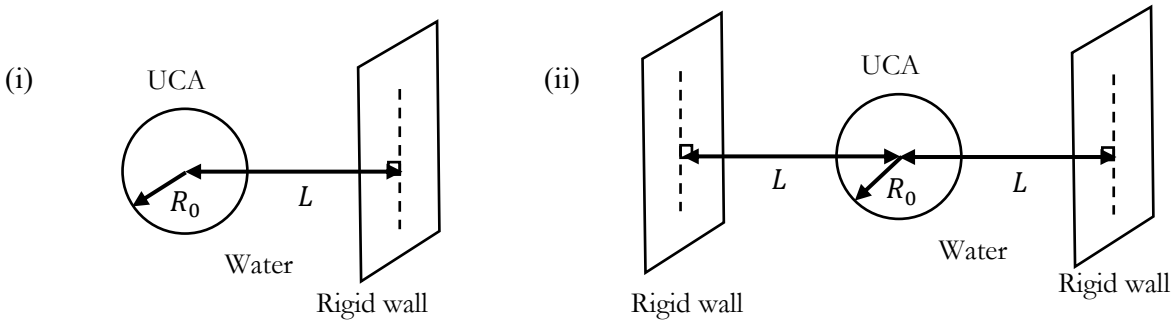

Figure 1: Schematic of both the cases under study in this work. (i) Bubble close to a rigid wall (ii) Bubble trapped equidistantly from two rigid walls.

References

[1] E Sassaroli and K Hynynen *Resonance frequency of microbubbles in small blood vessels: a numerical study* Phys. Med. Biol. 50 5293, 2005.

[2] H. N. Oğuz and A. Prosperetti *The natural frequency of oscillation of gas bubbles in tubes* J. Acoust. Soc. Am. 103 (6), June, 1998.

[3] A. A. Doinikov, S. Zhao, P. A. Dayton *Modelling of the acoustic response from contrast agent microbubbles near a rigid wall* Ultrasonics 49 (2009) 195–201

†Email: spush@iitm.ac.in
*Email: shambhu.anilkumar@gmail.com

Particle focusing in a microfluidic cavity

Subhas Nandy[1], Niladri Sekhar Satpathi[1], and Ashis Kumar Sen[1,2]

[1 1]*Fluid Systems Lab, Dept. of Mechanical Engineering, Indian Institute of Technology Madras, Chennai-600036, India*

[2] *Micro Nano Bio –Fluidics Group, Indian Institute of Technology Madras, Chennai-600036, India,* ashis@iitm.ac.in

Controlled manipulation and alignment of suspended microparticles and cells play a vital role in diverse engineering and biomedical applications, including tissue engineering, material science, and functionalization of microparticles for specialized drug delivery applications [1-3]. Using ultrasonic waves in fluid-filled cavities has emerged as a promising tool for controlling the arrangement of microparticles with high precision and low input power requirements while being non-invasive and label-free in nature. Most acoustofluidic devices reported in the literature rely on operations at resonant frequencies, corresponding to dimensions of devices conforming to integral multiples of the half-wavelength of the acoustic wave in the fluid. Dynamic- field-driven acoustofluidic devices have relied on the employment of multiple transducers which require complex peripherals and control, thus affecting the ease of handling of the devices. In this study, we present a novel acoustofluidic device design that allows clustering of particles in a microfluidic cavity coupled to a single piezoelectric transducer. The potential of the device design was studied through experiments, while our numerical results highlight the generality of the approach that can be extended to a multitude of applications.

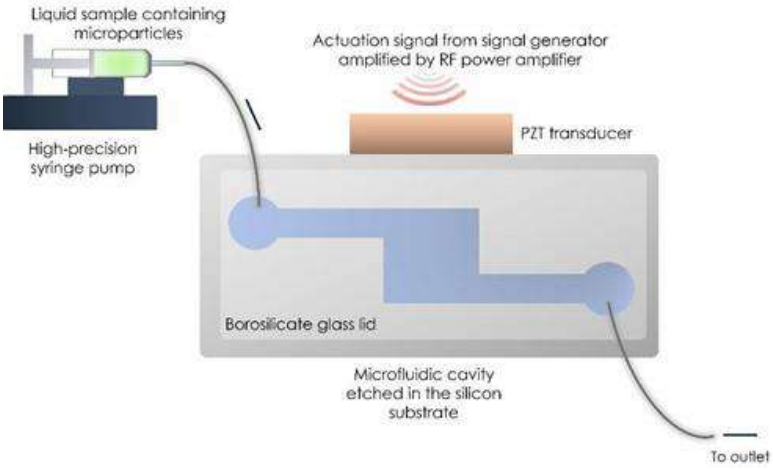

FIG. 1. Schematic illustration of the experimental setup for studying the acoustic field distribution in a microfluidic cavity. The PZT vibration source is coupled to a signal generator and a RF power amplifier (not shown in the figure for brevity).

An acoustofluidic device consisting of a glass-silicon-glass configuration was fabricated using standard photolithography techniques. A microfluidic cavity was etched at the center of the silicon substrate, with inlets and outlets connected at an offset w.r.t the center of the cavity and the silicon substrate was bonded to borosilicate glass, using anodic bonding. The experimental procedure has been reported in our previous work [4] and the arrangement has been schematically illustrated in Figure 1(a). A range of particle sizes was chosen for the purpose of this work. In order to prevent sedimentation of particles during the course of experiments, density-gradient medium Optiprep^{TM}, 15% by volume, and microparticles were added into the solution through micropipettes. The resulting solution was placed in an ultrasonic cleaner to ensure homogeneous mixing prior to starting of experiments.

The microparticle solution is injected into the device through a high-precision syringe pump (neMESYS pump, Cetoni, Germany). Once a uniformly distributed arrangement of microparticles is achieved in the microfluidic cavity, the syringe pump is turned off and experiments were performed under no-flow conditions. Under acoustic actuation, the particles migrate and form a cluster, and achieve a stable configuration. At the end of each experiment, the microparticles are flushed out through the outlet. The acoustophoretic particle focusing is found to be most efficient at the resonant frequency of the fabricated device. The experimental image of the particle aggregate formed in the microfluidic cavity is shown in

Figure 2(a).
The acoustic pressure distribution obtained from numerical simulations exhibits a distinct resonance peak which closely resembles experimental observations. The complex interplay of acoustic radiation forces and streaming-induced drag forces is illustrated in Figure 2(b), which influences the trajectories of the particles during acoustophoretic migration, resulting in interesting dynamics of suspended microparticles.

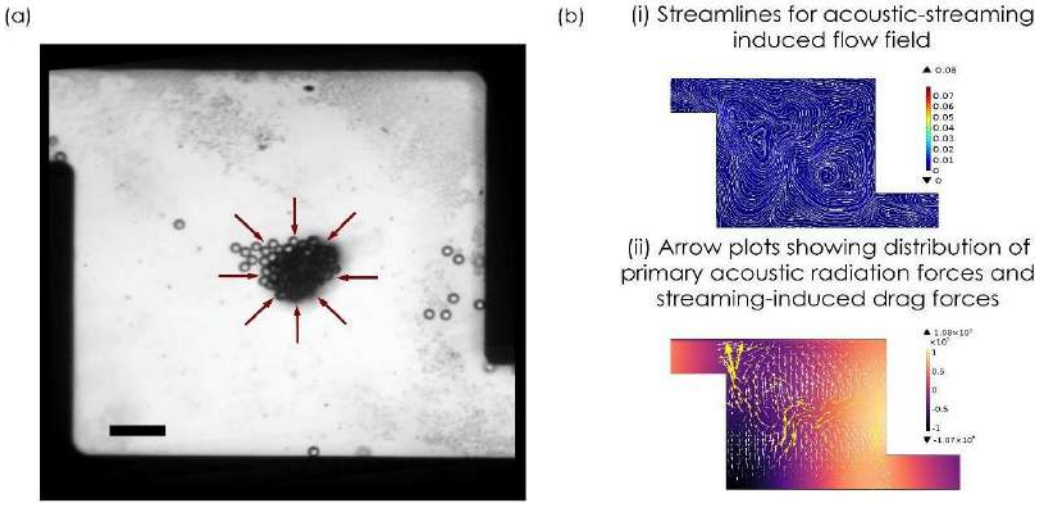

FIG. 2. (a) Experimental image showing the aggregation of microparticles in the microfluidic cavity under the combined effect of acoustic radiation forces and acoustic streaming induced drag forces (scale bar measures 100 μm), (b) Numerical simulation results showing the distribution of acoustic streaming patterns (top row), and arrow plots showing the complex interplay of primary acoustic radiation forces (white) and streaming-induced drag forces (yellow) (bottom row) corresponding to the dominant resonant frequency of the device. The color legend in the bottom row corresponds to the acoustic pressure distribution in the cavity for the respective frequency.

In this study, we report the development of an acoustofluidic device wherein, the inherent design of the microfluidic cavity facilitates the generation of acoustic fields under actuation from a single piezoelectric transducer source. It is worth noting that our experimental setup does not suffer from any significant depreciation in coupled acoustic energy density. The absence of complex synchronization among the electronic peripherals retains the dexterity of microfluidic approaches while making our acoustofluidic device suitable for a plethora of applications. Our continued efforts will be directed at understanding the underlying physics of particle dynamics and discovering the latent challenges.

[1] R. Barnkob, P. Augustsson, T. Laurell, and H. Bruus, *Measuring the Local Pressure Amplitude in Microchannel Acoustophoresis*, Lab Chip **10**, 563 (2010).

[2] P. Augustsson, C. Magnusson, M. Nordin, H. Lilja, and T. Laurell, *Microfluidic, Label-Free Enrichment of Prostate Cancer Cells in Blood Based on Acoustophoresis*, Anal. Chem. **84**, 7954 (2012).

[3] Z. Dong, D. Fernandez Rivas, and S. Kuhn, *Acoustophoretic Focusing Effects on Particle Synthesis and Clogging in Microreactors*, Lab Chip **19**, 316 (2019).

[4] L. Malik, A. Nath, S. Nandy, T. Laurell, and A. K. Sen, *Acoustic Particle Trapping Driven by Axial Primary Radiation Force in Shaped Traps*, Phys. Rev. E **105**, 1 (2022).

Pore-scale simulations of thinning-elastic fluids within idealized porous media

Sourabh Dhawan[1], Rahul Kailas Ovhal[1], Malay Kumar Das[1], and Pradipta Kumar Panigrahi[1]

[1] *Department of Mechanical Engineering, Indian Institute of Technology, Kanpur-208016, India*

I. ABSTRACT

Fluid flow in porous media is a topic that researchers and scientists are particularly interested in since it has many applications in biology [1], engineering, and earth sciences. Enhancing oil recovery in the petroleum sector is one significant application of fluid flow in the porous medium [2,3]. Researchers commonly use non-Newtonian viscoelastic fluids [4] made of polymer and water-based mixtures to extract oil from reservoir dead ends. Likewise, in the biomedical field, the analysis of non-Newtonian blood flow in the blood vessels is vital for managing cardiovascular diseases such as aneurysms and atherosclerosis. A prevalent therapeutic strategy for treating aneurysms involves the insertion of porous materials into the bulging section of the blood vessel [1]. Understanding blood flow through these porous materials is crucial; consequently, pore-scale simulations provide valuable insights into the complex fluid dynamics at play. These simulations deepen our understanding of hemodynamic behavior and guide the development of more effective treatment strategies.

In fluid flow investigation through porous media, simulations are generally performed at the macroscopic scale, where the governing equations are averaged over a Representative Elementary Volume (REV). This method absorbs the complex pore structure into macroscopic parameters such as porosity and permeability. Darcy's law $\left(q = -\frac{K}{\mu}\frac{dP}{dx}\right)$ must be brought up when talking about Newtonian fluid flow in porous media since it establishes a linear relationship between the macroscopic flow velocity (q) and the pressure drop $\left(\frac{dP}{dx}\right)$ across the porous medium at low Reynolds numbers. Yet, the fact that the viscosity of non-Newtonian fluid depends on the local shear rate makes it difficult to apply Darcy's law to it. Accurate determination of local viscosity necessitates a detailed understanding of pore-level flow dynamics, rendering Darcy's law impractical for non-Newtonian fluids. In an attempt to apply Darcy law, the equivalent viscosity, known as "porous medium equivalent viscosity", is proposed for non-Newtonian fluids in porous media at low Reynolds numbers [3]. This viscosity is further dependent on the porous medium shear rate. The relationship between the flow rate and the characteristic length scale of the porous medium is what determines this shear rate:

$$\dot{\gamma}_m = \alpha \frac{q}{\sqrt{K\varepsilon}} \tag{1}$$

where α is the scaling factor introduced to match the porous medium equivalent viscosity with the fluid's actual viscosity. The literature suggests that the scaling factor is influenced by both the properties of the porous medium and the rheological characteristics of the fluid. Jithin et al. [5] used the purely shear-thinning Carreau-Yasuda model to simulate blood flow through regular and stochastically reconstructed porous media. They proposed a correlation between equivalent viscosity and shear rate in porous media for various pore morphologies incorporating the scaling factor. Further, they relate the scaling factor to the quantifiable macroscopic characteristics of the porous medium. However, their study was restricted to fluids exhibiting purely shear-thinning behavior. Given the well-established viscoelastic properties of blood, this study aims to simulate its flow using the multimode sPTT (mm-sPTT) model, which accurately captures the rheological behavior of blood as it moves through idealized porous media with varying porosities [6,7].

In the present study, we employ the idealized porous media for pore-scale simulations, as they offer simplified yet representative structures that effectively capture essential flow and transport characteristics. We thoroughly modify geometric parameters to achieve variations in permeability and porosity, using distinct configurations shown in Figure 1(A). The geometries under examination include Inline Circle (In-Ci), Inline Square (In-Sq), Staggered Circle (St-Ci), and Staggered Square (St-Sq). This approach allows us to explore the porosity values of 0.4, 0.6, and 0.8 across all geometric configurations. Here, we model whole blood as an incompressible, shear-thinning, and viscoelastic fluid using the multi-mode sPTT models [6–8].

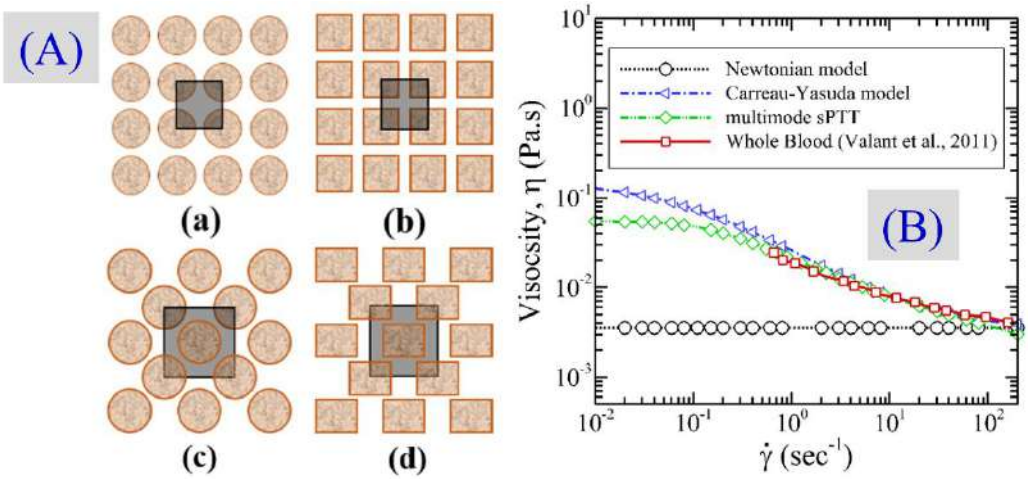

Figure 1(A) Different pore-scale geometries employed in the current numerical simulations, and (B) Comparison of the apparent viscosity predictions for human blood [9] between the mm-sPTT and the Carreau-Yasuda model.

For comparison, we also conduct simulations under the assumption that blood behaves as a Newtonian fluid (serving as a reference case) alongside a non-Newtonian thinning-elastic fluid. This approach allows us to investigate the impact of blood elasticity on hemodynamics at the pore scale. The model parameters of the mm-sPTT model are as follows:

Table 1: Parameters of the multimode sPTT model [6]

Modes (k)	Multimode sPTT model		
	$\eta_p^k(Pa.s)$	$\lambda_k(s)$	$\varepsilon_k(-)$
1	0.05	7	0.2
2	0.001	0.4	0.5
3	0.001	0.04	0.5
4	0.0016	0.006	0.5
5 (solvent)	$\eta_S = 0.0012$		

Further, Figure 1(B) illustrates the rheological behavior of human blood as predicted by the Newtonian model, the Carreau-Yasuda model, and the multi-mode sPTT model. Next, to validate the accuracy of our solver, we performed simulations of viscoelastic fluid flow governed by the mm-sPTT model and contrasted the results with those presented by Cruz et al. [10], as depicted in Figure 2.

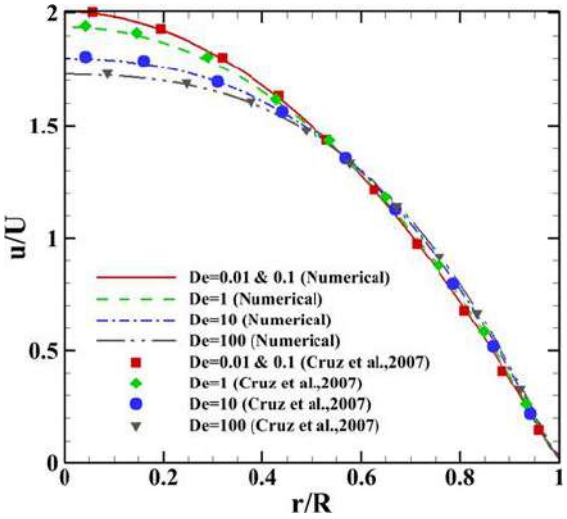

Figure 2. Normalized velocity profiles for multimode sPTT model across varying Deborah numbers in the pipe flow, compared with the results from [10].

In Figure 3, we present a comparative analysis of flow predictions from the Newtonian model and the mm-sPTT model at a Wi of 20, specifically examining In-Sq, In-C, St-Sq, and St-C pore configurations, all characterized by a porosity of 0.6. The velocity contours are normalized relative to the velocity at the inlet's center point. The streamlines superimposed on the velocity contours

demonstrate that the flow field for the Newtonian case is symmetric. However, in the viscoelastic flow scenario, two key observations emerge: (a) the flow field exhibits noticeable asymmetry, and (b) vortex tilting is observed within the inline geometries. This tilting phenomenon is attributed to the elastic hoop stresses generated along the curved streamlines in viscoelastic fluids. The elastic effects are particularly significant in the inline square and inline cylinder configurations due to the pronounced extensional forces caused by continuous large deformations as the fluid moves through contraction and expansion regions, where the expansion-contraction ratio is greater than that found in staggered geometries.

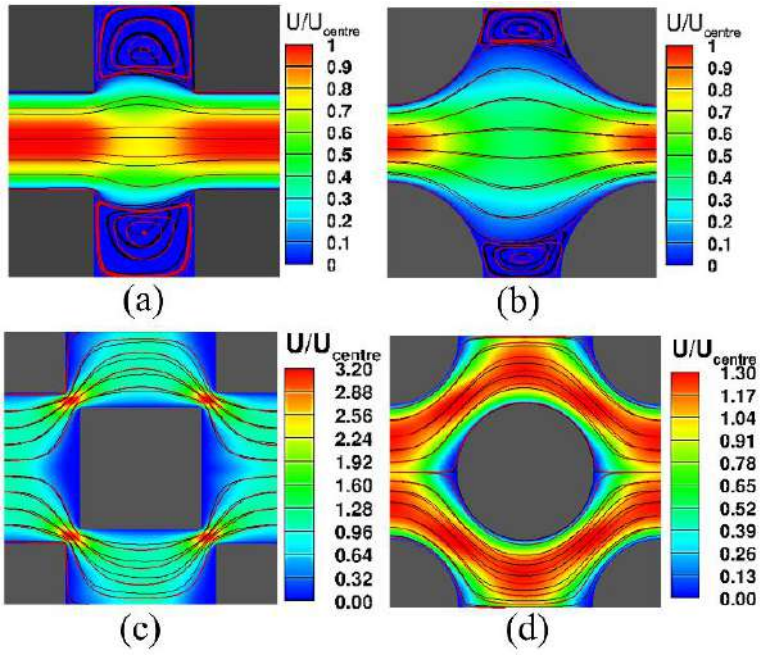

Figure 3: Normalized velocity contours overlaid with streamlines for viscoelastic fluid ($Wi = 20$, black color) and Newtonian fluid (red) illustrating flow fields in (a) In-Sq, (b) In-Cyl, (c) St-Sq, and (d) St-Cyl configurations.

In the analysis of blood flow through porous media, viscosity variations depend on shear rates, which are intrinsically related to the pore-scale characteristics of the porous structure. The Weissenberg number (Wi) serves as a critical control parameter, representing the fluid's elasticity in viscoelastic flows and being directly influenced by the shear rate. By adjusting the Wi, one can effectively regulate the shear rate. The apparent relative viscosity, defined as the ratio of the apparent viscosity of the viscoelastic fluid to that of a Newtonian fluid - both assessed using Darcy's law - is calculated using the following equation:

$$\eta_{app} = \frac{\left(\frac{\Delta p}{q}\right)_{Viscoelastic}}{\left(\frac{\Delta p}{q}\right)_{Newtonian}} \tag{2}$$

Figure 4(a) depicts the variation of apparent viscosity for the viscoelastic fluid as the Wi increases, across different levels of porosity. Importantly, the mm-sPTT model does not exhibit shear-thickening behavior with increasing Weissenberg numbers; instead, it consistently reveals shear-thinning behavior throughout the examined range of Weissenberg numbers, regardless of the geometry considered. The primary aim of this study is to understand how pore-throat configurations influence the estimation of apparent relative viscosity when accounting for blood elasticity. To achieve this, it is essential to incorporate pore structure information into a pore-length scale-based definition of the Wi. This approach allows for the consolidation of all graphs shown in Figure 4(a) into a single line of variation. Consequently, the Wi can be expressed in relation to the length scales of the porous media, as shown in the following equation:

$$Wi_k = \lambda_m \dot{\gamma}_{eff} = \lambda_m \alpha \frac{q}{\sqrt{K\phi}} \tag{3}$$

To ascertain the value of n for the fluid under investigation, we created a plot of apparent relative viscosity versus the dimensional shear rate $\left(q/\sqrt{K\phi}\right)$, as illustrated in Figure 4(b). A curve was fitted

to the data points using MATLAB's cftool, resulting in a constant value of $n = 0.7$ from the fitted model. Figure 4(b) illustrates that the apparent relative viscosity agrees well with the fitted line derived from the proposed model. Nonetheless, the observed deviation arises from the constraints of depending solely on the shear rate determined through dimensional analysis, as highlighted by the expression $\left(q/\sqrt{K\phi}\right)$.

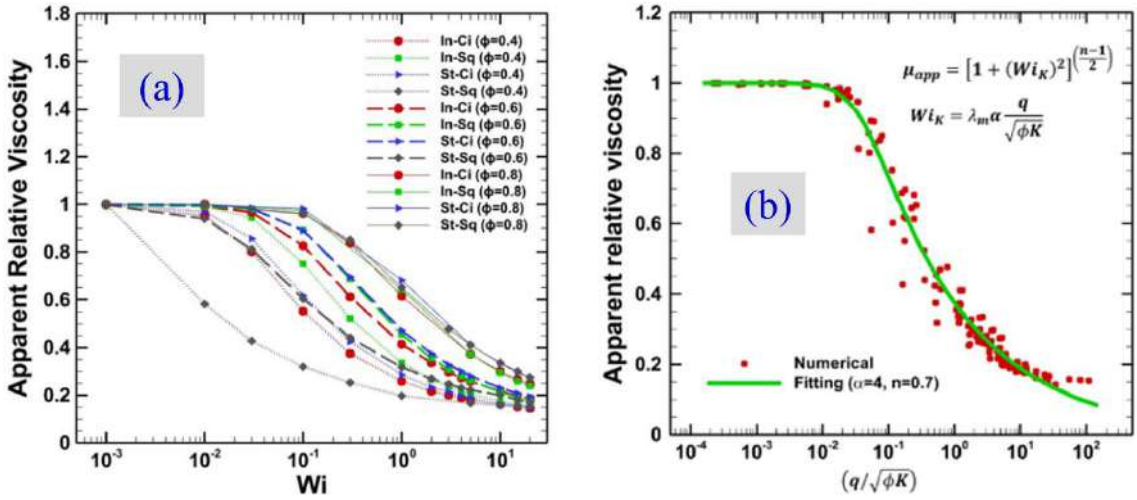

Figure 4(a) Variation of apparent relative viscosity with increasing Weissenberg number, and (b) variation of apparent relative viscosity with dimensional shear rate.

Consequently, analogous to the Newtonian viscosity employed in Darcy's law, we can derive a "porous medium equivalent viscosity" for the mm-sPTT model that accurately accounts for the shear-thinning and viscoelastic behavior of blood. This derivation is based on the macroscopic characteristics of the porous media utilized in aneurysm treatment. As a result, we can effectively apply Darcy's law to viscoelastic shear-thinning fluids using this equivalent porous medium viscosity. This study not only advances our understanding of blood flow dynamics within complex porous structures but also offers crucial insights for optimizing medical treatment strategies.

II. REFERENCES

[1] P.K. Pandey, M.K. Das, Effect of foam insertion in aneurysm sac on flow structures in parent lumen: relating vortex structures with disturbed shear, Phys. Eng. Sci. Med. 44 (2021) 1231–1248. https://doi.org/10.1007/s13246-021-01058-3.

[2] X. Lopez, P.H. Valvatne, M.J. Blunt, Predictive network modeling of single-phase non-Newtonian flow in porous media, J. Colloid Interface Sci. 264 (2003) 256–265. https://doi.org/10.1016/S0021-9797(03)00310-2.

[3] T. Tosco, D.L. Marchisio, F. Lince, R. Sethi, Extension of the Darcy-Forchheimer Law for Shear-Thinning Fluids and Validation via Pore-Scale Flow Simulations, Transp. Porous Media 96 (2013) 1–20. https://doi.org/10.1007/s11242-012-0070-5.

[4] S. Dhawan, M.K. Das, P.K. Panigrahi, Analysis of viscoelastic flow past a square cylinder in a channel with sudden contraction, Phys. Fluids 35 (2023). https://doi.org/10.1063/5.0149092.

[5] M. Jithin, N. Kumar, A. De, M.K. Das, Pore-Scale Simulation of Shear Thinning Fluid Flow Using Lattice Boltzmann Method, Transp. Porous Media 121 (2018) 753–782. https://doi.org/10.1007/s11242-017-0984-z.

[6] L. Campo-Deaño, R.P.A. Dullens, D.G.A.L. Aarts, F.T. Pinho, M.S.N. Oliveira, Viscoelasticity of blood and viscoelastic blood analogues for use in polydymethylsiloxane in vitro models of the circulatory system, Biomicrofluidics 7 (2013). https://doi.org/10.1063/1.4804649.

[7] S. Dhawan, P.K. Pandey, M.K. Das, P.K. Panigrahi, A Computational Analysis of the Impact of Blood's Viscoelastic Properties on the Hemodynamics of a Stenosed Artery, in: K.M. Singh, S. Dutta, S. Subudhi, N.K. Singh (Eds.), Fluid Mech. Fluid Power, Vol. 4, Springer Nature Singapore, Singapore, 2024: pp. 655–669.

[8] A. Chauhan, C. Sasmal, Effect of real and whole blood rheology on flow through an axisymmetric stenosed artery, Int. J. Eng. Sci. 169 (2021) 103565. https://doi.org/10.1016/j.ijengsci.2021.103565.

[9] A.Z. Valant, L. Žiberna, Y. Papaharilaou, A. Anayiotos, G.C. Georgiou, The influence of temperature on rheological properties of blood mixtures with different volume expanders-implications in numerical arterial hemodynamics simulations, Rheol. Acta 50 (2011) 389–402. https://doi.org/10.1007/s00397-010-0518-x.

[10] D.O.A. Cruz, F.T. Pinho, Fully-developed pipe and planar flows of multimode viscoelastic fluids, J. Nonnewton. Fluid Mech. 141 (2007) 85–98. https://doi.org/10.1016/j.jnnfm.2006.09.001.

Prediction of Droplet blockage through deformable stenosed microconfinement

Kumar Amit[1], Ashwani Assam[1], and Abhishek Raj[1]
[1]Department of Mechanical Engineering, IIT Patna, Bihar-801106, India

I. ABSTRACT

Understanding droplet migration in stenosed microchannels is crucial for various applications. This study explores how droplet properties (viscosity, surface tension, density, and diameter) and channel characteristics (stenosis degree and wall elasticity) affect droplet movement and blockage in deformable stenosed microchannels (see Fig. 1(a-e)). Higher viscosities lead to lubrication film formation between droplet and wall, reducing viscous resistance; while increased surface tension enhances wall adherence, amplifying Laplace pressure. Droplet entry is primarily influenced by viscosity, while passage is governed by surface tension and curvature effects at the droplet-wall interface. Surface tension dominates pressure generation in the channel and within the droplet, influencing wall deformation and hydrodynamic resistance. The study examines the relationship between droplet viscosity, density, surface tension, channel wall elasticity, and the maximum Capillary number (Ca_{max}) on the lubrication film thickness between the droplet and the channel wall. A lubrication film exists for $Ca_{max} \geq 0.095$, reducing blockage chances (see Fig. 1(f)). A critical range of the modified Ohnesorge Number ($Oh^* \times 1000 \leq 132$) and Capillary number ($Ca_{max} < 0.095$) indicates higher chances of droplet blockage *(see Fig. 1(g))*. Additionally, the study explores the impact of channel wall elasticity on droplet entry, transit, and hydrodynamic resistance. Higher wall elasticity facilitates faster entry but introduces curvature during passage, increasing frictional resistance and blockage likelihood as the wall softens.

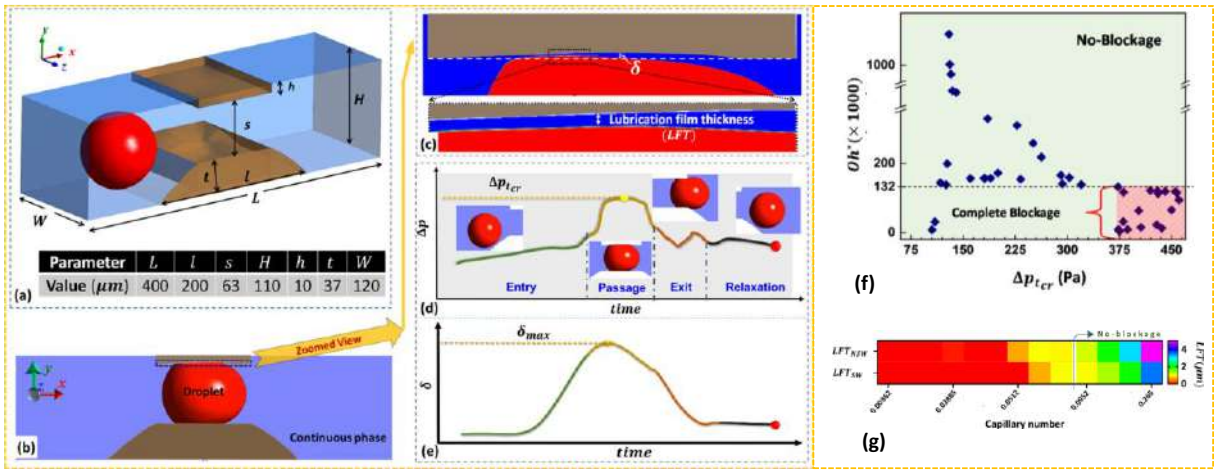

FIG. 1. Schematic of (a) the isometric view of the simulated 3D model with the parametric definition at the time when the flow is about to onset, and (b) the side view (x–y plane) of the model used in the study. The deformable solid domain is shown with a brown color. (c) The zoomed view near the top wall showing the wall deformation and the lubrication film thickness. The schematic of (d) the pressure across the stenosed region and (e) the wall deformation with time. (f) Critical modified Ohnesorge number for the prediction of complete blockage of confined microchannels, (g) Regime of no-blockage cases in terms of capillary number.

Radiation force and torque on a dielectric Janus particle

Mohd Meraj Khan[1*], Sumesh P. Thampi[2], Anubhab Roy[1]

[1] Dept. of Applied Mechanics, Indian Institute of Technology Madras, Chennai, India

[2] Dept. of Chemical Engineering, Indian Institute of Technology Madras, Chennai, India

Optical levitation to control and move microparticles is widely used in bio and medical sciences [1]. One type of microparticle that has received significant attention is the Janus particle, which has applications in nanotechnology, medicine, and biology [2]. Janus particles are characterized by their two different chemical properties, which have been extensively studied in the literature. In this study, we focus on the electromagnetic scattering of a two-dimensional Janus cylinder with different dielectric constants on each half. We investigate the radiation force and torque on the cylinder at various angular orientations relative to an incident electromagnetic wave. We use the lattice Boltzmann method (LBM) to compute the total (sum of incident and scattered) electric and magnetic fields at the surface of the cylinder. Our method has been validated for scattering by curved surfaces, following the work of Hauser and Verhey [3]. In our simulations, we consider a square domain with sides equal to 25 times the radius of the cylinder and place the Janus particle at the centre of the domain. We use a TM^z polarized monochromatic plane wave as the incident wave travelling in the x direction and compute the total electric and magnetic fields at the surface of the cylinder. Finally, we determine the radiation force ($\boldsymbol{F} = \oint(\mathbb{T}\cdot\hat{\boldsymbol{n}})dl$) and torque ($\boldsymbol{\Gamma} = \oint[\boldsymbol{r}\times(\mathbb{T}\cdot\hat{\boldsymbol{n}})]dl$) on the Janus cylinder, where $\mathbb{T}$ is the Maxwell stress tensor [4].

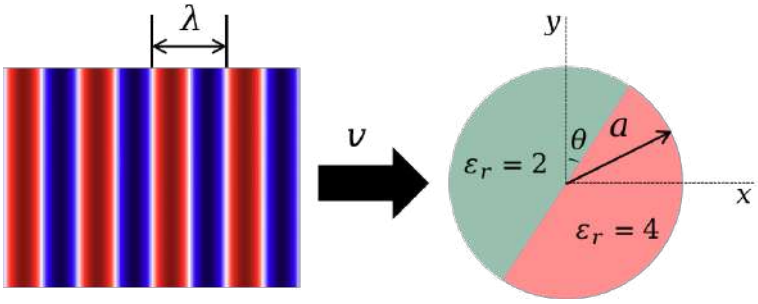

Figure 1: A monochromatic plane wave incident upon a dielectric Janus cylinder.

References

[1] J. Millen et. al., *Optomechanics with levitated particles* , Rep. Prog. Phys., **83**, 36pp, 2020.

[2] Wauer, Jochen, and Tom Rother *Electromagnetic scattering on Janus spheres* Journal of Quantitative Spectroscopy and Radiative Transfer **253** 2020

[3] A. Hauser and J. L. Verhey, *Stable lattice Boltzmann model for Maxwell equations in media*, Phys. Rev. E, **96**, 063306, 2017.

[4] Mishchenko, Michael I., Larry D. Travis, and Andrew A. Lacis. *Scattering, absorption, and emission of light by small particles* Cambridge university press, 2002.

*am19d041@smail.iitm.ac.in

RAYLEIGH-BÉNARD-MARANGONI CONVECTION IN A BINARY FLUID SYSTEM

Anubhav Dubey[1], Saumyakanta Mishra[2] , S.V. Diwakar[2] and Sakir Amiroudine[1]

[1]Université de Bordeaux, I2M, UMR CNRS 5295, Talence F-33400, France
[2]Engineering Mechanics Unit, Jawaharlal Nehru Centre for Advanced Scientific Research, Bangalore, 560064, India

Keywords: Binary fluids, Phase field method, Linear stability analysis

Abstract

A pair of partially miscible liquids, exhibiting an upper-critical solution temperature (UCST) is considered in order to investigate the effect of miscibility on the onset criteria of Rayleigh-Bénard-Marangoni convection. We deployed a modified phase-field approach to track the continuous evolution of the smearing interface from the state of immiscibility to miscibility via partially miscible states. The numerical methodology employed, in an improvement to our previous model[1], accurately captures the Korteweg stresses above the UCST. The proximity to the UCST (T_c) is characterized by a parameter r, where $r = \frac{T_c - T}{T_c}$. This parameter is incorporated while defining the free energy functional as a function of temperature. The convective flow could manifest in numerous ways depending upon the thermophysical and geometrical properties of the individual fluid layer[2]. A spectral[3] collocation-based linear phase field model is deployed to study the onset characteristics. The critical Rayleigh number and the growth rate was found to be a function of interface location in the domain and the parameter r. The window for the oscillatory mode of convection is found to a function of the parameter "r" due to the dynamic linking of interfacial tension with the localized concentration gradient.

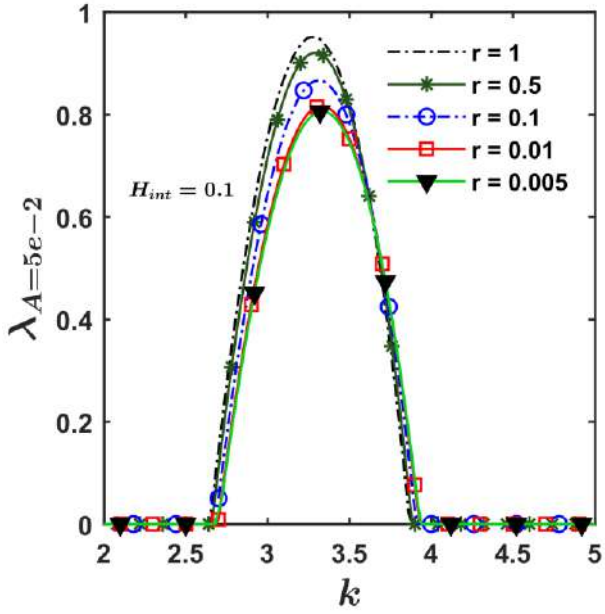

(a)

[1] M. Bestehorn, D. Sharma, R. Borcia and S. Amiroudine, "Faraday instability of binary miscible/immiscible fluids with phase field approach", Phys. Rev. Fluids, 6, 064002, (2021).
[2]D. Johnson and R. Narayanan, "Geometric effects on convective coupling and interfacial structures in bilayer convection", Physical Review E, 54(4), 3102-3104 (1997).
[3] S.V. Diwakar, S. Tiwari, S.K. Das and T. Sundararajan, "Stability and resonant wave interactions of confined two-layer Rayleigh-Bénard systems", J. Fluid Mech., 754, pp. 415-55 (2014).

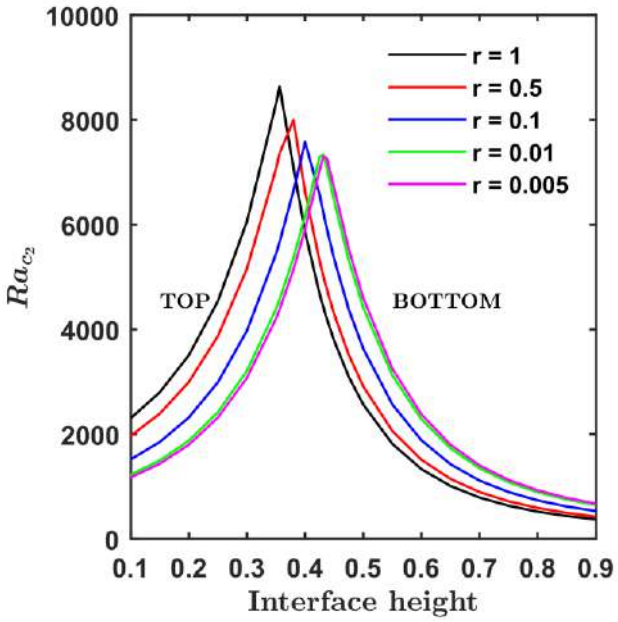

(b)

Fig1. (a) Variation of growth rate (calculated at $A = 5e - 2$, where $A = \frac{Ra - Ra_c}{Ra_c}$) with wavenumber for interface located at $h1 = 0.1$ for varying r, (b) Variation of critical Rayleigh number with interface height for varying r

Rheology and dynamics of soft attractive microcapsules

Hugues Bodiguel[1], Mehdi Maleki[1], Nishant Nair[1], Benjamin Cross[2], Romain Lhermerout[2], Clément de Loubens[1]
[1] *Univ. Grenoble Alpes, CNRS, Grenoble-INP, LRP UMR 5520, Grenoble, France*

Topic(s): Low Reynolds suspensions: from single particle to collective behavior

Key words: Micro-capsule, suspension, gel, electrostatic interactions

Abstract:

We are interested in the rheological properties of dense suspensions of deformable particles because of their biological (e.g. blood) and industrial (e.g. microcapsules) interest. We study as a system microcapsules of about 100 micrometers composed of a membrane obtained by complexation of polyelectrolytes at the water-oil interface (Xie et al., Soft Matter, 2017). Homogeneous suspensions in size and mechanical properties are generated through a membrane emulsification process. In addition, the elastic properties of the particles are characterized through automated measurement of their deformation in a microfluidic elongational flow chamber (Maleki et al. Chem. Eng. Sci., 2021). The rheological properties of the suspensions are characterized in oscillatory rotational rheometry, steady-state rheometry, and shear reversal experiments for volume fractions ranging from 20 to 55%.

Surprisingly, the suspensions obtained show a Bingham-like behavior with a flow threshold for volume fractions of 25%. The threshold increases with the volume fraction. Oscillation measurements show that the elastic modulus of the suspension increases with time, signature of aggregations in the system over time, cf figure showing clusters of microcapsules. The elastic properties of the microcapsules have little influence on the results. The viscoelastic behavior of the suspension after a pre-shearing, in order to break the clusters of capsules, is characteristic of a behavior of attractive colloidal suspensions (Trappe and Weitz, PRL, 2000). We perform various shear reversal experiments. These experiments highlight that the flow threshold is associated with the formation of a microstructure under flow. Above the threshold, the behavior of the microcapsule suspension is very similar to that of rigid sphere suspensions with lubricated contacts.

In conclusion, the microcapsule system formed by polyelectrolyte complexation has attractive colloidal particle behavior for particle sizes of several hundred micrometers. The flow threshold is related to underflow structuring, while above this threshold the suspension behaves as a suspension of non-crushing spheres.

In order to better understand the physical origin of the attraction between capsules, we perform direct observation of the interaction between two particles, under an AC electric field. Depending on the frequency, different regimes are observed. At high frequency, the capsules attract each other, and this behavior is in agreement with electrically induced dipole-dipole interaction. Decreasing the frequency down to a few Hz, we observe a more complex and surprising behavior. The capsules attract themselves until close contact and then repel each other before attracting again. This periodic bouncing of the capsules is interpreted as the result of electrostatic interaction between capsules, in addition to the Coulomb force due to the electric field. This interpretation indicates that the capsules are charged and exchange surface charge when come into contact.

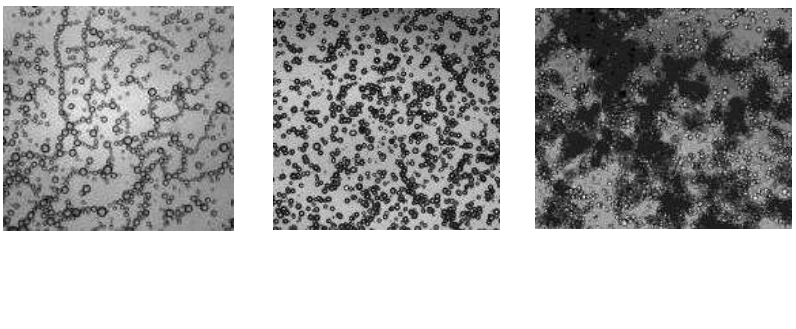

Figure 1:: From left to right: image of the suspension of microcapsules under an electric field; in a high permittivity silicone oil (AK1000); in a low permittivity silicone oil (AP1000); flow curve of suspensions of microcapsules in AK1000 at various volume fraction. The suspensions exhibit a yield stress at low shear rates, even at very low volume fraction.

Ribbing and fingering instabilities in liquid entrainment

J. John Soundar Jerome[1], Pierre Trontin[1] and Jean-Philippe Matas[1]

[1] *LMFA & Université Claude Bernard Lyon 1, 43 Bd du 11 Novembre 1918, , 69622, Villeurbanne, France*
jean-philippe.matas]univ-lyon1.fr

Emmanuel Nault[2,3], Juliette Cayer-Barrioz[3] and Denis Mazuyer[3]

[2]*Renault Group France*
[3]*LTDS, CNRS, Ecole Centrale de Lyon, 36 av. Guy de Collongue, 69130 Ecully, France*

I. RIBBING INSTABILITY

The entrainment of liquid along the outer rising wall of a cylinder is a common phenomenon observed in many applications, particularly in coating processes. While extensive research has been conducted on this flow at low Reynolds numbers, identifying various ribbing or fingering instabilities, our focus here is on scenarios where inertial effects become significant and even predominant.

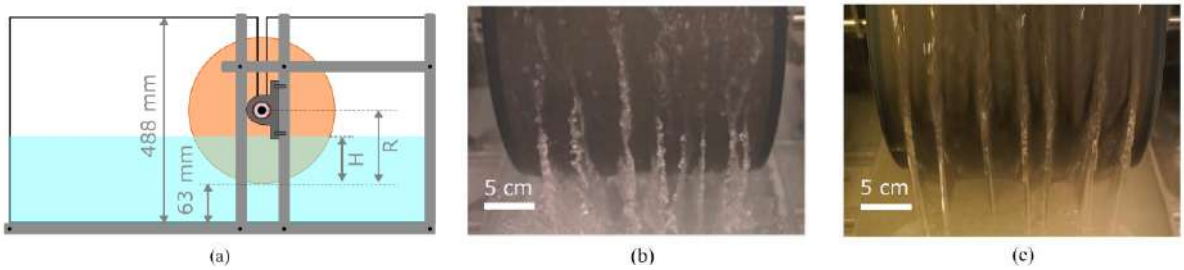

FIG. 1. Side view of experimental setup. Water depth can be changed to control the drum immersion b) Examples of ribbing patterns in water, linear velocity 3.8 m/s and c) water/UCON mixture of approximately 100 times the viscosity of water, 1.6 m/s. Immersion is 10% of drum radius in both cases.

A wheel of radius R = 19.5 cm and width 30 cm, partially immersed in a reservoir, is rotated about its horizontal axis, entrained by an asynchronous motor. The depth of immersion of the wheel is H. The bottom of the wheel is located at 6.3 cm above the tank floor. The liquid used can be either water, or a mixture of water and UCON oil (30% of UCON in mass), with dynamic viscosity up to 100 times that of water. We capture images of the liquid structures formed as the wheel drags the liquid out and analyze these images to extract intensity profiles along the wheel's width. MATLAB is then used to analyze these profiles and determine the location of each rib.

Additionally, we perform Direct Numerical Simulations (DNS) of this setup. The simulations involve solving the 3D, two-phase, incompressible Navier-Stokes equations using Basilisk [1]. A spatial adaptive octree grid is employed to handle the multi-scale nature of the problem effectively. The interface between the two immiscible fluids is tracked with a sharp geometric Volume-Of-Fluid (VOF) method. The computational domain consists of a cubic box of size Lb = 80 cm and a half cylinder with a radius of R = 20 cm and a length of Lb = 80 cm.

Our experimental results indicate that the wavelengths of the observed patterns are relatively insensitive to changes in rotation speed and immersion depth within the tested conditions. The

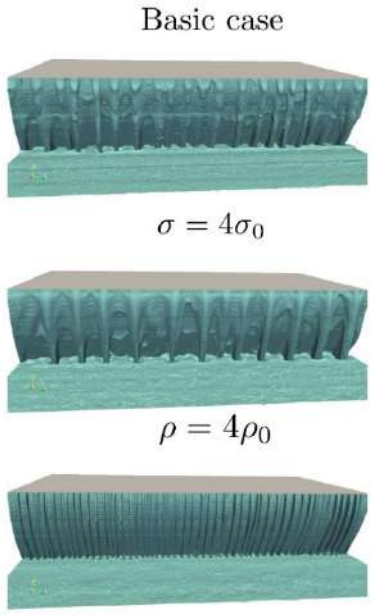

FIG. 2. Results of numerical simulation for: top, the experimental conditions of Fig. 1c ; middle : same velocity with surface tension increased by a factor 4 ; bottom : same as top with 4 times denser liquid.

measured wavelength is also very similar for both fluids investigated, varying between 3.5 and 4.5 cm. We propose that these axial patterns arise from a mechanism similar to the Saffman-Taylor (ST) instability [2,3] as the origin of such axial patterns. The most probable rib spacing predicted from this model is $\lambda* = 2\pi l_c 3/\xi$, where ξ is the nondimensional average adverse pressure gradient for the corresponding inclined flat plate drag-out flow under lubrication approximation, and l_c is the capillary length. This prediction agrees well with both the experimental and numerical data, in particular also when the liquid density and surface tension are varied (figure 2 where rib spacing can be doubled, or halved).

II. FINGERING INSTABILITY

We now look at the lubricating flow behind a contact, when a metal sphere rolls without slipping on a rotating disk covered in oil. Four oil viscosities are studied. The speed of the ball and of the rotating disk upon which it is pressed at a constant force can be controlled precisely on our tribometer. The disk is transparent, and the flow around the contact can then be visualized easily. The contact appears as a dark disk on Fig. 3, surrounded by Newton rings. A cavitation bubble forms behind the contact above a threshold velocity, due to the steep pressure variations in the lubricated contact (Fig. 3).

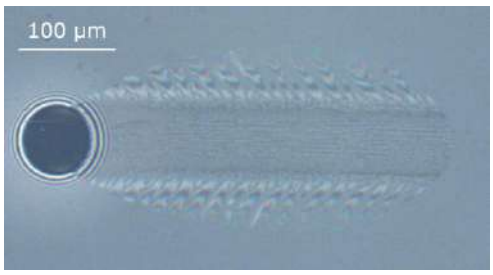

FIG. 3. Stationary elastohydrodynamic contact, steel bead, glass disk, 5 N normal force, viscosity 77 mPa.s, 5 cm/s. A bubble forms downstream of the contact.

A fingering instability is observed just after the contact, and along the walls of the bubble. The wavelength and growth rate of this instability are observed to respectively decrease and increase when oil viscosity and speed are increased (see Fig. 4). We demonstrate that these fingers arise because of the Couette-Poiseuille flow established downstream of the Hertzian contact, as in the well-known Printer's instability between two cylinders [3]. As we will illustrate, a simple model based on Saffman-Taylor instability captures the good order of magnitude of wavelength and growth rate for these fingers as a function of the local thickness, and of the Capillary number.

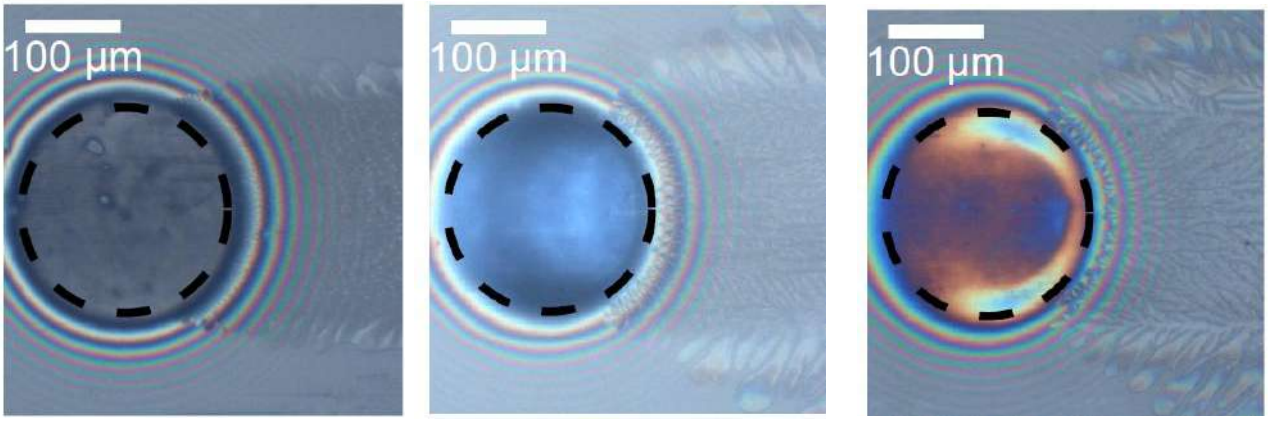

FIG. 4. Visualization of the flow downstream the contact when a sphere rolls on a lubricated plane at 1 cm/s: oil viscosity is (from left to right) 0.074 Pa.s ; 0.71 Pa.s and 3.3 Pa.s.

[1] Popinet S. *An accurate adaptive solver for surface-tension-driven interfacial flows*, J. Comp. Phys. 228, 5838-5866 (2009).
[2] Saffman P.G. & Taylor G.I. *The penetration of a fluid into a porous medium or hele-shaw cell containing a more viscous liquid*, Proc. R. Soc. London 245 (1242), 312-329 (1958).
[3] Reinelt D.A. *The primary and inverse instabilities of directional viscous fingering*, J. Fluid 285 (1242), 303-327 (1995).

Sedimentation and adhesion of red blood cells to a solid surface

Sainath H and Sarith P Sathian

S rpartmrnt of Applird Mrchanics and Biomrdical Enginrrring, IIT Madras, Chrnnai 600036,
hsainath92@gmail.com

I. Introduction

Blood is an excellent indicator of health. Hematological disorders cause significant changes in biophysical and morphological properties of the red blood cells (RBCs) [1], eventually affecting the rheology and physiological functions of blood. Sedimentation tests help in analyzing the aggregation behaviour of RBCs which usually takes place at rest/low shear rates in the presence of blood plasma proteins (esp. fibrinogen) forming large structures known as the rouleaux [2]. The subsequent deposition of red blood cells on a model surface is also simulated to investigate the extent of aggregation and analyze its preferred morphological configurations. The clustering of cells under healthy and pathological conditions can eventually be explored through comprehensive numerical modeling of RBCs, and altering the shape, viscoelastic properties of the cell membrane, plasmatic factors and surface characteristics.

II. Methodology

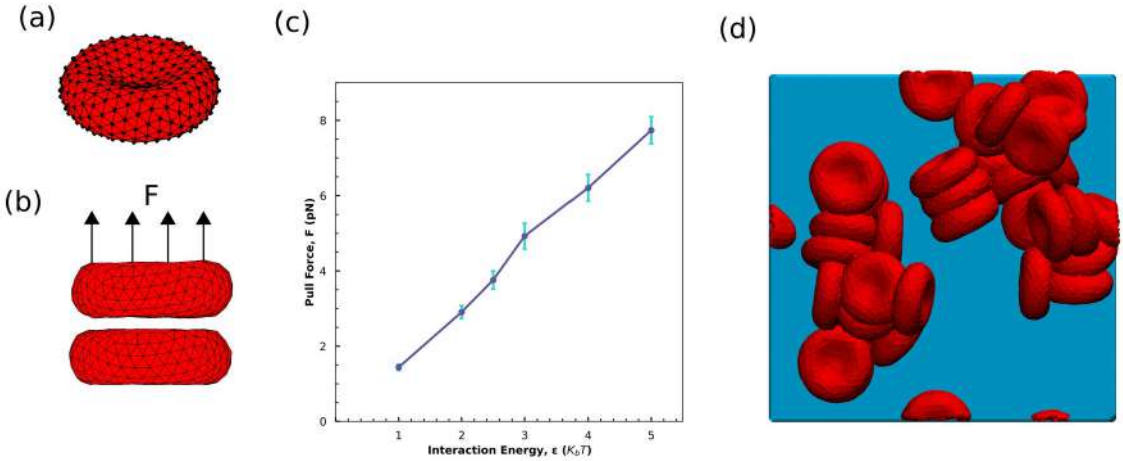

Figure 1: (a) Healthy 3D RBC model of diameter 7.8μm used for this study (356 nodes), (b) Simulation snapshot of two RBCs in aggregated state with the upper cell acted upon pull force F, c) Variation of pull force with cell-cell interaction energy, d) deposition of RBCs onto the surface.

The RBC model used in this study addresses a) membrane viscoelasticity described by viscous contribution of the lipid bilayer and an elastic contribution of the spectrin network, b) area-incompressibility of the lipid bilayer and volume incompressibility of the inner cytoplasm and, c) bending resistance of the lipid bilayer, all of which critical to capture the viscoelastic nature of cells [3]. Cell mechanics along with it's cytoplasm and blood plasma, the physiological fluid surrounding the cell are simulated by using a mesoscopic, particle-based computational approach, called Dissipative particle dynamics (DPD). The interaction between the cells is modeled using a soft repulsive core LJ potential capable of imitating cell aggregation and the force required to pull them apart is determined to study their aggregation strength.

[1] Tomaiuolo, G., *"Biomechanical properties of red blood cells in health and disease towards microfluidics"*, Biomicrofluidics, 8(5), (2014).

[2] Baskurt O. K., Meiselman H. J., *"Erythrocyte aggregation: basic aspects and clinical importance"*, Clinical Hemorheology and Microcirculation, 53(1-2):23-37, (2013).

[3] Sainath H, Sarith P. Sathian, *"Dynamic response of red blood cells in health and disease"*, Soft Matter, 19, 1219-1230, (2023).

The value of force (F = 3.76pN) required to detach healthy cells obtained from simulations is close to those measured experimentally in autologous blood plasma with optical tweezers [4]. The simulations were performed in a cubic box of side 40μm incorporating 35 RBCs (hematocrit = 0.05) embedded in blood plasma placed at a mean height of 35μm above the surface. The cells are subjected to downward force due to existing density differences between RBC and plasma, mimicking sedimentation. The strength and nature of cell-wall adhesion is assumed to be similar to cell-cell interactions.

III. Results and Discussion

Radial distribution function (RDF) of the cell centers reveal the local microstructure of the suspension and its peaks indicate likely configurations of the interacting RBC doublets. We observe that at higher cell-cell interactions (RDF peak at 3μm), the RBCs doublets primarily remain aligned maintaining their biconcave contact zones, pertaining to sigmoid-concave or S-shape. The second peak at 5μm refers to doublets with the biconcave part of one cell attached to the rim part of the other. Finally the third peak at 8μm shows the presence of isolated cells deposited at the surface. We also recognized relatively smaller occurences of parachute and male-female doublets with either aligned or offset configurations in our simulations as typically found in blood smear studies [5].

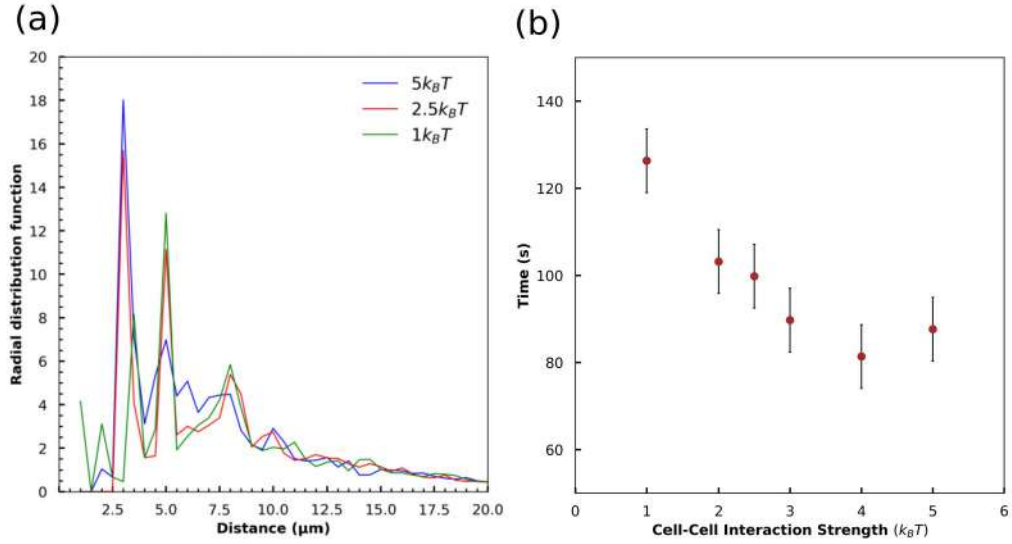

Figure 2: a) Radial distribution function of cell centers after adhering to the surface, and b) the total aggregation time against the cell-cell interaction strength.

The aggregation time is a sum total of settling time and the time required to form aggregates upon deposition. The aggregate formation itself is characterized by two phases, slow (primary rouleaux) and fast (large 3D aggregates) and completes in time of $O(10^2 s)$ [6]. Figure 2b presents a faster sedimentation rate as cell-cell interaction strength increases. The increase in interaction strength increases the propensity of RBCs to aggregate, forming large structures. This leads to lesser drag being experienced by the larger aggregate as the exposed surface area is less compared to isolated RBCs falling through the suspension, thus leading to faster settling. Finally, the projected area of the aggregates onto the surface and the evaluation of aggregation indices are performed through image segmentation to compare the different microstuctures.

---

[4] Ermolinskiy P., Lugovtsov A., Yaya F., Lee K., Kaestner L., Wagner C., Priezzhev A., *"Effect of red blood cell aging in vivo on their aggregation properties in vitro: Measurements with laser tweezers"*, Applied Sciences, 10, 7581 (2020).

[5] Flormann D., Aouane O., Kaestner L., Ruloff C., Misbah C., Podgorski T., Wagner C., *"The buckling instability of aggregating red blood cells"*, Scientific reports, 7(1), 7928 (2017).

[6] Hardeman, M., Goedhart P., Dobbe J., Lettinga K., *"Laser-assisted optical rotational cell analyser (lorca); i. a new instrument for measurement of various structural hemorheological parameters"*, Clinical hemorheology and microcirculation, 14(4), 605–618, (1994).

Self-propulsive micromotors and their force mechanics

Thilak Raj [a], Srestha Roy [b], Ashwin Kumar [c], Basudev Roy [b], Ethayaraja Mani [c d], Swathi Sudhakar [a d]

Abstract

Hypothesis: Synthetic micro/nanomotors are gaining extensive attention for various biomedical applications (especially in drug delivery) due to their ability to mimic the motion of biological micro/nanoscale swimmers. The feasibility of these applications relies on tight control of propulsion speed, direction, and type of motion (translation, circular, etc.) along with the exerted self-propulsive force. We propose to exploit the variation of both self-propulsion speed and force of active colloids with different patch coverages (with and without supporting layer) for engineering diffusiophoretic micro/nanomotors.

Experiments: The microswimmers were designed at various patch coverages (10°, 30°, and 90°) with (Ti/Pt) and without (Pt) an adhesion layer for the catalytic patch through glancing angle metal deposition (GLAD) technique. Mean-square displacement (MSD) analysis was performed to obtain the self-propulsion parameters like speed and angular speed. Using optical tweezers (OT), the self-propulsive force was measured from the force power spectral density.

Findings: The findings of our experiments suggest the non-requirement of any adhesion layer preceding the catalyst deposition since the Pt 10° colloidal batch had the maximal self-propulsion speed (4.61±0.3μm/s) and force (345±57fN) for 5% w/v H_2O_2 fuel concentration. Moreover, the self-propulsion speed and force decreased with increasing patch size, contrary to theoretical estimates. Also, the self-propulsive force obtained from MSD is 2 to 4 times lower in magnitude than the OT based force values. We believe that the self-propelling motion of the micromotors is possibly hindered due to interactions with the surface of the quartz cuvette during the optical microscopic analysis. Further, the MSD is limited to the self-propulsive motion in two dimensions. On the other hand, OT based force measurement involve trapping the particles in the bulk of the solution entirely avoiding the particle–substrate interactions. Hence, OT based force measurements are better than the propulsion velocity based stokes drag force estimates. We believe that this study can lay the foundation in designing efficient micro/nanomotors for translational biomedical applications.

Self-Organization of Micro/Nano Plastics

Dipankar Bandyopadhyay and Saurabh Dubey
Department of Chemical Engineering, Centre for Nanotechnology & Jyoti and Bhupat Mehta, School of Health Sciences and Technology, Indian Institute of Technology Guwahati

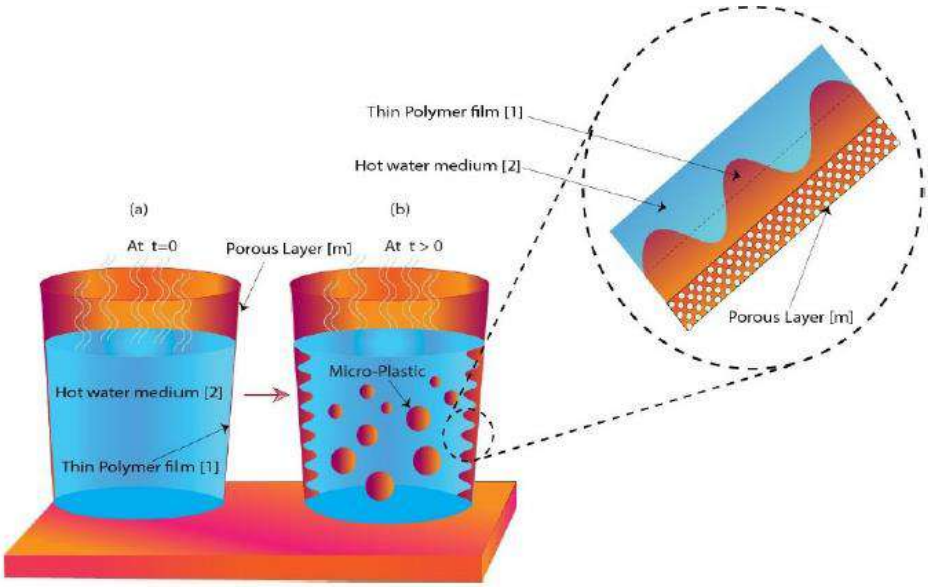

An average person drinking three regular cups of tea or coffee daily, in a paper cup, may ingest ~75,000 tiny micro/nano plastic particles, which has the potential to deposit in heart, kidney, liver, blood, and blood vessels of a human body. The characteristics of such occurrences can be studied employing a model system wherein the adhesion failure of a metastable thin film of polymer happens when it is sandwiched between bulk of hot water bath (e.g. coffee or tea) and a porous medium (e.g. paper cup). The ultrathin polymer film dewet and disintegrate under such a scenario to mimic the length scales that are typically identified during the micro/nano plastic formation. The influence of film thickness, surface physicochemical heterogeneities – polymer-water and porous-polymer, thermal gradients, and solvent exposure have been explored systematically to identify the typical length and times scales of the micro/nano plastic formation. The study suggests that, for micron thick polymer films, the phenomena may follow the length and time scales obtained from the classical Rayleigh-Taylor instabilities to engender micro plastic formation while the ultrathin polymer films may form nanoplastics under the influence of the van der Waals forces. We also show the example cases wherein magnetic microrobots can be used to remove such micro/nano plastics from such solutions in a non-invasive way.

Self-organized intracellular flows: computations and coarse-grained theory

Brato Chakrabarti[1]

[1] *International Center for Theoretical Sciences (ICTS), Bengaluru, India,* brato.chakrabarti@icts.res.in

Large cells often rely on cytoplasmic flows for intracellular transport, maintaining homeostasis, and positioning of cellular components. Understanding the mechanisms of these flows is essential for gaining insights into cell function, developmental processes, and evolutionary adaptability. Here, we focus on a class of self-organized cytoplasmic stirring mechanisms that result from fluid-structure interactions between cytoskeletal elements at the cell cortex. Drawing inspiration from streaming flows in late-stage fruit fly oocytes, we develop a computational framework to understand such emergent dynamics. This computational method combines ideas from fast kernel summation, efficient time integrators, and asymptotic reduction of fluid-structure interaction phenomenon. Using our simulations involving over half a million degrees of freedom, we reveal the conditions under which cytoplasmic flows emerge.

To understand such high dimensional problem, we then propose an analytically tractable *active carpet* theory. This model deciphers the origins and three-dimensional spatio-temporal organization of such flows. Through a combination of simulations and weakly nonlinear theory, we establish the pathway of the streaming flow to its global attractor: a cell-spanning vortical twister. Our study reveals the inherent symmetries of this emergent flow, its low-dimensional structure, and illustrates how complex fluid-structure interaction aligns with classical solutions in Stokes flow. Through a combination of theory, experiments, and computation, we then illustrate how the role of geometry is intrinsically tied to the spatiotemporal organization of the flow.

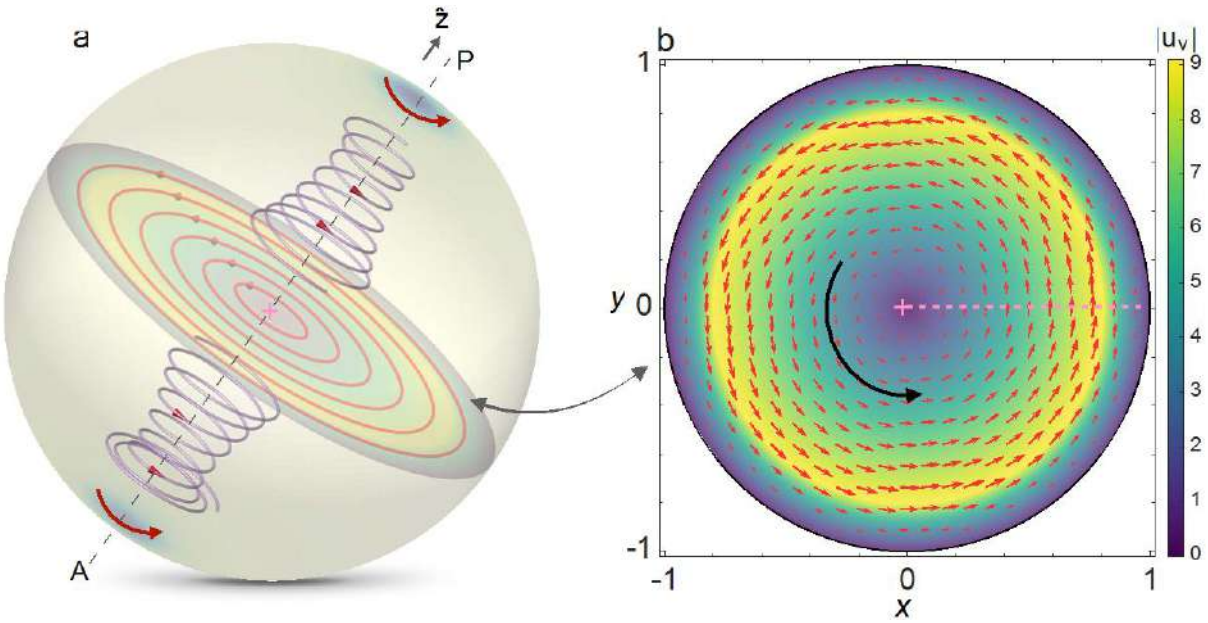

Figure 1: (a) Emergent flows inside a spherical egg cell. (b) Flow in the plane of vortex

Shear Stresses Alters Bacterial Physiology

Siddhant Jain[1], Anmol Singh[2], Nivedita Tiwari[1], Aparna Naik[1], Ritika Chatterjee[2], Dipshikha Chakravortty[2] and Saptarshi Basu[1]

[1] *Department of Mechanical Engineering, Indian Institute of Science, Bengaluru, sbasu@iisc.ac.in*

[2] *Department of Microbiology and Cell Biology, Indian Institute of Science, Bengaluru, dipa@iisc.ac.in*

From the tissue of humans, animals and plants to the deep tortuous soil pores and sea vents, motile bacteria live in different sophisticated and challenging habitats. Thriving in such stressful situations demands real-time evolution both morphologically and at cellular levels [1]. A lot has been studied about bacteria in the last century, however the physiological changes that bacteria experience due to the various types of stresses is less explored especially from Bio-Fluid Dynamics point of view.

In this study, we investigate how fluid-induced stresses affect the morphology and virulence of bacteria in microfluidic channels [2 , 3]. Our model organism is Klebsiella pneumoniae (KP), a clinical isolate and ESKAPE pathogen linked to various infections, including bloodstream infections. We create four distinct stress conditions by manipulating flow rates and channel geometries, which alter shear rates and exposure times. Our findings reveal notable structural changes in the bacteria under stress, with increased stress correlating with decreased viability. Interestingly, stressed bacterial samples show enhanced proliferation within RAW264.7 murine macrophages compared to unstressed ones. These results illuminate the intricate relationship between flow stresses and bacterial virulence. Additionally, we challenge the bacterial samples with ciprofloxacin to observe their responses under varying stress conditions. The insights from this research could inform models of severe infections like bacteremia and enhance our understanding of bacterial pathogenicity in realistic environments using organ-on-a-chip technology.

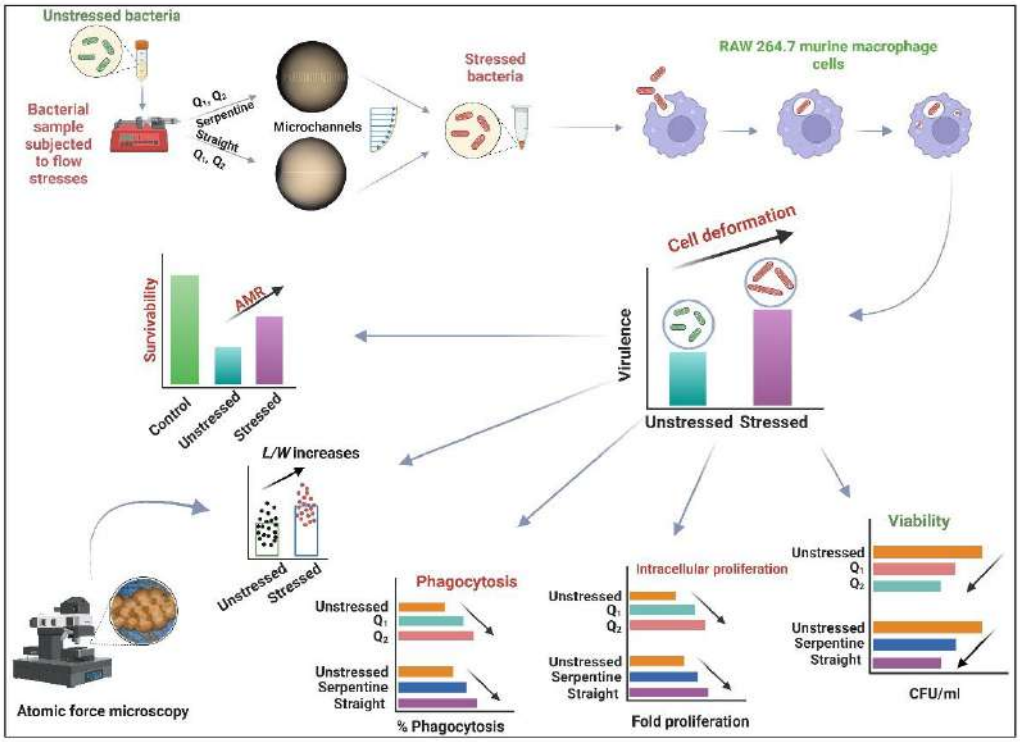

FIG. 1. Summary of the work.

[1] G. C. Padron et al., Bacteria in Fluid Flow. Journal of bacteriology, 205, 4 (2023)

[2] S. Jain et al., Observations on phenomenological changes in Klebsiella Pneumoniae under fluidic stresses, Soft Matter, 19, 9239-9253 (2023)

[3] S. Jain, D. Chakravortty, S. Basu, Interfacial Stresses within Droplets and Channels Influence Bacterial Physiology: A Perspective, Langmuir, 40, 33, 17161–17169 (2024)

Some Aspects Of Contact Line Dynamics

Stephane Zaleski
Sorbonne Universite

Contact line dynamics offers a challenging problem of computational fluid dynamics. Among the most difficult issues is the very wide range of scales involved, from orders of magnitude below the nanometer to the macroscopic scale in some cases. Attempts at investigating the contact line problem have been made from various approaches, the closest to first principles being molecular dynamics, while diffuse interface methods and sharp interface methods with several variants have also been put forward.
The talk will review the corresponding efforts made on a number of problems, including plunging and withdrawing plates, the sheared droplet, sessile droplets on oscillating or accelerating substrates, menisci in nanopores and the hydrodynamics assist problem. The issues involved in nucleate boiling and accelerated sessile droplets will be addressed both from the point of view of experiments performed by various colleagues and from simulations.

Spatio-temporal focussing of surface waves

Ratul Dasgupta

Indian Institute of Technology Bombay
Powai, Mumbai, Maharashtra-400076 - India

We study the spatio-temporal focussing of progressive capillary and gravitocapillary waves on the surface of a gas bubble and on a cylindrical deep pool of liquid respectively, originating from localised interface distortions. For moderate interface distortion, we find that near the focal point, large amplitude oscillations are generated. Linear theory is inadequate to describe these oscillations at the focus and nonlinearity through bound wave components play an important role. Analytical results will be compared to numerical simulations showing very good agreement [1, 2]. Viscosity has a non-intuitive effect in these and this will be discussed further using the linearised viscous equations as well as the nonlinear viscous, potential-flow equations.

References-

[1] Focussing of concentric free-surface waves, Kayal, Sanjay, Yewale, Kumar and Dasgupta (under review), 2024
[2] Capillary waves on a distorted bubble, Kayal, Sanjay and Dasgupta (in preparation), 2024.

The Regimes around Spreading and Splashing due to Falling Drops

Gautam Biswas and Ashwani K Pal
Department of Mechanical Engineering
Indian Institute of Technology Kanpur
Kanpur-208016, UP, India

Abstract

When a drop of a liquid passes through a gaseous medium and impacts on the gas-liquid interface of a liquid pool, depending on the size and velocity of the drop, it may create several outcomes. Based on the shape of the crater and its expansion and contraction time, the outcome can be one of the regimes within a wide range of regimes between coalescence and splashing (Rein, 1996).

The transition regimes between complete-coalescence and splashing of drops include jet formation with single or multiple tip drops. One of the main features in this regime is the formation of a central liquid jet followed by breakup of the jet in the form of tip-drops.

We perform investigations based on a coupled level-set and volume-of-fluid method to elucidate the earlier observations on this topic. The investigations reveal the creation of a variety of tip drops depending on the impact conditions. The present study also reveals that tip drops, larger than the initial drop, can be obtained at higher impact velocities. We identify the importance of capillary forces and cavity shapes on the formation of jets and other pertinent parameters that are responsible for drop ejection (Das et al., 2022).

In addition, we examine the coalescence dynamics of two ethanol drops of equal and unequal size, impacting an ethanol pool at low impact velocities (Kirar et al., 2022). By altering the separation distance between the drops and their size ratios, different coalescence outcomes, such as total coalescence, interacting partial coalescence, and non-interacting partial coalescence, have been observed.

One of our recent studies highlighted the salient features of splashing, specifically transition between spreading and splashing and expressing the transition as a function of Weber number and pool depth (Paul et al., 2024).

References:

[1]. M. Rein, 1996 The transitional regime between coalescing and splashing drops. ***J. Fluid Mech***. Vol. 306, pp. 145–165, (1996).
[2]. S. K. Das, A. Dalal, M. Breuer, G. Biswas, Evolution of jets during drop impact on a deep liquid pool, ***Physics of Fluids***, Vol. 34, pp. 022110-1 -- 022110-10, (2022).
[3]. P. K. Kirar, S. D. Pokale, K. C. Sahu, B. Ray, G. Biswas, Influence of the interaction of capillary waves on the dynamics of two drops falling side-by-side on a liquid pool, ***Physics of Fluids***, Vol. 34, pp. 112114-1 -- 112114-10, (2022).
[4]. A. Paul, A.K. Pal, A- B. Wang, G. Biswas, Splashing impact of a falling liquid drop, ***Physics of Fluids***, Vol. 36, (2024).

Thermocapillary Instability of a Surfactant-laden Heated Falling Film

Arnab Choudhury[1] and Arghya Samanta[2]

[1] *Department of Applied Mechanics, IIT Delhi, New Delhi-110016, India,* arnab.choudhury@am.iitd.ac.in
[2] *Department of Applied Mechanics, IIT Delhi, New Delhi-110016, India,* arghya@am.iitd.ac.in

The linear thermocapillary instability of a two-dimensional gravity-driven shear-imposed incompressible viscous film flowing over a uniformly heated inclined wall is studied when the film surface is contaminated with an insoluble surfactant. We intend to extend the prior research of Wei [1] to the case of a non-isothermal viscous film. As a result, the energy equation is incorporated into the governing equations along with the mass conservation and momentum equations. In the present study, we have found two additional thermocapillary S- and P-modes in the low to moderate Reynolds number regime, along with the known H-mode (surface mode) and surfactant mode reported by Wei [1]. The long-wave analysis predicts that the surfactant Marangoni number (M_S) has a stabilizing impact on the H-mode, but the thermal Marangoni number (M_T) has a destabilizing impact. These opposing effects produce an analytical relationship between them for which the critical Reynolds number for the H-mode instability of the non-isothermal film flow coincides with that of the isothermal film flow. On the other hand, the numerical result exhibits that the surfactant Marangoni number has a stabilizing influence on the thermocapillary S-mode and P-mode. More specifically, these thermocapillary instabilities diminish with an increase in the value of the surfactant Marangoni number. However, these thermocapillary instabilities can be made stronger by increasing the value of the thermal Marangoni number. The ensuing results are depicted in the Fig. 1, when $Ka = 500$, $\theta = 15^{\circ}$, $Pr = 7$, $B = 1$, and $Pe_S = 1000$. Here, Ka, Pr, B, Pe_S and θ denote Kapitza number, Prandtl number, Biot number, surfactant Peclet number and angel of inclination of the plane respectively. Furthermore, the thermal Marangoni number destabilizes the surfactant mode instability, but the onset of instability is not affected in the presence of the thermal Marangoni number, which is in contrast to the influence of the surfactant Marangoni number on the onset of surfactant mode instability. Interestingly, the Biot number, which measures the ratio of heat convection and heat conduction, shows a dual role in the surfactant mode instability, even though the threshold of instability remains the same. In the high Reynolds number regime, the shear mode appears and is stabilized by the surfactant Marangoni number but destabilized by the thermal Marangoni number. Moreover, the comparison of results with inertia and without inertia exhibits a stabilizing role of inertia in the surfactant mode.

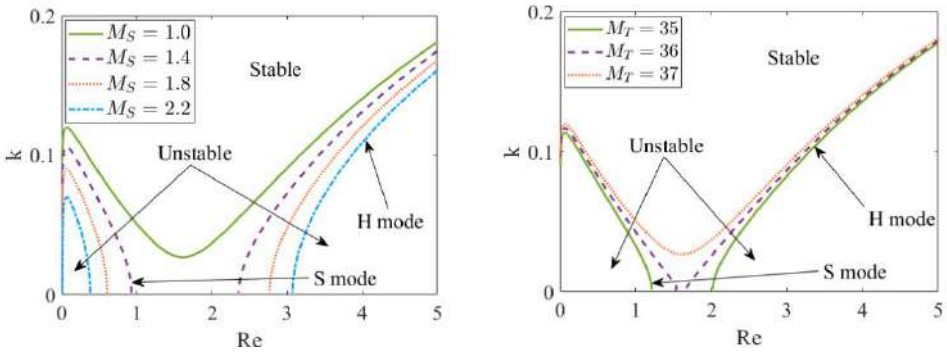

FIG. 1. (a) Variation of the neutral stability curves for the H-mode (surface mode) and S-mode in (Re, k) plane for different values of M_S when $M_T = 37$ and $\tau = 0.5$. (b) Variation of the neutral stability curves for the H-mode and S-mode in (Re, k) plane for different values of M_T when $M_S = 1$ and $\tau = 0.1$. Here, τ denotes the dimensionless imposed shear stress at the free surface.

REFERENCES

[1] H. H. Wei, Effect of surfactant on the long-wave instability of a shear-imposed liquid flow down an inclined plane, Phys. Fluids **17**, 012103 (2005).

Thermo-Electro-Hydrodynamic (TEHD) convection induced by dielectric loss

Harunori Yoshikawa[1] and Innocent Mutabazi[2]

[1] *Faculty of Science and Engineering, Doshisha University, 1-3 Tatara Miyakodani, Kyotanabe-shi, Kyoto 610-0321, Japan* hayoshik@mail.doshisha.ac.jp

[2] *Université Le Havre Normandie, Normandie Université, Laboratoire Ondes et Milieux Complexes,53 Rue de Prony, 76058 Le Havre Cedex, France,* innocent.mutabazi@univ-lehavre.fr

Dielectric liquids in an electric field **E** are subject to an electrohydrodynamic body force $\mathbf{f}_{EHD}$,

$$\mathbf{f}_{EHD} = \rho_e \mathbf{E} + \boldsymbol{\nabla}\left[\frac{\rho}{2}\left(\frac{\partial \epsilon}{\partial \rho}\right)_T \mathbf{E}^2\right] - \frac{\mathbf{E}^2}{2}\boldsymbol{\nabla}\epsilon,$$

where ρ_e is the net density of electric charge, ρ and ε are, respectively, the mass density and permittivity of the fluid, and T is the temperature. The first and second terms of this force represent Coulomb forces on free charges and the electrostriction. The last term arises from differential polarization of fluid and called *dielectrophoretic (DEP) force*. In electric fields of periods shorter than the charge relaxation time $\tau_e = \sqrt{\epsilon/\sigma}$ (σ: electric conductivity), the DEP force dominates the other components, unless the flow is compressible, and the fluid is bounded by mobile interfaces. The permittivity varies with fluid temperature. Its behavior can be modeled by a linear equation,

$$\hat{\epsilon} = \epsilon'\left(1 - e'\theta\right) + i\epsilon' \tan\delta\left(1 - e''\theta\right), \quad \text{with} \quad \theta = T - T_{\text{ref.}}$$

where $\hat{\epsilon}$ is the complex permittivity, ε' is the permittivity at a reference temperature T_{ref}, $\tan\delta$ is the loss tangent, and e' and e'' are the coefficient of thermal permittivity variation. The permittivity variation coupled with an alternating electric field results in the following DEP force component that can generate thermal convection inside the fluid even in microgravity environments,

$$\mathbf{f}_{conv.} = -\rho_{\text{ref.}}\alpha\theta\mathbf{G}_e + \mathbf{f}_R, \quad \text{with}$$

$$\mathbf{G}_e = \frac{\epsilon' e'}{2\rho_{\text{ref.}}\alpha}\left[\boldsymbol{\nabla}\left(\hat{\mathbf{E}}\cdot\hat{\mathbf{E}}^*\right) - ie_r\tan\delta\left((\boldsymbol{\nabla}\hat{\mathbf{E}}^*)\cdot\hat{\mathbf{E}} - (\boldsymbol{\nabla}\hat{\mathbf{E}})\cdot\hat{\mathbf{E}}^*\right)\right],$$

where $\hat{\mathbf{E}}$ is the complex amplitude of the electric field and * stands for the complex conjugate. The coefficient of thermal expansion of the fluid is denoted by α. The term $\mathbf{G}_e$, called *electric gravity*, is an analogue to Earth's gravity in the generation of thermal convection. The last force component $\mathbf{f}_R$ is a residual term independent of the temperature deviation θ.

The ability of DEP force to transport mass and momentum has been studied in view of applications, e.g., in biomedical engineering. Thermal convection due to the DEP force, i.e., TEHD convection, has also been investigated because of its analogy to the thermal convection under the gravity field. The effects of the dielectric loss have not been considered much [1]. We consider TEHD convection in liquid filling the gap of a horizontal parallel plate capacitor without any external source of temperature gradient. The dielectric loss creating a temperature gradient inside the fluid, the resulting force $\mathbf{f}_{conv.}$ can generate convection. The critical parameters and flow patterns will be discussed (Fig. 1). An energetic analysis will also be presented to determine the energy transfer mechanism from base to perturbation flows.

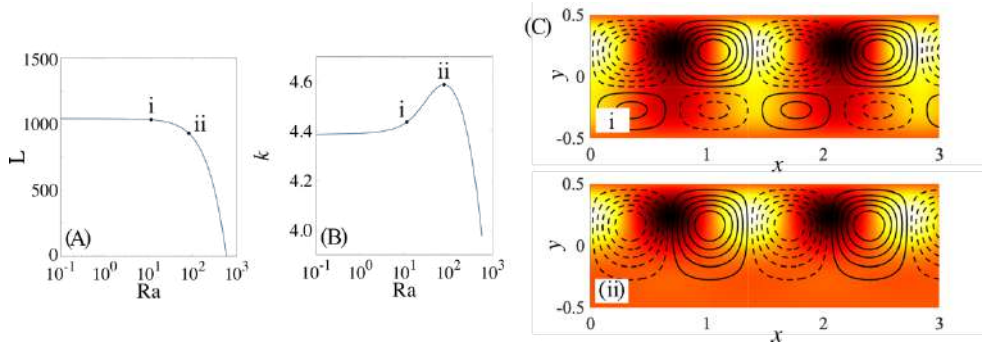

Fig. 1 Critical Rayleigh number L based on $\mathbf{G}_e$ (A) and wavenumber k (B) in function of the Rayleigh number Ra and critical eigenfunctions represented by streamlines and color-coded temperature fields (C).

[1] H. Yoshikawa, C. Kang, I. Mutabazi, F. Zaussinger, P. Haun, C. Egbers, Phys. Rev. Fluids, **5**, 113503 (2020).

THE ORIENTATION DYNAMICS OF A MASSIVE ELLIPSOID IN SIMPLE SHEAR FLOW

Sangamesh Gudda[1], Giridar Vishwanathan[2], Ganesh Subramanian[3]
[1] *Engineering Mechanics Unit, Jawaharlal Nehru Centre for Advanced Scientific Research, Bengaluru, India, sangameshguddabk@jncasr.ac.in*
[2] *nEye Systems, Berkeley, California, USA, vgiri1908@gmail.com*
[3]*Engineering Mechanics Unit, Jawaharlal Nehru Centre for Advanced Scientific Research, Bengaluru, India, sganesh@jncasr.ac.in*

Abstract:
The orientation dynamics of a massive ellipsoid in simple shear flow is studied in detail, where 'massive' refers to the limit of dominant particle inertia, as characterised by large Stokes number ($St \gg 1$). The dynamics consists of a fast conservative motion on a time scale of $O(\dot{\gamma}^{-1})$, involving a combination of spin, precession and nutation, and a slower dissipative component that modulates the angular momentum and rotational kinetic energy on asymptotically longer time scales of $O(St\dot{\gamma}^{-1})$; $\dot{\gamma}$ being the characteristic shear rate of the ambient flow. The spheroid is a special case where the fast motion comprises only a spin and a precession. The separation of time scales allows for use of the method of multiple scales for a spheroid, and the method of averaging for a triaxial ellipsoid, to derive an autonomous system of ODE's that govern motion on the four-dimensional slow manifold consisting of the three angular momenta and the rotational kinetic energy.

The case of an ellipsoid in simple shear flow is analysed in detail using the averaging method. There are three equilibrium (fixed) points in the slow manifold, corresponding to each of the principal-axis-aligned rotations. Rotation about the shortest axis is a stable node, and that corresponding to rotation about the longest axis is a saddle point. The intermediate-axis-aligned rotation is a singular fixed point that only plays a passive role in organizing the dynamics in its vicinity. For a spheroid, there are only two fixed points: a stable node, corresponding to equatorial rotation, and a saddle point, corresponding to axial rotation, owing to the singular fixed point merging with the stable node or the saddle point (the nature of the merger is determined by the aspect ratio).

Keywords: Ellipsoid, Method of Averaging, Stokes number.

Introduction:
This work involves understanding the effect of inertial forces on the dynamics of an ellipsoid in the limit where particle inertia is dominant, and the particle Stokes number is therefore assumed to be large. This limit arises for gas-solid systems owing to the particle density (ρ_p) being much greater than the fluid density (ρ_f). The fluid inertia and gravitational torque are neglected, so the particle Reynolds number based on either the shear rate or settling speed is zero. In this limit, the equations of motion of the ellipsoid reduce to those of an asymmetric Euler top with the addition of a weak viscous torque. This analytical effort is motivated by earlier numerical efforts that have examined the effect of dominant particle inertia on spheroids [1, 2] and ellipsoids [3] in simple shear flow.

The parameters relevant to ellipsoidal orientation dynamics in a Newtonian fluid are the Reynolds($Re = \frac{l^2\dot{\gamma}}{\nu}$) and Stokes($St = \frac{\rho_p l^2 \dot{\gamma}}{\rho_f \nu}$) numbers, and the limiting scenario examined here corresponds to $Re = 0$ and $St \gg 1$, with the particle aspect ratios being arbitrary. In the above parameters, $\dot{\gamma}$ is a characteristic shear rate, ν is the kinematic viscosity, l is the longest semi axis, and ρ_p and ρ_f are the particle and fluid densities, respectively. For an ellipsoid, the semi-axis lengths are a, b and $c\,(a > b > c)$, and l equals a; spheroids have semi-axes (a, c, c), being characterized by a single aspect ratio $\kappa = a/c$; $\kappa > 1$ and $\kappa < 1$ for prolate and oblate spheroids, respectively.

Results and discussion:
The slow variables, that constitute the averaged description, are the three angular momenta (L_x, L_y, L_z) and

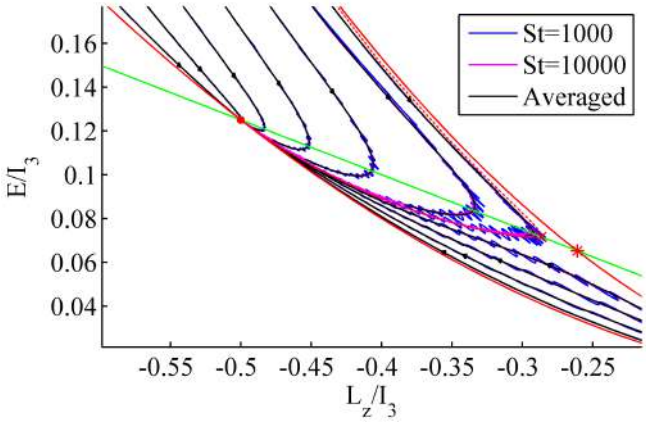

Figure 1: $L_z - E$ phase plot for an ellipsoid ($a = 1, b = 0.95, c = 0.3$) with $L_x, L_y = 0$, showing good agreement between the slow-manifold solution trajectories and the full solution ones for $St = 1000$ and 10000.

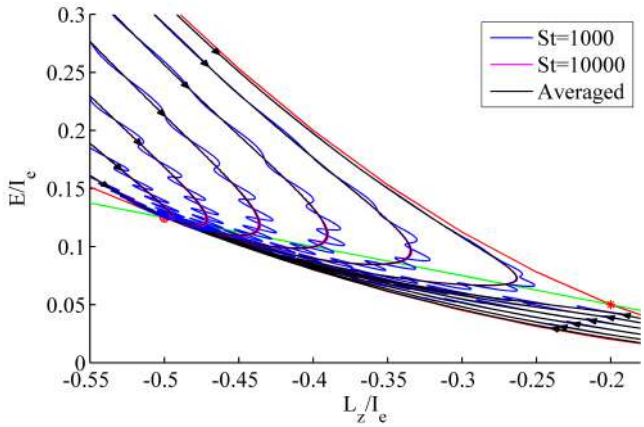

Figure 2: $L_z - E$ phase plot for a spheroid of $\kappa = 2$ with $L_x, L_y = 0$, showing good agreement between the slow-manifold solution trajectories and the full solution ones for $St = 1000$ and 10000.

the rotational kinetic energy (E). Figure 1 shows the $L_z - E$ phase plot for an ellipsoid. The three fixed points are: a stable node $(L_z/I_3, E/I_3) \equiv (-1/2, 1/8)$ marked by a red spot, a saddle point $(L_z/I_3, E/I_3) \equiv (I_1/I_3)(-1/2, 1/8)$ marked by a red asterisk and a singular fixed point $(L_z/I_3, E/I_3) \equiv (I_2/I_3)(-1/2, 1/8)$ marked by a red cross. The $L_z - E$ plot for a spheroid is shown in figure 2. The fixed points are a stable node $(L_z/I_e, E/I_e) \equiv (-1/2, 1/8)$ and a saddle point $(L_z/I_e, E/I_e) \equiv (I_a/I_e)(-1/2, 1/8)$.

Conclusion:

In this work we have used the method of multiple scales and method of averaging to obtain the system of ODE's governing the slow variables for both an ellipsoid and a spheroid. The numerical solution, and an analysis of the fixed points, of this system have allowed for a complete characterisation of the particle motion. Scaling arguments show the time required, to converge to the averaged description, to be $O(St^{1/2}\dot{\gamma}^{-1})$, an asymptotically smaller time in relation to the slow time scale of $O(St\dot{\gamma}^{-1})$.

References

[1] Lundell, F. & Carlsson, A. *Heavy ellipsoids in creeping shear flow: Transitions of the particle rotation rate and orbit shape*, Phys. Rev. E. **81**, 016323 1-8 (2010).

[2] Challabotla, N. R. & Nilsen, C. & Andersson, H. *On rotational dynamics of inertial disks in creeping shear flow"*, Physics Letters A. **379**, 157–162 (2015).

[3] Lundell, F. *The effect of particle inertia on triaxial ellipsoids in creeping shear: From drift toward chaos to a single periodic solution*, Physics of Fluids. **23**, 011704 1-4 (2011).

Time-domain motion of a floating or obliquely submerged non-uniform elastic plate

Mansi Singh[1,*], Michael H. Meylan[2] and Rupanwita Gayen[1]

[1] *Department of Mathematics, Indian Institute of Technology Kharagpur, 721302, West Bengal, India,* mansi.maths.iitkgp@gmail.com; rupanwita.gayen@gmail.com

[2] *School of Information and Physical Sciences, University of Newcastle, 2308, New South Wales, Australia,* mike.meylan@newcastle.edu.au

I. ABSTRACT

We consider the scattering of surface gravity waves by a thin elastic plate with non-uniform thickness in the context of linear water wave theory. The plate is either completely submerged and has some inclination with the vertical or is floating on the upper surface of the water. The associated boundary value problem is solved using the integral equations approach and the Green's function technique. Green's function arising from the fourth-order boundary condition (with variable coefficients) for the non-uniform plate (which we refer to as plate Green's function) is determined using two different methods in terms of the vibrating modes of the plate – the direct method and the eigenfunction method. These, in turn, are derived from the modes of a plate with constant thickness. The problem is finally reduced to a boundary integral equation involving the plate Green's function and the fundamental Green's function. The resulting integral equation has a hypersingular kernel in the case of a submerged plate. A numerical solution to the integral equation is used to find results for elastic plates with variable thicknesses. The results are validated by comparing them with those of an elastic plate with uniform thickness. We also present simulations of the time-domain motion when the plate–fluid system is subject to an incident wave pulse using Fourier transform.

II. TIME-DOMAIN SNAPSHOTS

Fig. 1 depicts the time-dependent results for a wave packet incident from $x = -\infty$ that interacts with the elastic plates having two different thickness profiles (denoted by solid and dotted curve). The sub-figure on the left is for the obliquely submerged plate, while the one on the right is for the floating plate. The blue curves correspond to the free surface, while the black lines represent the elastic plate. As the wave interacts with the plates, both the free surface and the plate exhibit deformations, which are shown at four different time stamps, t. The figure provides a comparative view of the dynamic deflections for the two configurations of the non-uniform plate, highlighting how the thickness variation affects the interaction between the wave and the elastic structure over time.

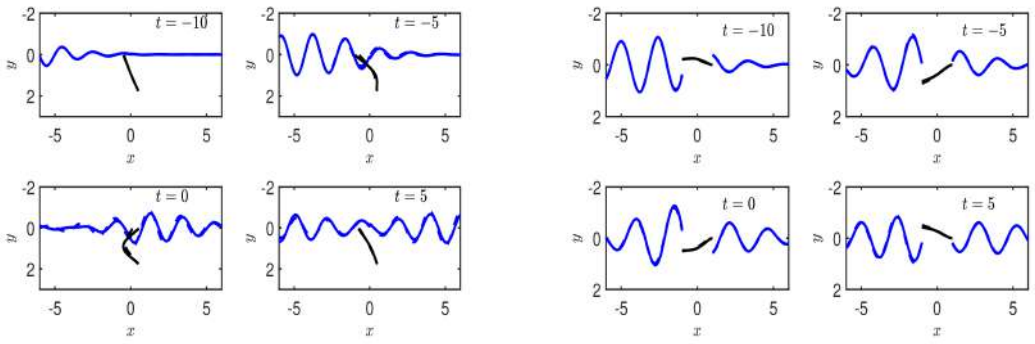

FIG. 1. Comparison of time-dependent motion between elastic plates of constant thickness (dotted line) and cubically varying thickness (solid line). Left: submerged inclined; Right: floating.

** Presently at: *Department of Applied Mechanics, Indian Institute of Technology Madras, 600036, Tamil Nadu, India.*

Towards a universal law for blood flow

Chaouqi MISBAH

Laboratoire Interdisciplinaire de Physique, Université Grenoble Alpes and CNRS, F-38000 Grenoble, France

Despite decades of research on blood flow, an analogue of Navier-Stokes equations that accurately describe blood flow properties has not been established yet. The reason behind this is that the properties of blood flow seem, a priori, non-universal as they depend on various factors such as global concentration of red blood cells (RBCs) and channel width. We have discovered a universal law when the stress and strain rate are measured at a given local RBCs concentration. However, the local concentration must be determined in order to close the problem. We propose a non-local diffusion equation of RBCs concentration that agrees with the full simulation. The universal law is exemplified for both shear and pressure driven flows. The theory is not limited to blood, as the approach is not explicitly dependent on RBC-specific properties. While the theory is restricted to a simplistic geometry (straight channel) it provides a fundamental basis for future research on blood flow dynamics and could lead to the development of a new theory that accurately describes blood flow properties under various conditions, such as in complex vascular networks.

Reference

Alexander Farutin, Abdessamad Nait-Ouhra, Mehdi Abbasi, Gopal Dixit,
Hamid Ez-zahraouy, Othmane Aouane, Jens Harting, and Chaouqi Misbah, Towards a universal law for blood flow, arXiv:2112.13801

Ultrasound reforms droplets

Ashis Kumar Sen, Lokesh Malik, Subhas Nandy, Niladri Sekhar Satpathi, Debasish Ghosh

Micro Nano Bio Fluidics Unit, Department of Mechanical Engineering, IIT Madras, India, ashis@iitm.ac.in

Microfluidic drop generation pivots around a few undisputed designs that hydrodynamically force two immiscible fluids, eventually breaking the interface into drops [1, 2]. Monodispersity in emulsions is a prerequisite to their successful implementation in the cosmetics, food, and pharmaceutical industries. Generation of monodisperse and homogenous droplets is also extremely critical in biochemical assays such as high-throughput screening. Commercial non-microfluidic emulsification recipes such as mechanical shearing inherit non-uniform shear stresses, thus leading to wide distribution in drop size and poor reproducibility. Although carefully designed microfluidic devices can produce monodispersed emulsions, however at certain operating conditions polydispersity is inevitable. For instance, polydisperse emulsions can result from fluctuations at the fluid supply source in simple microfluidic setups or while operating in the jetting regime that is inherently unstable. Further, to the best our knowledge, none of the available microfluidic devices are capable of reforming the size and uniformity of an already existing polydisperse emulsion, without losing part of the emulsion or distributing them through sorting. We introduce acoustomicrofluidics-based trapping-coalescence-splitting technique to reform existing polydisperse emulsion into size-controlled drops with improved monodispersity (see FIG. 1). In contrast to conventional approaches, our platform enables: controlling drop characteristics in-situ by regulating acoustic power without altering hydrodynamical parameters thereby improving response time; nozzle-less clogging-free drop generation from a liquid plug in a chamber instead of a liquid stream at a narrow junction. The technique can reform polydisperse drops produced not only due to fluid-source fluctuations or unstable regimes but also by non-microfluidic simple setups. Our study uncovers the universal dependency of generated drop size on a new dimensionless number – acousto-visco-capillary number, $Ca_{av} = (CaCa_a)^{1/2}$. Our theoretical scaling suggests the sum of capillary (Ca) and acoustocapillary (Ca_a) numbers $\sim O(1)$, and predicts the generated drop size, both agreeing well with the experimental findings. The underlying physics is uncovered by exploring the drop trapping-coalescence-splitting kinematics and dynamics. Distinctively, our platform is amenable to continuous mixing of inhomogeneous drops, offering monodisperse mixed-sample drops, and holds the potential to match current throughput standards through suitable design modifications.

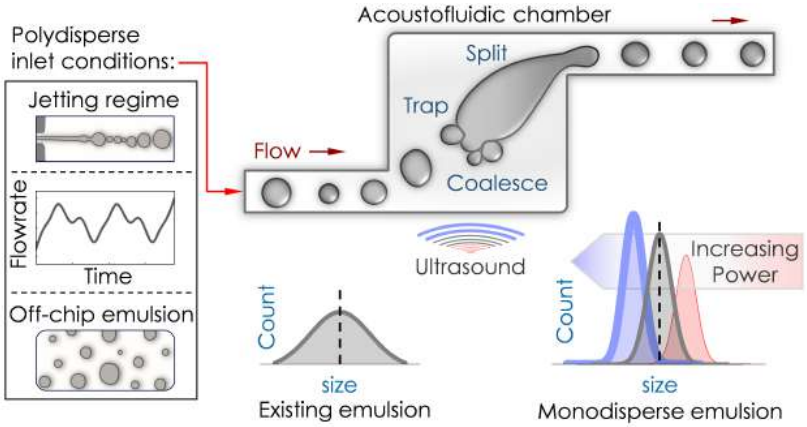

FIG. 1. Schematic diagram showing modification of droplet characteristics via trap-coalesce-split mechanism in a chamber. Droplets of varying size go through trapping, coalescence, and splitting to generate size-controllable droplets with improved monodispersity. Various inlet conditions: unstable jetting regime, fluid-source fluctuations, and off-chip emulsification; which may lead to polydispersity in the incoming emulsion, are also shown.

[1] A. S. Utada, A. Fernandez-Nieves, H. A. Stone and D. A. Weitz, Physical Review Letters, 2007, 99, 1–4.
[2] C. N. Baroud, F. Gallaire and R. Dangla, Lab on a Chip, 2010, 10, 2032–2045.